TÉCNICO LISBOA

Polymer Nanoparticles Containing Gold Nanoclusters

Bárbara Augusta Pereira Casteleiro

Thesis to obtain the Master of Science Degree in

Chemical Engineering

Supervisors:
Prof. Dr. José Paulo Sequeira Farinha
Prof. Dr. Marie-Thérèse Charreyre

Examination Committee

Chairperson: Prof. Dr. Carla Isabel Costa Pinheiro
Supervisor: Prof. Dr. José Paulo Sequeira Farinha
Member of the Committee: Prof. Dr. José Manuel Gaspar Martinho

November 2017

This page was intentionally in blank

Acknowledgements

Finishing a master degree in Instituto Superior Técnico is not something you can do alone. I did it with the patience of my family and friends, and the shared knowledge from my professors. There are a few people who deserve a special thank you for different reasons.

Starting with Prof. J. P. Farinha, who is one of my supervisors. He deserves a big thank you for accepting me in his laboratory 3 years ago, where I learned a lot about research work and discovered the subject of my dissertation, which I adore.

Prof. Marie-Thérèse Charreyre, my other supervisor, was one of the kindest people I met. She helped me to find my way in Lyon, in the university and out.

Tânia Ribeiro, who helped during most of these 3 years, especially with my master thesis. She shared with me her work and helped with mine, answering all my two thousand questions, being as happy as me for the good results and never giving up when it was difficult.

Arnaud Favier, with who I learned more than I could write in this thesis during my 6 months in Lyon. He was not only a great teacher, as well as an amazing person. He heard all my ideas, patiently discussed with me all my results and taught me how to think better.

Prof. Martinho who shared with me a lot of knowledge, always ready to discuss my news about gold nanoclusters and all the odd results that came with it.

My mother and my boyfriend deserve as well be thanked for all the times they remind me to breath and keep going.

Abstract

Gold nanoclusters (AuNCs) have unique properties and a wide range of applications, for example imaging. The objective of this work was to encapsulate AuNCs in polymer particles by miniemulsion polymerization and polymerization induced self-assembly (PISA) to improve their stability. Miniemulsion polymerization produces surfactant-stabilized polymer particles with diameters between 50 and 500 nm. And, PISA produces ''hairy'' polymer nanoparticles.

The project is divided into three sections. The first one consists in the synthesis of AuNCs and study of their properties. The AuNCs studied were AuNCs with 25 ($Au_{25}(MHA)_{18}$), 5 (Au_5) and 11 (Au_{11}) atoms. The size of $Au_{25}(MHA)_{18}$ was studied by HR TEM, being the average diameter of (1.8±0.6) nm. For $Au_{25}(MHA)_{18}$, the fluorescence emission spectrum has one band (810 nm) and the UV-Vis absorption spectrum has two bands (440 and 670 nm). For the Au_5/Au_{11}, the fluorescence emission spectra have 2 bands (380 and 500 nm) while the absorption spectra don't have any. The reducing agent:Au and ligand:Au molar ratios were studied to better understand the size evolution of AuNCs.

The second section is the study of miniemulsion polymerization incorporating AuNCs, using styrene and butyl methacrylate. The size determined by TEM and DLS was about 60 nm for polystyrene nanoparticles and 30 nm for poly butyl methacrylate nanoparticles. UV-Vis spectroscopy and fluorescence showed that the AuNCs keep their properties upon incorporation in the polymer nanoparticles.

The third section is the study of PISA-RAFT incorporating AuNCs. Different temperatures and macroCTA:Initiator ratios were studied. ^{1}H NMR was used to determine the kinetics of PISA-RAFT with and without AuNCs. The average size without AuNCs is 50 nm and with AuNCs is about 20 nm, determined by DLS, TEM and cryoTEM. The optical properties were studied and confirmed the incorporation of AuNCs in the polymer nanoparticles.

Key-words

Gold Nanoclusters, Miniemulsion polymerization, PISA-RAFT, Gold Nanoclusters stability, hybrid gold-polymer nanoparticles

Resumo

Nanoclusters de ouro (AuNCs) têm propriedades incomparáveis e grande diversidade de aplicações. O objetivo deste trabalho é incorporar os AuNCs em partículas de polímero produzidas por polimerização por miniemulsão e PISA (*polymerization induced self-assembly*). Polimerização por miniemulsão produz partículas poliméricas estabilizadas por surfactante com dimensões entre 50 e 500 nm. Por outro lado, PISA produz partículas estabilizadas por cadeias de polímero.

O projeto está dividido em três secções. A primeira corresponde à síntese de AuNCs e estudo das suas propriedades. Os AuNCs estudados foram AuNCs com 25 ($Au_{25}(MHA)_{18}$), 5 (Au_5) e 11 (Au_{11}) átomos. O tamanho dos $Au_{25}(MHA)_{18}$ foi estudado por HRTEM, sendo o diâmetro médio de (1.8±0.6) nm. Os $Au_{25}(MHA)_{18}$ têm duas bandas de absorção (440 e 670 nm), e uma banda de emissão de fluorescência (810 nm). Os Au_5/Au_{11} não têm nenhuma banda no espectro de absorção, mas têm duas bandas de emissão de fluorescência (380 e 500 nm). Os rácios molares ligando:ouro e redutor:ouro foram estudados para compreender melhor os mecanismos de formação dos AuNCs.

A segunda secção consiste no estudo de polimerização por miniemulsão incorporando AuNCs, usando estireno e butil metacrilato. O tamanho determinado por TEM e DLS é cerca de 60 nm para as partículas de poliestireno e 30 nm para as de PBMA. Espectroscopia de absorção UV-Vis e de fluorescência mostraram que não há alteração das propriedades óticas do AuNCs depois da incorporação.

A terceira secção é a incorporação dos AuNCs em partículas poliméricas sintetizadas por PISA-RAFT. Diferentes temperaturas e rácios molares de macroCTA:iniciador. ^1H RMN foi usado para determinar a cinética de PISA com e sem AuNCs. O diâmetro, determinado por TEM, cryoTEM e DLS, é 50 nm sem AuNCs e 20 nm com AuNCs. As propriedades óticas foram estudadas e confirmaram a incorporação dos AuNCs nas partículas de polímero.

Palavras-chave

Nanoclusters de ouro, polimerização por miniemulsão, PISA-RAFT, estabilização de Nanoclusters de ouro, partículas hibridas de ouro-polímero

Contents

Figure Index

Table Index

Glossary

^{1}H NMR (NMR)	Proton nuclear magnetic resonance
a	Box dimension
ACPA	4,4'-azobis (4-cyanopentanoic acid)
Ag	Silver atomic symbol
AIBN	2,2'-azobis(isobutyronitrile)
Ar	Argon
ATRP	Atom-transfer radical polymerization
Au	Gold atomic symbol
AuNCs	Gold Nanoclusters
AuNPs	Gold Nanoparticles
BDDA	1,4-butanediol diacrylate
BMA	Butyl methacrylate
c	Speed of light
C_{70}	Fullerene
CA	Cetyl alcohol
$CDCl_3$	Chloroform-d
CRP	Controlled radical polymerization
cryoTEM	Cryo transmission electron microscopy
CTA	Chain transfer agent
CTAB	Hexadecyltrimethylammonium bromide
Đ	Dispersity
DLS	Dynamic light scattering
DP	Degree of polymerization
DVB	Divinylbenzene
E	Energy
E_F	Fermi's energy
E_g	Band gap
E_n	Energy
f	Dilution factor
FID	Flame ionization detector
GC	Gas chromatography
GPC	Gel permeation chromatography
h	Plank's constant
$\hbar$	Reduced Plank's constant
HD	Hexadecane
HOMO	Highest occupied molecular orbital
HR TEM	High resolution transmission electron microscopy
IR	Infra-red
IUPAC	International union of pure and applied chemistry
K_b	Boltzmann's constant
KPS	Potassium persulfate
LUMO	Lowest unoccupied molecular orbital
m	Electron mass
macroCTA	Macro chain transfer agent
MHA	Mercapto hexanoic acid
MWD	Molecular weight distribution

n	Principal quantum numbers
N	Number of electrons in the box (section 1.1)
N	Number of Au atoms per AuNCs (section 3.1.2)
N'	Number of state with energy En
NaBH$_4$	Sodium borohydride
NaHCO$_3$	Sodium bicarbonate
NAM	N-acryloylmorpholine
NaOH	Sodium hydroxide
nBA	Butyl acrylate
NIR	Near infra-red
NMP	Nitroxide-mediated polymerization
P	Packing parameter
PAA	Polyacrylic acid
pBA	Poly (butyl acrylate)
PDI	Polydispersity index
PEG	Polyethylene glycol
PGMA	Poly (glycerol monomethacrylate)
PISA	Polymerization induced self-assembly
PMPC	Poly(2-methacryloyloxy) ethyl phosphorylcholine
PNAM	Poly(N-acryloyl morpholine)
PNPs	Polymer nanoparticles
PS	Polystyrene
RAFT	Reversible addition-fragmentation chain transfer polymerization
RuO$_4$	Ruthenium tetroxide
SDS	Sodium dodecyl sulphate
SEC-MALLS	Size exclusion chromatography - multi angle light scattering
SPR	Surface resonance plasmon
SR	Thiol ligand
Sty	Styrene
T	Temperature
tBDB	Tert-butyl dithiobenzoate
TEM	Transmission electron microscopy
UV	Ultra violet
Vis	Visible
α	Absorption coefficient
δ	Inverse of density of states
δ (NMR)	Chemical shift
λ	Wavelength
λ$_{exc}$	Excitation wavelength (nm)
v	Radiation frequency

Unit List

μA	microampere
a.u.	arbitrary units
eV	electron volt
g	gram
g/mol	gram per mol
h	hour
J	Joule
K	Kelvin
kV	kilo volt
M	molarity (mol/L)
mg	milligrams
mg/mL	milligrams per millilitre
min	minute
mL	millilitre
mM	millimolarity
mol/nm^2	mol per square nanometre
N/m	newton per metre
nm	nanometres
ppm	parts per million
rpm	rotations per minute
V	volt
μL	microliter
μm	micrometres

1. Introduction

Gold use started in the prehistory [1] and kept on being this important element until the present. From the Vedic civilization, when it was used mixed with ashes for medicinal purposes, to the romans, when it was used in decorations like the Lycurgus' cup (4th century AD), or the monetary and financial uses present until this day, gold has been part of humankind for a while now [1].

From a scientific point of view, before the modern sciences came along, gold was the fascinating goal of alchemists, when ''soluble gold" would be known as the ''elixir of life"[2]. In the modern age context, its stability and inertness as a bulk material, for a long time, made most of the scientific community lose interest in it. Faraday was the first one, in 1857, to see gold as a potentially interesting element in the eyes of science when he wrote ''the gold was there in separated particles, and that such specimens afforded cases of extreme division" [3], in between other observations related with the gold as a fine small particle.

This subject raised interested in the end of the XX century, more precisely in the beginning of the 1980's. By this time, the technology had evolved enough to allow the study of small particles and characterize, for example, the particles obtained by Faraday. So nowadays it is known that their sizes go from 3 to 300 nm, which puts them in the colloids' family.

1.1. Gold Nanoclusters (AuNCs)

According to the IUPAC, colloidal particles are defined as particles with at least one dimension between 1 nm and 1 μm and with a dispersity superior to 15% [2]. But there are other categories of particles that have been, with the boom of nanotechnology, interesting to scientists. Ones are the nanoparticles, which are characterized by having at least one dimension inferior to 100 nm. These particles maintain some of the properties of bulk materials, like almost continuous density of states (no emission) and crystalline structure, which allows them to keep metallicity (Figure 1). But new properties arise, such as superparamagnetic behavior and surface plasmon resonance (SPR) [4]. In the case of SPR, it results from the ''collective oscillation of the electrons in the conduction band" [4] from the energy levels below Fermi level. It is characterized by an absorption band at 520 nm in spherical gold particles, which stops being noticeable as the quantum size effects starts to gain importance (sizes below 2 nm) [2]. The other group is the gold nanoclusters or just gold clusters (AuNCs). They are characterized by dimensions inferior to 2 nm with a well-defined structure and organization (Figure 1) [2]. They are the in-between molecules and atoms, since it encounters properties of both: discrete electronic structure, photoluminescence, HOMO-LUMO transition and intrinsic magnetism [5]. Due to the loss of metallic character since all electrons are localized [6], there is no surface plasmon resonance. But on the other hand, the quantum confinement effects, due to their size being comparable with Fermi's wavelength, confer them discretization of energy levels and consequently emission in different wavelengths. The focus of this work will be the gold nanoclusters (AuNCs).
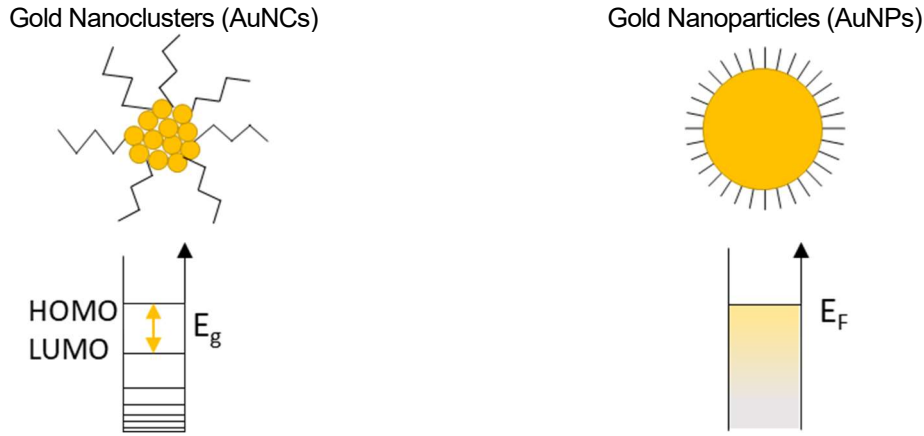
Figure 1. Main differences between gold nanoclusters and gold nanoparticles.

They can be small AuNCs, medium AuNCs and large AuNCs [4]. The first ones, small AuNCs, correspond to less than 5 atoms, not needing a stabilizer like thiols and having the largest band gap of the 3. The medium AuNCs are between 5 and 10 atoms, establishing weak bonds with the thiol stabilizer. The last ones, large AuNCs, with more than 10 atoms, not only establish strong bonds with the stabilizer molecule, but also have smaller band gaps. While the bigger ones have absorption spectra similar to semiconductors, the smaller ones are a more molecular like spectra [6].

AuNCs are not the only metal clusters studied in the last years, but the higher resistance of gold to oxidation and its stability as a cluster have drawn more and more attention to them [5], as well as made them an interesting subject for further studies and manipulation as it is intend in this work.

1.1.1. Characteristics and properties of gold nanoclusters

To better understand these particles, it is important to look with more detail into some of their characteristics, starting with the discrete electronic structure. It results from the relevance of electronic energy quantization and it is related to the cluster size. For example, in the bulk gold, the energy levels are close together which origins bands and the quantization of energy is less evident [7]. When we start reducing the material/particle size, the energy levels start to be more far apart, and the quantization is more evident, like in the clusters. To know from which size this effect is relevant it is possible to calculate the critical diameter through the free-electron model following the explanation of Jin [5]. Starting by the Schrödinger equation for 1 electron, in a Cartesian coordinate system, considering a cube of N electrons with volume a^3 [5]:

$$E_n = \frac{\pi^2 \hbar^2}{2ma^2} n^2 \tag{1}$$

In equation 1, n represents the principal quantum numbers being the sum of the squares of n_x, n_y and n_z. From this point, considering N' as the number of energy states with energy E_n and as being represented by the volume of a sphere, equation 2 correlates N' with the principal quantum numbers through n.

$$N' = \frac{1}{8} \left(\frac{4}{3} \pi n^3 \right) \tag{2}$$

By substituting n from equation 1:

$$N' = \frac{\pi}{6} \left(\frac{2ma^2}{\pi^2 \hbar^2} \right)^{\frac{3}{2}} E^{\frac{3}{2}} \tag{3}$$

And differentiating equation 3 with respect to E, the density of energy states is obtained:

$$\frac{dN'}{dE} = \frac{a^3}{4\pi^2}\left(\frac{2m}{\hbar^2}\right)^{\frac{3}{2}} E^{\frac{1}{2}} \tag{4}$$

The spacing between levels correspond to the inverse of the energy states' density, being then defined by:

$$\delta = \frac{4\pi^2}{a^3}\left(\frac{\hbar^2}{2m}\right) E^{-\frac{1}{2}} \tag{5}$$

Using the thermal energy at 298 K, about the room temperature, it is possible to calculate at which size the quantization energy is comparable with the thermal energy (equation 6). And with this obtain the critical size [5]:

$$Tk_B = \frac{4\pi^2}{a^3}\left(\frac{\hbar^2}{2m}\right) E^{-\frac{1}{2}} \tag{6}$$

being k_B Boltzmann's constant, T=298 K, $\hbar$ the reduced plank's constant and m electron mass. Being the Fermi's energy, for gold, 8.8 x 10 $^{-19}$ J [5], the value obtained for a is about 1.7 nm. This value is taken as the cluster's diameter and, given all the approximations of the method, it can be taken as being approximately 2 nm, the value mentioned before as the diameter from which gold particles start to behave as nanoclusters. At this size the levels start to be closer, including HOMO and LUMO, which means a decrease in the band gap, and consequently emission closer to IR. For the same reason, smaller AuNCs will have emission in the UV or closer to it, having larger band gaps.

1.1.2. Applications of Gold Nanoclusters

AuNCs have strong photoluminescence. Some of them conjugate this with some other properties, such as long fluorescence lifetime, large Stokes shift, biocompatibility, photostability [8], low toxicity [4] and catalytic activity [5] confers them the high range of applications

One of the most important applications of these nanostructures is as catalyst due to its catalytic activity mentioned previously. According to Buceta, et al [4], the catalytic capacity of AuNCs can be explained by the HOMO-LUMO gap. Increasing the number of gold atoms, the gap decreases and the bonding to the thiol group starts to be stronger. For the oxidation reactions, the bond between AuNCs and the thiol group can't be too strong, to allow the interaction with the oxygen. So, in this case the AuNCs with intermediate size (between 5 and 10 atoms) are the ideal. But for different types of reaction, different AuNCs size are required, for example, for hydrogen oxidation reaction, bigger AuNCs are needed (10 to 40 atoms), because these ones will have a lower HOMO, making it lower than the antibonding resonance, allowing the reaction to happen [4]. Furthermore, the small size of AuNCs in general allows them to have a higher superficial area which is an advantage in heterogeneous catalysis (high density of active sites). Some examples of this application are the oxidation of α-hydroxyl ketones by encapsulated AuNCs which gives them an ''excellent reusability'' [9], aerobic oxidation of alcohols to aldehydes with AuNCs produced by a method called Red-Al® [10], and aerobic oxidation to produce esters from alcohols through micro-encapsulation of AuNCs in polystyrene copolymers [11]. Fang and co-workers studied Au$_{25}$MHA$_{18}$ as a precatalyst for styrene oxidation and nitrobenzene hydrogenation [12] obtaining high conversions and selectivities for both. This is an example of application of AuNCs synthesized by the same protocol of the ones studied in the present work.

Chemiresistors as MIME (metal-insulator-metal ensemble) sensors are another important application of AuNCs [13, 14]. Electron tunneling allows the AuNCs to do electron conduction in between the AuNCs' cores,

when in an insulating surface. These sensors allow not only high sensitivity, but high selectivity too. This last point is achieved due to the different thiols and other stabilizing groups that can be used, while the first one is due to the tunneling modulation and high density of tunnel junctions [14]. One of the most used are the AuNCs with mercapto hexanoic acid (MHA) as ligand, being extremely sensitive to amines, responding even to low concentrations.

In the sensing field, there are AuNCs sensible to different compounds such as heavy metal ions, biomolecules, inorganic ions and even drug molecules, pH and temperature. Some examples to consider, in the heavy metal and inorganic ions are Hg^{2+} or CN^- detection, while in the other ones there is folic acid, cholesterol and vitamin B_{12} detection by AuNCs functionalized with different ligand such as BSA or glutathione [8]. One of the most tested in terms of pH response is the AuNCs functionalized with glutathione [15]. While, as temperature sensitive, have now been functionalized with peptide nanofibers [16].

Imaging has been strongly investigated too, with special emphasis in bioimaging using AuNCs with emission in the biocompatible region (near IR) [17, 18]. In combination with stabilizers such as folic acid, AuNCs are used for detection of cancer cells [8].

In the biological field, there are more applications such as biolabeling and biosensing. In biolabeling, cancer cells, as human hepatocarcinoma and leukaemia, have been studied since they naturally reduce gold salt, allowing cell imaging, unlike normal cells in which this phenomenon does not occur. The identification of bacteria using lysozyme functionalized AuNCs has been achieved as well, not only for *Escherichia coli* as well as for *Enterococcus faecalis*, *Staphylococcus aureus* and a few more [8].

In the biomedical field, there is also gene and siRNA delivery, drug control release and delivery as well as photodynamic and radiation therapy [8]. In the case of drug release, it can be achieved not only through thiol/sulphite exchange of the ligand, but by AuNCs encapsulated in nanoparticles [19-22], combining diagnostic with therapy - theranostic.

1.1.3. Gold Nanoclusters Synthesis

The synthesis of AuNCs can be made by two distinct strategies: top-down and bottom-up [6]. Top-down synthesis start from bigger particles to obtain smaller ones, which is mainly done by etching with different ligands. Bottom-up synthesis, on the other hand, start with atomic precursors like gold salt using then a reducing agent.

This subject had a big impulse with the synthesis by bottom-up using thiols as ligands achieved by M. Brust in 1994 [23]. Since then, it has been optimized being now possible to synthesize monodisperse AuNCs in only one phase and in multiple solvents.

In the present work, the synthesis strategy used is bottom-up, starting with a gold salt ($HAuCl_4$) as precursor. The other important reagents are the reducing agent and stabilizer (ligand). The mainly used chemical reducing agents are sodium borohydride ($NaBH_4$ - the one used in the present work), sodium citrate, hydrazine hydrate, tetrakis(hydroxymethyl) phosphonium chloride and ascorbic acid [8]. Besides chemical reduction, other options can be considered, such as photoreduction, bioreduction and electroreduction.

The stabilizers, also denominated ligand, which have been most used are thiolates, peptides, proteins, DNA oligonucleotides, dendrimers and polymers [8]. The ligands can influence the AuNCs applications and features. For example, acid folic or proteins can be used to achieve biocompatibility or affinity with certain cells,

or glutathione can be used to produce pH responsive AuNCs. Nevertheless, the ligand is essential to achieve different AuNCs sizes, and consequently different electronic and optical properties. In between these, the more common ones are $NaBH_4$ as reducing agent and glutathione, in the thiolate family, as stabilizer. Thiolates are widely used due to the S-Au covalent bond, stabilizing quite efficiently the AuNCs. The more common AuNCs, due to their high stability are Au_{25}, Au_{38} and Au_{144} [24]. Au_{25}, for example, structurally, are composed by a Au_{13} core capped with 6 Au_2SR_3 motifs [25]. This is a characteristic that varies with the number of atoms: different motifs are obtained for different curvatures which depend on the number of atoms (higher number of atoms means smaller curvature). The mechanism is based in an equilibrium between stabilization and etching ("digestion of the newly formed nanoparticles" [26]) from the ligand and reduction by the reducing agent. To be more precise, it is believed that it involves two steps. The first one is the reduction of Au(I) with kinetical control, and the second one is the size differentiation with thermodynamic control [24].

1.1.4. Stabilization of Gold Nanoclusters with Polymers

The main problems related with gold nanoclusters are the lack of stability as well as handling and storage conditions. To solve these issues, the present work proposes to incorporate the clusters into a polymer matrix, producing materials from the nanocomposites family (more than one compound with at least one phase with less than 100 nm). Different teams have been trying this approach through different types of polymerization and with different goals, as it is shown in the following examples.

Yu's team has developed a material that acts as a catalyst being constituted by AuNCs encapsulated in dendrimer-like micelles [9]. The encapsulation allows the AuNCs to be reused as catalysts. They prepared AuNCs with emissions between 330 and 380 nm without the use of external reducing agents. The micelles are produced with polyethylene glycol (PEG) with a four steps process, in which the gold salt is only added after the micelles formation.

Carotenuto's team developed a protocol to produce Au thiolate complexes embedded in amorphous polystyrene, which can be used as "invisible ink" for polymer, paper or wood [27]. The method used is a solvent based one with heating of AuNCs. In this field, it is still difficult to change in a controllable way the size of AuNCs, and consequently, to tune the emission since this is size dependent. Carotenuto's team followed two different approaches: Au alloyed with Ag and Au coated with aromatic molecules. These allowed them to obtain a polymer with high fluorescence intensity which can be used as probe for different applications.

Polymer nanogels have been studied as an efficient way to deliver "therapeutic agents and diagnostic probes" [17]. So, Chen's team tried to put together AuNCs and nanogels to combine their properties for bioimaging, using polyacrylic acid (PAA) nanogels with hollow core and porous shell with about 150 nm of diameter. These authors, by testing *in vivo* the nanocomposites with emission and excitation in the near-infrared (NIR), proved the potential application of it as bioimaging and therapeutic agents [17].

Miyamura and Kobayashi worked in the development of AuNCs encapsulated in polystyrene copolymers for catalytic applications [11]. They developed "one-pot tandem reactions" based in two processes: microencapsulation and crosslinking. Different catalytical tests are made after the encapsulation, where the AuNCs show a high catalytical activity. The same group developed the Red-Al® method [10], very similar with the method before mentioned. The main difference between them is the stage in which the crosslinking groups are added: incorporated in the polymer or added after to the reaction.

Another example is the incorporation of AuNCs in amphiphilic polymeric nanocarriers by Chen's team [20], used in multifunctional theranostic. Besides polymers, folic acid is also used due to its known affinity for tumor cells. Firstly, fluorescence spectroscopy shows emission maximum is at 610 nm, and TEM images allowed to locate the AuNCs in the polymer. Secondly, the accumulation of the nanocarriers was positively tested in the tumor cells. So, in this case, the conjugation of AuNCs with different components allows the production of an efficient material for tumor targeting and drug release, like in some other cases above mentioned.

The last case presented is the self-assembly of peptides nanofibers containing AuNCs [16]. The particles are both used for thermos-sensing and cell imaging. They also report the increase in luminescence intensity after incorporation, obtaining a quantum yield of 21.3%, which is quite high compared with most AuNCs reported.

1.2. Polymerization in dispersed medium

Miniemulsion polymerization and polymerization induced self-assembly (PISA) are part of a larger family: free radical polymerization, like most of the examples above presented.

In this family, the polymerization can be carried out in different media, which divides it in different methods of polymerization: bulk, solution and dispersed medium polymerization. In the current work, in both cases (miniemulsion polymerization and PISA), it corresponds to dispersed aqueous medium. It has been strongly developed in the past decades due to its popularity between academia and industry [28].

When compared with bulk polymerization in emulsion polymerization, the final mixture has lower viscosity which not only facilitates the product removal as well as avoids hot spots and helps the heat removal (polymerization is an exothermic process). Nowadays, the drawback of producing a lower amount of polymer has mostly been overcome due to the high solid content processes available.[28, 29]

In addition, when compared with solution polymerization, there is the advantage of using water as solvent instead of organic solvents. It makes the process more environmentally friendly, reduces health issues and toxicity and it is less expensive [29], even though the water may interfere with the polymerization itself [28].

Overall, the main advantages of this kind of polymerization are [30]:

$\rightarrow$ Good control of polymerization;

$\rightarrow$ Low viscosity;

$\rightarrow$ High concentration of copolymer;

$\rightarrow$ High yield of polymerization;

$\rightarrow$ High solid content;

$\rightarrow$ Good for environment;

1.2.1. Miniemulsion polymerization

Miniemulsion polymerization was first designed to overcome the limitations of emulsion polymerization (only works well for radical homopolymerization and in a limited groups of monomers), without adding other limitations, such as excess of surfactant, low colloidal stability or high costs [28]. It was J. Ugelstad, in 1973, with polystyrene polymerization, who was the first to publish a paper on the subject: miniemulsion [29].

It consists of a system of heterophases originating monomer droplets between 50 and 500 nm [28], with 4 main components: water, monomer, surfactant and costabilizer. J. Asua presents a table of different monomers, surfactants, costabilizers and initiators commonly used in miniemulsion [31]. The most common monomer is styrene, but monomers with different water-solubilities have been successfully used (completely soluble to not soluble at all). For the surfactant, the most common is sodium dodecyl sulfate (SDS), an anionic surfactant, while the costabilizers are hexadecane (HD) and cetyl alcohol (CA). For the initiator it is mostly potassium persulfate (KPS), which is water-soluble.

Starting with a two phases system: aqueous phase and oil phase (monomer phase), the system is stirred creating an emulsion (Figure 2). Then a shear force is applied, with a sonifier or homogenizer, causing the particles to be deformed and disrupted. The nucleation in miniemulsion occurs mainly by monomer droplets nucleation as opposite to homogeneous and micellar nucleation in emulsion polymerization, being this a special feature, which confers miniemulsion a broad range of applications. To maximize the number of particles by droplet nucleation there are two important factors: surfactant amount and homogenization method. If the homogenization process is not efficient or intense enough, larger particles will be formed. With larger particles, less surfactant is needed to stabilize it, and more free surfactant will be in solution leading to the formation of micelles and micellar nucleation. On the other hand, smaller particles need more surfactant and less will be available to form micelles. This way, efficient homogenization and no excess of surfactant will lead to monomer droplets nucleation and less or non-existent micellar nucleation. [31]
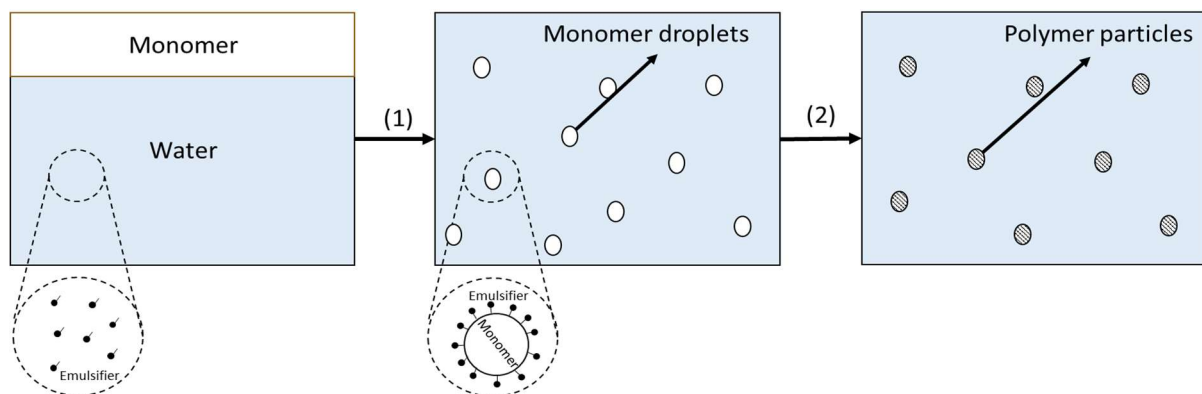
Figure 2. Miniemulsion polymerization according to nanoreactor's principle [28]: (1) sonication, (2) polymerization.

The droplets are stabilized by the surfactant, which avoids coalescence by droplet's collision. J. Asua enunciates some of the main characteristics of a surfactant [31] as: presence of polar and apolar groups, soluble in aqueous phase but easily adsorbed in the monomer phase, the surface tension must be 0.005 N/m or less, it must resist particles collision and it must work in small concentrations.

The costabilizer, also known as hydrophobe, on the other hand, reduces the diffusion of monomer in the aqueous phase, avoiding Ostwald ripening, by decreasing the surface energy of the smaller droplets. To make the monomer droplet's nucleation the main nucleation process, the presence of costabilizer is needed. As opposite to the surfactant, the effect produced by this component is a bulk effect instead of surface stabilization. This is a highly hydrophobic component, usually with low molecular mass, such as hexadecane and cetyl alcohol. By adding small amounts of this component, the surface energy of the small droplets is reduced, making them more stable and reducing the diffusion of monomer from the small droplets to bigger

ones (Ostwald ripening). But these components remain in the particles after polymerization, which constitutes a disadvantage of this technique when they are volatile and most of the time toxic compounds. Other options such as using polymer or chain transfer agents (CTA) as hydrophobes have also been explored. The first one presents some issues such as the droplets lack of stability. The second one overcomes this issue, but only low molecular weight polymers can be produced [31].

Inside the droplets, the polymerization proceeds as bulk polymerization being that each droplet behaves like an individual nanoreactor [28, 31]. Depending on the type of initiator, different process can occur. If it is a water-soluble initiator, the radicals go inside of the particles, after forming more hydrophobic oligomers. On the other hand, if the initiator is oil-soluble (monomer-soluble), the decomposition occurs mainly inside the monomer phase, followed by the desorption of one radical by unit of radicals. So, water-soluble initiators favor homogeneous nucleation (emulsion polymerization), while oil-soluble initiator favors monomer droplet nucleation. In terms of polymerization rate, miniemulsion using oil-soluble initiator is the fastest, followed by conventional emulsion and, at last, miniemulsion using water soluble initiator [31].

The homogenization of the system, as mentioned before, can be done using different apparatus. In laboratory environment, the main technique is ultrasounds, first reported in 1927 as used in emulsion technique [28]. The droplets are broken by the shock waves produced, but only in a limited radius around the ultrasounds' source. So, to assure that all particles go through this area, additional stirring is needed. A direct correlation between sonication time and droplets size was also shown: by increasing the time of sonication, the droplets size decreases. For larger amounts, high pressure homogenizers and roto-stator dispersers can be used [28]. While roto-stators use turbulence to emulsify, high pressure homogenizers, such as microfluidizers, use mostly shear forces with help of cavitation and impact forces to break the droplets. Regardless of the technique, the more efficient it is, higher is the number of particles (and smaller) and higher the rate of polymerization [31].

Miniemulsion polymerization allowed the production of latex with high solid content but low viscosity, polymerization in reactors of continuous production, controlled radical polymerization in dispersed media, catalytic polymerization, incorporation of hydrophobic monomers, hybrid polymer particles and some others [31].

The incorporation of inorganic compounds goes from pigments to produce paint (one of the main applications) to magnetic particles to couple with antibodies or enzymes for biological application (like drug release) [32], different kinds of dyes [33-35], compounds such as fullerenes (C_{70}) [36] and some metal salts such as Co and Ag [37]. The incorporation of inorganic compounds in latex particles started in 1980s, starting with about 50 papers per year published in the area, that fast increased to 100 papers per year in the first decade of 2000.[32]

1.2.2. Polymerization induced self-assembly (PISA)

Polymerization induced self-assembly, also known as PISA, is a relatively new method of polymerization in dispersed medium. It consists in the self-assembly of amphiphilic copolymer part soluble in the solvent, part insoluble that are formed during synthesis [38]. Different controlled radical polymerization (CRP) techniques can be used such as nitroxide-mediated polymerization (NMP), atom-transfer radical polymerization (ATRP) and reversible addition-fragmentation chain transfer polymerization (RAFT), being the last one the more common [39]. In this project, only PISA via RAFT(PISA-RAFT) was studied.

RAFT ''is based on an equilibrium between active and dormant species, achieved by a degenerative chain transfer process'' [40] (Figure 3). It has a high control of molecular weight distribution (MWD) and architecture, using a source of free radicals like in conventional free radical polymerization, allowing obtaining polymers with different compositions and structures.
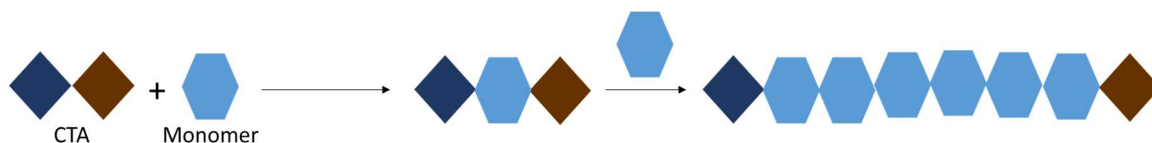
Figure 3. Scheme of RAFT polymerization.

The polymerization is divided into different steps: initiation, addition-fragmentation, pre-equilibrium, reinitiation, addition-fragmentation main equilibrium and termination. Initiation correspond to the decomposition of the initiator leading to the formation of primary free radicals, similarly to conventional free radical. RAFT is conducted with lower initiator concentration to limit the influence of termination. The number of polymer chains is mainly controlled by the quantity of chain transfer agent (CTA – Figure 4) which is a thiocarbonylthio-compounds.
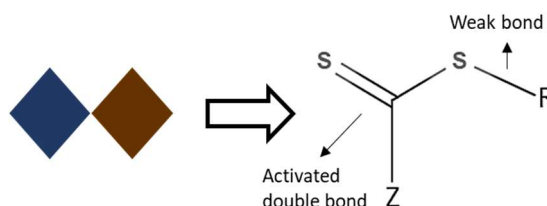
Figure 4. General structure of a RAFT-CTA.

When the RAFT polymerization is stopped, the chains are mainly ''dormant'', meaning that they can be re-activated (macroCTA). These macroCTA polymer chains are used to start the PISA. Besides this component, the other components of PISA are: monomer, initiator and solvent(s).

The macroCTA is usually a solvent-philic living polymer chain, that can add the solvent-phobic monomer units (only partially soluble in the continuous solvent phase) thanks to the RAFT mechanism to form an amphiphilic ''block'' copolymer. In PISA-RAFT, the block copolymerization usually starts in the continuous solvent phase after the decomposition of the initiator. Soluble macroCTA chains add few monomer units. When the solvent-phobic block reaches a critical size, the solubility is disrupted, and auto-assembly occurs through the formation of block copolymer micelles. From this point the polymerization proceeds similarly to bulk/solution polymerization in the interior of the micelles (Figure 5), while the solvent-philic part of the chain act as a steric stabilizer.
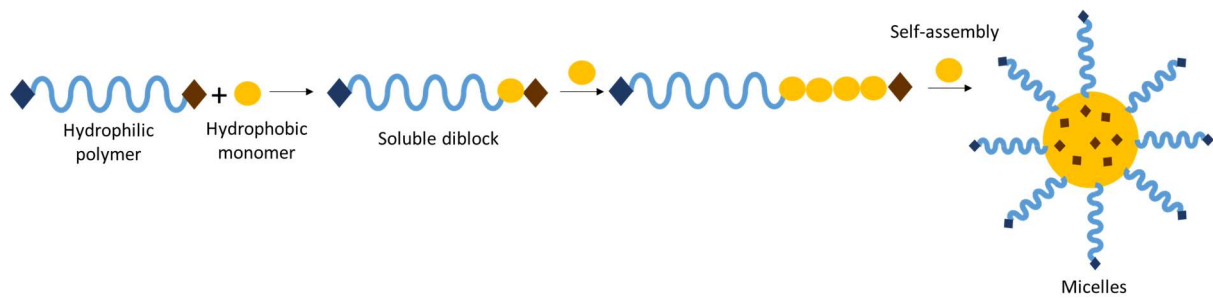
Figure 5. Principles of PISA via RAFT

For PISA-RAFT, in aqueous media, there are some important parameters to consider, such as pH, temperature, degree of polymerization (DP) of macroCTA, initial concentration of the hydrophobic monomer and targeted DP of the hydrophobic block.

In terms of pH, for alkaline solutions, the macroCTA chain-end tends to suffer hydrolysis, especially when it is a dithiobenzoate macroCTA [38]. On the other hand, for pH between 6 and 3, this macroCTAs leads to high conversion and low polydispersity. But the pH does not affect only the macroCTA, but also the morphology of the particles. Depending of the pH, electrostatic repulsions between the chains can be screened, changing particle conformation [41].

A variety of monomers can be used, from more solvent-phobic to less. But it has been discovered that using a less hydrophobic monomers is one of the parameters which can lead to thermo-responsive gels [38]. The variety of monomer which can be used for PISA in organic solvents is also higher than the one for PISA in aqueous medium [41].

Different morphologies can be obtained such as spherical micelles, worm-like micelles and vesicles, being defined essentially by volume fraction of the hydrophilic and hydrophobic blocks [38]. The different morphologies can be rationalized with the packing parameter (P). The packing parameters is a function of the volume and length of the hydrophobic bock and the effective interfacial area of the block junction. Lower P values produce micelles (until 1/3), then the worms (1/3<P<1/2) and for higher values vesicles (1/2<P<1) are obtained. This value tends to increase during the polymerization, which lead to an evolution of the morphology during the synthesis. Other factor that influence the morphology are the nature and average mass of the 2 blocks, initial monomer concentration and solvent properties.

The main advantages of PISA are [30, 38]:

→ Simple, direct and reproducible process;
→ Low number of purification and synthesis steps;
→ Wide range of surface functionality;
→ Controlled morphology;
→ No use of tensioactives.

The main applications of PISA, until now, are drug and gene delivery [30]. The studies in this field are mainly about the optimization of the different parameters of PISA-RAFT, such as monomer, solvent or particles morphology [42]. But with the development of the technique and functionalization of the polymer particles, new applications will appear soon. Some of the potential applications are nanostructured films, materials to heterocoagulates, rheology modifiers and responsive gels depending on the morphology [42].

The particles obtained by PISA-RAFT differ from the ones obtained by miniemulsion polymerization (Figure 6). By miniemulsion polymerization the particles are mainly stabilized by the surfactant, being the particles formed by a large number of solvent-phobic polymer chains. The size depends on the surfactant concentration. On the other hand, the particle by PISA-RAFT are "self-stabilized" by the solvent-philic block ("hairy" nanoparticles), and can be used to access to different morphologies [41].

Miniemulsion Polymerization
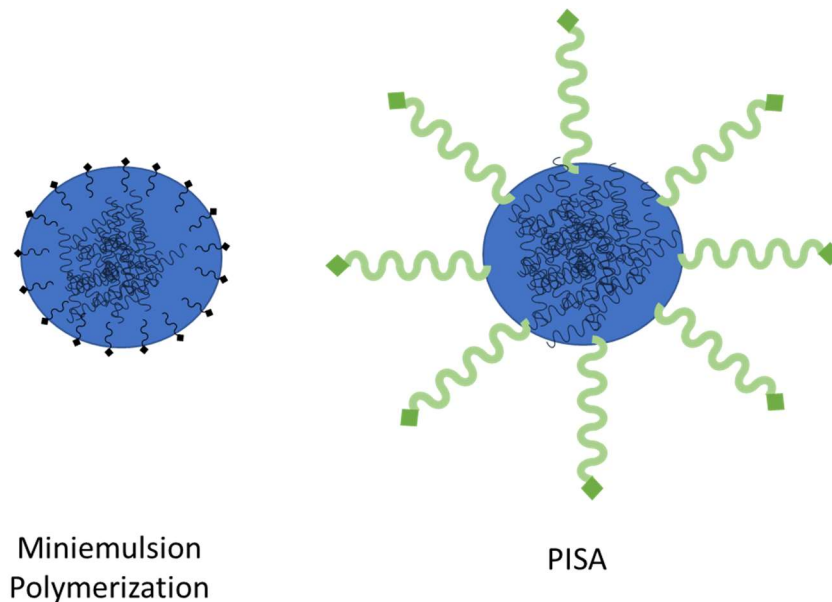
PISA

Figure 6. Scheme of common structure for polymer particles synthesized by miniemulsion polymerization (spherical polymer nanoparticles stabilized by surfactant) and PISA (spherical "hairy" nanoparticles stabilized by polymer chains).

The report is divided in 4 sections. It starts with the present introduction with the theoretical background of the studied topics: AuNCs, miniemulsion polymerization and PISA.

The second section corresponds to the methods and techniques applied. The main ones are UV-Vis spectroscopy and fluorescence spectroscopy for the study of the optical properties of AuNCs in different conditions, different TEM techniques and DLS to study the size and morphology of the PNPs and AuNCs, and ^{1}H NMR for kinetic studies of PISA. GC and SEC were also applied to study the composition of certain solutions and the Mn of macroCTA, respectively.

The third section corresponds to the results and discussion. The characterization and stability of two different kind of AuNCs is discussed: Au_{25} (AuNCs known for their high stability) and Au_5 and Au_{11} (with higher fluorescence intensity). Then incorporation of the first one into PNPs by miniemulsion polymerization is studied. Lastly, PISA-RAFT is also studied as a polymerization technique for the incorporation of AuNCs into PNPs. Different parameters, such as temperature and amount of initiator, are optimized in order to favor the AuNCs stability.

The last section presents the conclusions and future perspectives of the subject. This is a quite recent topic, with still a lot of options to explore and optimize.

2. Materials and Methods

2.1. Materials

Gold(III) chloride trihydrate (HAuCl$_4$.3H$_2$O, ≥99.9% trace metals basis, Sigma-Aldrich), 6-Mercaptohexnoic acid (MHA, 90%, Sigma-Aldrich), sodium hydroxide (NaOH, pure, EKA Pellets) and sodium borohydride (NaBH$_4$, >98.5%, Sigma-Aldrich) were used for the synthesis of gold nanoclusters (AuNCs). Deionized water, used in the synthesis, was generated by a Millipore Milli-Q system (≥18 MΩcm, Merck).

Hexadecyltrimethylammonium bromide (CTAB, 99+%, ACRÔS organics), and absolute ethanol (EtOH, 99.8%, Sigma-Aldrich) were used to phase transfer the gold nanoclusters from water to various monomers and toluene (99.5+% toluene ACS, Sigma-Aldrich).

Hexadecane (99%, Sigma-Aldrich), divinylbenzene (DVB, 80%, Sigma-Aldrich), 2,2'-azobis(isobutyronitrile) (AIBN, Fluka), and deionized water (≥18 MΩcm, Merck) were used in the mini-emulsion synthesis. The monomers used in different mini-emulsions synthesis were styrene (Sty, Fluka) and butyl methacrylate (BMA, 99%, Sigma-Aldrich).

N-acryloyl morpholine (NAM, Sigma-Aldrich, 97%, distilled at 120°C and 10 mmHg [30]), Tert-butyl dithiobenzoate (tBDB, synthesized according to Favier et al [43]), 1,4-dioxane (Sigma-Aldrich, ≥99%, distilled with LiAlH$_4$ at 110°C [30]), 2,2'-azobis(isobutyronitrile) (AIBN, Fluka, ≥98% (GC), recrystallized in ethanol [30]) and 1,3,5-trioxane (≥99%, Sigma-Aldrich) were used in the RAFT polymerization of PNAM.

Poly(acryloyl morpholine (PNAM, synthesized by RAFT), n-butyl acrylate (nBA, Sigma-Aldrich, ≥99%, distilled with hydroquinone at reduced pressure [30]), acetonitrile (Ficher, HPLC grade, distilled [30]), 4,4'-azobis(4-acide cyanopentanoique) (ACPA, Fluka, ≥98%), sodium bicarbonate (NaHCO$_3$, Merck), and 1,4-butanediol diacrylate (BDDA, Aldrich, 90%, purified using an inhibitor remover column (Aldrich)) were used to synthesize particles by PISA.

2.2. Experimental techniques

2.2.1.   Transmission Electron Microscopy (TEM)

Transmission electron microscopy (TEM) is a microcopy technique which uses an electron beam instead of a light source. This allows to achieve higher resolutions, going until the electron wavelength, visualizing theoretically until 0.1 nm [44].

In the present work, TEM, HR TEM (high resolution TEM) and cryoTEM were employed to characterize the AuNCs and polymer nanoparticles. The main limitations of these techniques are [45]:

→   Sampling reproducibility and the small area analyzed.

→   Interpretation of transmission images.

→   Sample damage by electron beam (specially in polymers).

The main advantages and limitations of each method for this project are presented in Table 1.

Table 1. Comparison between the different TEM techniques used to study the morphology and size of AuNCs and PNPs.

Technique	Advantages	Limitations
TEM	Minimum damage of sample. Good resolution and contrast.	Dried samples – changes in morphology.
CryoTEM	Visualization of sample in the same condition as in solution (no changes in size or morphology).	Lower resolution. Issues with charged particles.
HR TEM	Visualization of crystalline structure. Higher resolution.	Damage of sample (mostly polymeric materials)

The TEM apparatus used to characterize the miniemulsion PNPs was Hitachi transmission electron microscope of model H-8100 with LaB_6 filaments (Hitachi, Tokyo, Japan) and operated by Tânia Ribeiro. The acceleration voltage was 200 kV and the current was 20 µA. The images were acquired by the camera KeenView of Soft Imaging System, using the software iTEM. The sample preparation consisted in immersion of the grid into the solution without dilution and left to dry overnight.

The TEM apparatus used to characterize the PISA-RAFT PNPs was Philips transmission electron microscope of model CM120, both for regular TEM and cryoTEM, and operated by Pierre Alcouffe.

For the sample preparation for regular TEM, a droplet of the diluted sample (dilutes 100 times in water from **PISA1** to **PISA14** and f=1000 in water from **PISA15** to **PISA27**) was deposited onto a carbon film coated on a copper grid. Before observation the sample was stained by RuO_4 vapor (2%wt in water) during 30 min to enhance polymer contrast. The accelerating voltage used for the observation was 80 kV.

In the sample preparation for cryoTEM, a small drop of sample (ca. 5 µL) diluted 100 times in water was pipetted onto an advanced holey carbon film (Quantifoil, EMS) coated on a copper grid. The excess of sample was removed by quick blotting with filter paper leaving a thin spanned film of the sample in the grid, and the grid was immediately vitrified by plunging it into liquid ethane cooled by liquid nitrogen (Cryoplunge, Orsay University, Laboratory Physique des solids). The sample was transferred into liquid nitrogen and inserted into the cold cryo-holder (Gatan). Subsequently, the cooled holder was quickly transferred into the vacuum column of TEM microscope (PHILIPS CM120) maintained at liquid nitrogen temperature. The accelerating voltage used for the observation was 120 kV. The visualization of the PNPs incorporating AuNCs by cryoTEM does not allow to fully visualize the PNPs since they were positively charged (by CTAB) and would not go to the wells in the grid.

The HR TEM apparatus used to characterize the AuNCs was a JEOL2100F TEM, operated by Pierre Alcouffe. The accelerating voltage used for the observation was 200 kV. The samples, without dilution, were deposited onto an ultrathin carbon film coated on copper grid (ref.CF400-CU-UL, EMS). The excess solution was carefully blotted off using filter paper and air-dried at room temperature.

2.2.2. Dynamic Light Scattering (DLS)

Dynamic light scattering (DLS) measures the autocorrelation function. These data are then analyzed by models which correlate the diffusion coefficient with the size of a sphere. Being the obtained value the hydrodynamic diameter, which is, in this case, ''the size of a hypothetical hard sphere that diffuses in the same fashion as that the particles being measured'' [46].

The miniemulsion PNPs (IST, Lisbon, Portugal) and PISA PNPs (CNR – IMP, Lyon, France) were analyzed using Zetasizer Nano ZS from Malvern Instruments (UK) from model ZEN3600 with the detector 173°. This apparatus measures a size range from 0.3 nm to 10 μm, using a 633 nm laser.

For miniemulsion samples, the dilution was performed gradually until the solution was almost transparent. It was then filtrated with a 0.2 μm cellulose acetate filter for aqueous solutions. The samples were analyzed with groups of 5 runs, which one with an optimized number of measurements by the apparatus. For PISA-RAFT samples, we started by diluting 10 μL of sample into 2 mL of milliQ water (mother solution). The final solution was prepared with 85 μL of mother solution in 3 mL of milliQ water. The sample was then filtrated with a 0.45 μm CME filter for aqueous solution. The measurements consist in 3 sets of 10 measurements with 10 runs of 10 s in each.

2.2.3.   UV-visible Absorption Spectroscopy

To analyze the absorption properties of the particles the apparatus used was an UV-660 UV-VIS Spectrophotometer from JASCO International (Tokyo, Japan) with a double monochromator and photomultiplier detector for high resolution, using a temperature control with Peltier effect. The solutions were analyzed in quartz cells without dilution or filtration, except for miniemulsion PNPs in which was used the same dilution technique as in DLS.

It was also used a microplate reader from BioTek using the software Gen5. It was deposit between 125 μL and 175 μL of sample without filtration or dilution.

2.2.4.   Fluorescence Spectroscopy

Emission and excitation fluorescence spectra of the particles were measured with a Horiba Jobin Yvon Fluorolog 3-22 spectrofluorimeter with a xenox lamp of 450 V. The software used was FluorEssence®.

The samples were prepared without any dilution or filtration. The settings used were generally slits 14.7 nm and shutter completely opened.

2.2.5. ^{1}H NMR Spectroscopy

The analysis using NMR was done at 298 K in an apparatus Spectro BRUKER AVANCE US+ 400MHz with a probe 5 mm BBFO+ Inverse detection multinuclear dual-broadband with Z-gradients.

The samples were prepared by diluting the samples withdrawals from the synthesis with 1 mL of chloroform-d (CDCl$_3$), being then transferred around 700 μL to the NMR tubes.

This technique was used to calculate a conversion of RAFT (Figure 7) and PISA-RAFT (Figure 8) synthesis, as well as confirm the purity of the PNAM. The conversion is calculated by 3 methods for the RAFT polymerization and the PISA experiments. For the RAFT samples the methods are the following:

- Method 1: evolution of vinylic protons from NAM, identified as b, b* and c in Figure 7 (δ between 7 and 5ppm) comparing with trioxane (δ =5.1 ppm) as marker.
- Method 2: relation between the peak b in Figure 7 (corresponding to NAM, δ=6.5 ppm) and b$_p$ (corresponding to PNAM, δ=1.2 ppm).
- Method 3: relation between the peak c in Figure 7 (corresponding to NAM, δ=6.3 ppm) and c$_p$ (corresponding to PNAM, δ=2.6 ppm).
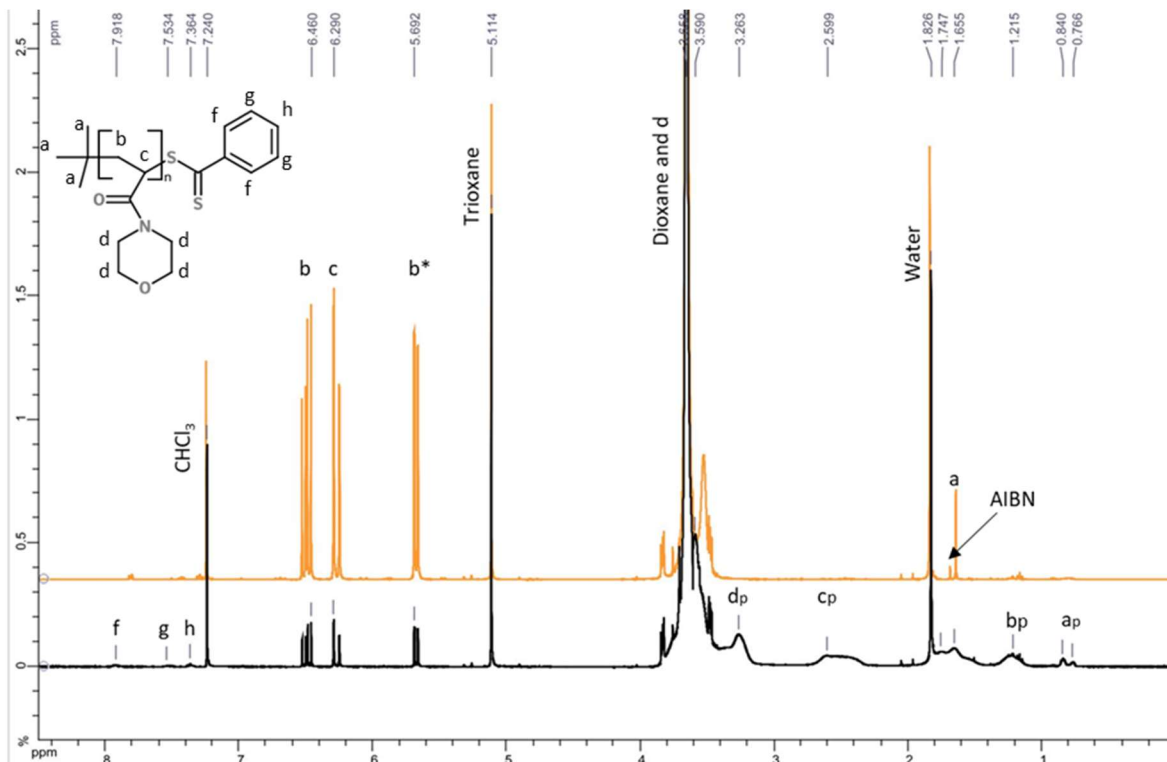
*Figure 7. NMR spectra of the initial (orange) and final (black) sample of the RAFT polymerization (**RAFT1**) and PNAM structure.*

To the PISA samples the methods are the following:

- Method 1: evolution of vinylic protons from nBA, identified as 1, 1* and 2 in Figure 8, (δ between 7 and 5 ppm, identified as) comparing with trioxane (δ =5.1 ppm) as marker.
- Method 2: relation between the peak 3 in Figure 8 (corresponding to NAM, δ=4.2 ppm) and 3p (corresponding to PNAM, δ=4.0 ppm).
- Method 3: relation between the peak 1 in Figure 8 (corresponding to NAM, δ=6.4 ppm) and 1p (corresponding to PNAM, δ=2.3 ppm).
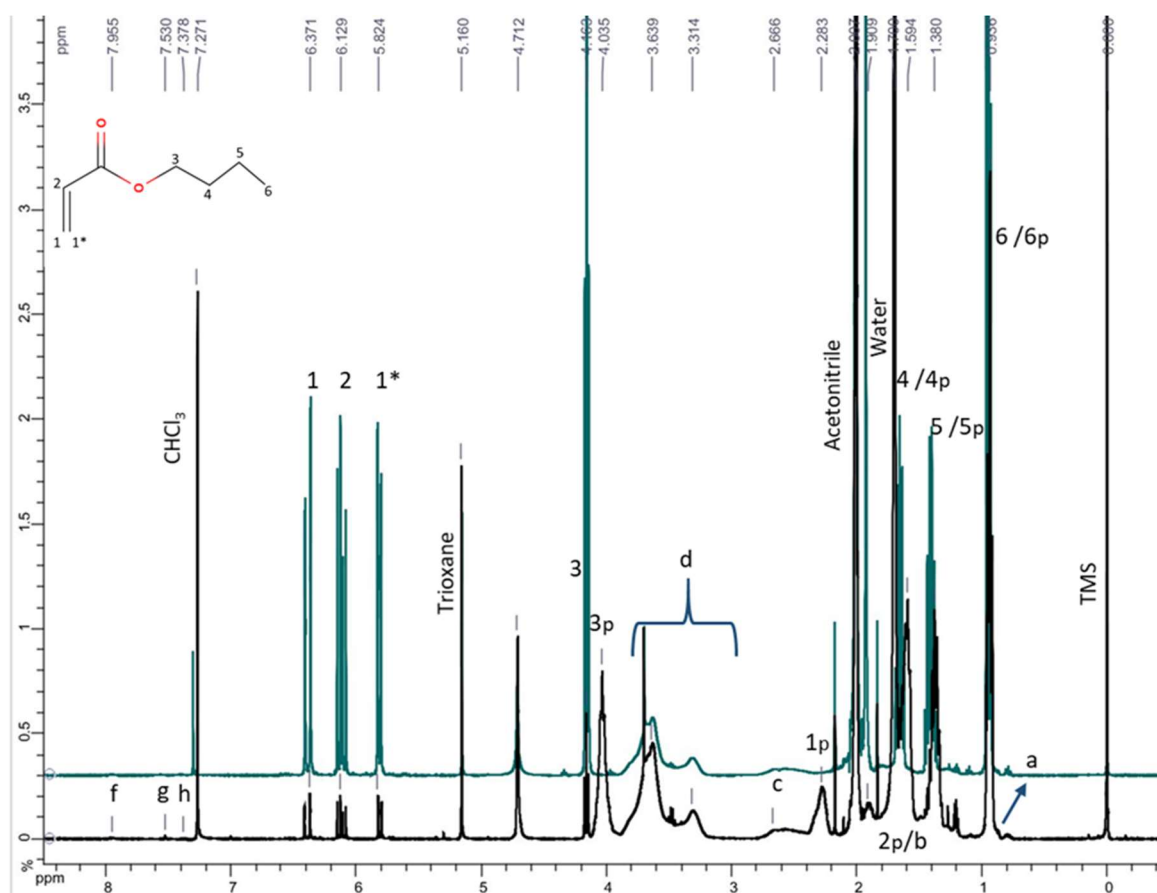
*Figure 8. NMR spectra of the initial (blue) and final (black) sample of the PISA-RAFT (**PISA2**) and nBA structure.*

All these methods have advantages and drawbacks. Methods 2 and 3, for RAFT and PISA-RAFT, use polymer peaks. These peaks are broader and with a less well-defined baseline, increasing the error. On the other hand, method 1, for PISA-RAFT and RAFT, uses trioxane which is extremely volatile. But this method, since the vinylic protons are in a δ where there are no other peaks, is the more reliable.

2.2.6. SEC-MALLS analysis

Gel permeation chromatography (GPC) or size exclusion chromatography (SEC) is a technique based on size separation. The column containing a gel allows the separation of compounds, like polymer chains, based on their size. Through different detectors like multi angle light scattering, refractometer or viscosity detector. Depending on the gel, different ranges of sizes are separated, and the effluent can be an organic solvent, such as chloroform, or water.

The apparatus, operated by Agnès Crepet, was constituted by, first, an auto-injector Perkin Elmer, series 200 Autosampler injecting a volume of 1mL. Secondly, there is a pump from Shimadzu model LC-20AD (1.0 mL/min). Then the column from Shimadzu model CTO-20A working at 30°C. And, at the end, the 2 sensors used were the multi angle light scattering MiniDawn treos with 3 angles and the refractometer from Shimadzu model RID-10A.

The sample consisted in the preparation of solution of 2.5 mg/mL, using 2 mL of chloroform (CHCl₃) as solvent. The samples are filtrated with a filter with porous of 0.45 µL for organic solvents. The eluent used was the same (CHCl₃) used as solvent to the samples.

2.2.7. GC analysis

Gas chromatography (GC) works for volatile compounds, which are vaporized before entering the separation column. The separation occurs based on the vapor pressure of the components. The samples are transported by the mobile phase, going through a liquid stationary phase.

The apparatus is Agilent model 6890 Series, operated by Valentin Cinquin. The program starts at 40°C. Then with a ramp of 20°C/min, it goes to 300°C, staying at this temperature for 5 min. The injector temperature is 240°C. The flow is 1 mL/min using ethanol, using a flame ionization detector (FID).

With a FID, the effluent from the column is mixed with hydrogen and air and then ignited. The current resulting from the pyrolysis of the compounds is then converted into a weight percentage. This detector is a robust one, even though it destroys the samples.

The samples preparation was made with a dilution factor of 1000 in different solvents. The solvents used were ethanol, toluene and methanol.

2.3. Methods

2.3.1. Gold Nanoclusters Synthesis

Gold Nanoclusters with 6-mercaptohexanoic acid (MHA) were synthesized according to a reference [47], with minor modifications. The procedure is the dissolution of $HAuCl_4 \cdot 3H_2O$ (1eq.) to deionized water, to obtain a concentration of 6.50 mM. Then, the solution is placed in a bath at 27ºC with magnetic stirring. MHA is added then to the solution followed by deionized water to obtain a concentration of 0.93mM in $HAuCl_4 \cdot 3H_2O$, the color change from yellow to orange and then colorless. To control pH, a solution of NaOH with 1.09 M (44.6 eq) is added to the solution, which turns completely transparent. Lastly, a solution of $NaBH_4$ in water and NaOH (0.22 M) is added dropwise to the solution. Depending in the amount of $NaBH_4$ and MHA the solution acquires different colors, from brown to transparent. The reaction is left for 3h stirring at 27ºC.

The 2 AuNCs synthesis studied in detail have the following molar ratios:
- ✓ Au_{25}: MHA: Au=2.05 and $NaBH_4$: Au=2.19.
- ✓ Au_5/Au_{11}: MHA: Au=6.00 and $NaBH_4$: Au=0.50.

2.3.2. Gold Nanoclusters Phase Transfer

To transfer AuNCs from water to the monomer or toluene, the procedure from a reference [47] was adapted.

Firstly, for miniemulsion, a solution of CTAB in ethanol with the concentration of 0.1 M is prepared. In the case of PISA, the solvent was 80% (v) acetonitrile and 20%(v) water. The same volumes of AuNCs aqueous solution and CTAB solution are added together.

In the case of styrene, the ratio of monomer per Au added was 0.25, in volume. For the other monomers, it was 0.12, while in the case of toluene, it is a ratio of 1. The mixture is then stirred magnetically for 5 min. After that, the 2 phases will start to separate and the AuNCs will migrate to the organic phase.

2.3.3. Miniemulsion polymerization incorporating Gold Nanoclusters

Miniemulsion polymerization incorporating the gold nanoclusters, was done accordingly to the protocol from reference [36], after this one have been transferred to the monomer phase, altering mainly the stabilizer and initiator in order to be compatible with the CTAB around the AuNCs.

First, a solution of CTAB in deionized water is prepared to have a concentration of 0.014 g of CTAB/g water. The dispersion of AuNCs in monomer (1 eq.) is placed in a bath at 30ºC with magnetic stirring. To this mixture of AuNCs in monomer, it is added hexadecane (1.06 eq.), DVB (0.35 eq.), AIBN (0.25 eq.) and the solution of CTAB (1.00 eq.) previously prepared. The reactional mixture was stirred at 30ºC for 30 min. Then the emulsion is sonicated, with 3 cycles with the parameters: output 3, duty cycle: 50% and timer: 6 min.

The mixture is then added to a three-necked 500 mL round-bottom reactor, equipped with argon inlet, condenser and mechanical stirring. The mixture is degassed for 30 min while stirring with constant velocity. After that time, the bath is turned on at 65ºC and the reaction is kept at this temperature with a low flow of argon for 8h.

2.3.4. RAFT polymerization

The RAFT polymerization was done following the procedure of the reference [30]. First, the pump is warm up for 5 to 10 minutes, while the oil bath is turned on to warm until 80°C. Using a peroxides' detector (paper strip), the distilled dioxane is checked. A solution of tBDB in dioxane with a concentration of 100 mg/L is prepared. Then, 1.784 mL of tBDB solution was added to 10 mg of NAM in the 150 mL Schlenk tube. A solution of 10 mg/mL of AIBN in dioxane is prepared, and 1.393 mL of this are added to the mixture of tBDB and NAM. 540.2 mg of trioxane are added to the mixture as well as 23.329 mL of dioxane. Three cycles of degassing with freeze-pump-thaw are performed. After, with a stirring of 1000 rpm and a temperature of 80°C, the Schlenk tube is immersed in the bath.

The polymer is then purified by precipitation with 800 mL of diethyl ether, being then filtrated. The polymer is dried by vacuum for 20h. The purity (elimination of solvent, monomer and other reagents) is verified by ^{1}H NMR.

2.3.5. PISA polymerization

The PISA polymerization followed to procedure on reference [30]. A solution of 0.184 g of PNAM synthesized by RAFT [30] (**RAFT1**, Mn= 10 300 g/mol) and 0.902 mL of MilliQ water is prepared. To this 0.301 mL of a solution of ACPA (0.048 M) and NaHCO$_3$ (0.166 M) were added. This is transferred to a 20 mL Schlenk tube and 1.203 mL of acetonitrile and 0.403 mL of nBA are added.

One of the following degassing methods was then performed:
1. 3 cycles of freeze-pump-thaw.
2. 30 min of argon flushing.
3. 30 min under argon with ice condenser.

The tube is introduced in an oil bath at 80°C. The reaction, with stirring velocity between 1000 rpm and 1250 rpm, was kept in this conditions for about 20h. During the reaction samples are withdrawn with a canula at different times to study the kinetics through NMR analysis. The samples start to be taken 10 min after the beginning, since the polymerization haven't started yet, but the reaction medium is already well stirred.

2.3.6. PISA polymerization incorporating Gold Nanoclusters

The PISA polymerization is conducted accordingly to reference [30]. A solution with 0.184 g of PNAM (**RAFT1**, M_n= 10 300 g/mol) and 0.902 mL of MilliQ water was prepared. To this one 0.301 mL of a solution of ACPA (0.048 M) and $NaHCO_3$ (0.166 M) were added. This was transferred to a 20 mL Schlenk tube.

Then the AuNCs were transferred to the monomer using the procedure described in section 3.3.2. By GC analysis it was determined that the organic phase was composed by 49.7% (v) of nBA and 50.3% of acetonitrile. To the Schlenk tube is added 811 µL of organic phase (nBA, acetonitrile and AuNCs) and 795 µL of acetonitrile. The degassing method applied was one of the previously presented in section 2.3.5.

The tube was introduced in a bath at 80°C, and procced in the same conditions as PISA-RAFT without AuNCs (section 2.3.5.).

3. Results and discussion

3.1. Gold Nanocluster's synthesis

To better understand the synthesis of AuNCs as well as the influence of different parameters, such as MHA:Au and NaBH$_4$:Au molar ratios, different synthesis were performed (Table 2).

Table 2. Different AuNCs synthesis. (NA means not applied to that synthesis).

Synthesis	Molar ratio		[NaOH] (M)	Color
	MHA: Au	NaBH$_4$: Au		
Au1	2.05	2.19	1.02	Brown
Au2	3.87	2.05	0.98	Brown
Au3	3.58	1.89	1.01	Brown
Au4	4.14	2.46	1.02	Colorless
Au5	3.99	2.31	1.02	brown
Au6	2.00	1.16	1.02	Brown
Au7	2.05	2.19	1.09	Brown
Au8	4.10	2.19	1.09	Colorless
Au9	4.10	1.09	1.09	Colorless
Au10	4.10	4.38	1.09	Red/brown
Au11	4.14	1.12	1.06	Brown
Au12	4.08	0.97	1.07	Colorless
Au13	4.07	1.07	1.02	Colorless
Au14	4.08	1.07	1.07	Brown
Au15	4.08	1.08	1.04	Brown
Au16	4.08	1.07	1.00	Brown
Au17	4.10	1.09	1.02	Brown
Au18	4.10	1.10	1.06	Colorless
Au19	4.10	1.10	1.06	Slightly brown
Au20	4.08	0.97	1.09	Brown
Au21	4.00	1.00	1.09	Brown
Au22	4.00	0.75	1.09	Brown
Au23	6.00	0.25	1.09	Colorless
Au24	6.00	0.50	1.09	Colorless
Au25	6.00	0.75	1.09	Slightly brown
Au26	6.00	1.00	1.09	Colorless
Au27	6.00	0.25	1.09	Colorless
Au28	4.10	0.25	1.09	Brown
Au29	2.05	2.19	1.09	Brown
Au30	2.05	2.19	1.09	Brown
Au31	2.05	2.19	1.09	Brown
Au32	2.05	2.19	1.09	Brown
Au33	2.05	2.19	1.09	Brown
Au34	2.05	2.19	1.09	Brown
Au35	2.19	4.00	1.09	Brown
Au36	2.19	6.00	1.09	Colorless
Au37	6.00	0.50	1.09	Colorless
Au38	6.00	3.00	1.09	Colorless
Au39	2.05	2.19	1.09	Brown
Au40	2.05	2.19	1.09	Brown
Au41	2.05	2.19	1.09	Brown
Au42	2.05	2.19	1.09	Brown
Au43	6.00	0.50	1.09	Colorless

3.1.1. Mechanism of AuNCs synthesis

One of the more stable AuNCs are the ones with 25 atoms. The evolution of the AuNCs synthesis is studied through these ones ($Au_{25}(MHA)_{18}$).

The synthesis of AuNCs can be summarized in 2 major steps (Figure 9). The first one is the reduction of the gold salt from gold (III) to gold (I) by the ligand, which in this case is MHA. And the second one is the reduction of gold (I) to gold (0) by $NaBH_4$.
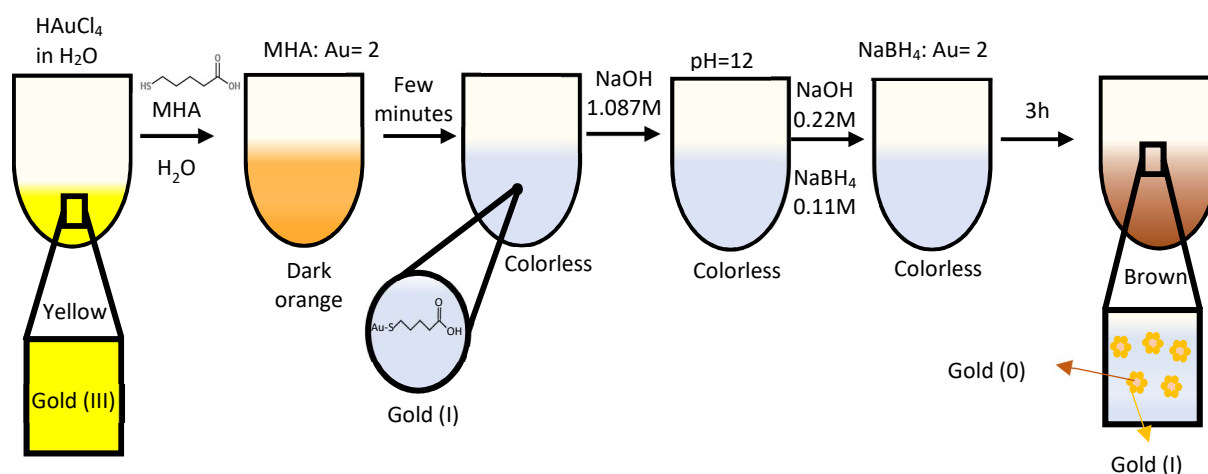
Figure 9. Scheme of different steps from AuNCs of $Au_{25}(MHA)_{18}$.

As shown in Figure 9, during the synthesis, the solution of gold salt is yellow, changing quickly to dark orange right after the addition of MHA (ligand), regardless of the amount of MHA added. It then slowly starts to turn colorless, a process which is accelerated by the addition of NaOH, which increases the etching capacity of the free MHA [26] and its solubility in water. The change from orange to colorless is due to the reduction from gold (III) to gold (I) by the ligand. In the end, the reducing agent is added together with NaOH to the mixture. By adding NaOH, $NaBH_4$, which usually behaves as a strong reducing agent, behaves now as a milder one. This pH control allows to obtain AuNCs instead of AuNPs (more than 2 nm) without having to use a milder reducing agent such as carbon monoxide (CO) or ascorbic acid [24], since the hydrolysis of $NaBH_4$ is delayed [26]. NaOH tunes the kinetics and thermodynamic step. After this step, depending on the ratio of $NaBH_4$: Au, the dispersion acquires a brown color or remains colorless, since this characteristic depends on the different AuNCs size. In the case of $Au_{25}(MHA)_{18}$, it is brown.

3.1.2. $Au_{25}(MHA)_{18}$ characterization

3.1.2.1. Visual Aspect

The dispersion presents a brown color (Figure 10). A change in the color is noticeable with time: from a light brown to a darker one over time.

Over time, there isn't sedimentation of particles or any compound, being the dispersion homogeneous in the space of, at least, three months. This shows the stability of $Au_{25}(MHA)_{18}$ in dispersion, since these do not have tendency to form bigger particles and precipitate.

*Figure 10. Visual aspect of Au$_{25}$(MHA)$_{18}$ (**Au31**).*

3.1.2.2.　　　**Optical properties**

Au$_{25}$(SR)$_{18}$, regardless the ligand, are one of the most stable AuNCs, as mentioned in the section 1.2, being this the starting point for further study of AuNCs properties, especially absorption and emission, using MHA as ligand.

Figure 11a shows the absorption spectra for Au$_{25}$(MHA)$_{18}$ (**Au1**) during a period of 91 days. The absorption bands, in the four spectra, have two bands, one at 440 nm and another one at 670 nm. This values are in agreement with the ones obtained by Yao, Q. et al [47] and Yuan, X. et al [26], who performed the synthesis in similar conditions. Yuan, X. and his co-workers did ESI mass spectra which confirms the size of the clusters that exhibit these absorption bands. In the absorption spectra, there are no bands around 520 nm, which shows the absence of AuNPs.

The color change previously mentioned can be detected in the absorption spectrum as an increase in scattering caused by the aging of the AuNCs. The aging of the AuNCs can result in the formation of non-emissive species, such as other AuNCs or return to gold salt. The oxidation may be due to the contact of the dispersion with oxygen (storage without degassing).

The emission spectra (Figure 11b) were obtained using different excitation wavelengths, between 440 and 680 nm. Outside this range no emission was detected, which goes accordingly with the absorption bands detected. The Au$_{25}$(MHA)$_{18}$ (**Au1**) show an emission maximum at 810 nm. The fact that there is only one band in the emission spectra confirms that there is only one population of AuNCs – they are monodispersed. The absence of a band at 520 nm in the absorption spectra over time, characteristic of gold surface resonance plasmon, shows that there isn't any AuNPs and that they are stable over large periods of time.
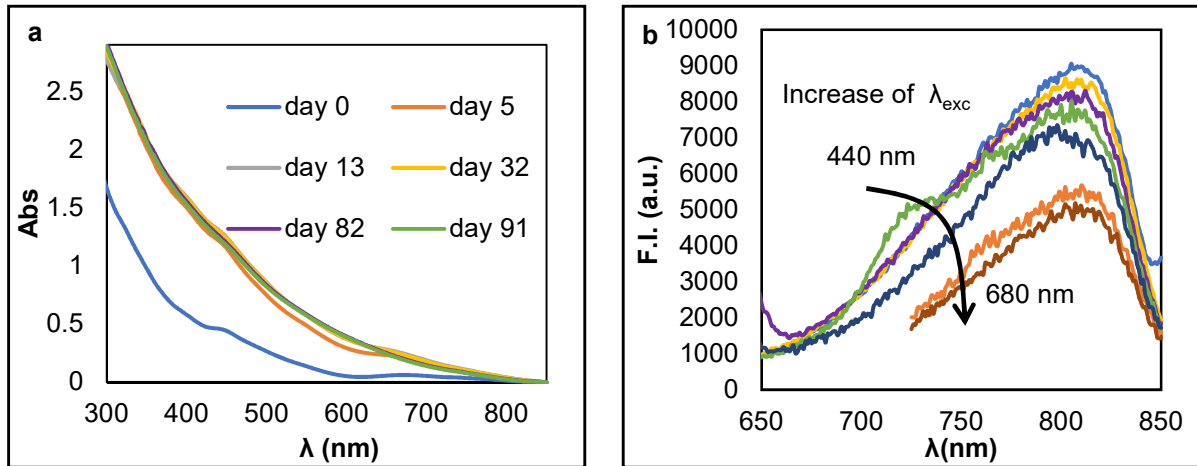
*Figure 11. a) Absorption spectrum of **Au1** with time evolution: day 0 (blue), day 5 (orange), day 13 (grey), day 32 (yellow), day 82 (purple) and day 91 (green); b) Emission spectra of **Au1** with different λ_{exc}: 440 nm (light blue), 480 nm (yellow), 520 nm (purple), 580 nm (green), 620 nm (dark blue), 670 nm (orange) and 680 nm (red).*

3.1.2.3. Theoretical Number of Atoms

To do an estimation of the band gap, as well as the number of atoms, Tauc's plot [48] and Jellium model [49] were used. The Tauc's plot corresponds to equation 7 [6], in which α is the absorption coefficient, h is Plank's constant, v is the radiation frequency ($v=c/\lambda$, being c the velocity of light and λ the wavelength), Eg is the band gap, n is a coefficient defined by the nature of the transition and A is a constant.

$$(\alpha h v) = A\big(h v - E_g\big)^n \tag{7}$$

The value of n can be 2 for indirect transitions or ½ for direct ones. This model and concepts are adapted from semiconductors theory. The band gap, for semiconductors, is ''the difference of energy between the lowest point of the conduction band and the highest point of the valence band" [50]. In the direct transition the lowest point of the conduction band occurs at the same wavevector as the highest point of the valence band, while in the indirect transition the band edges of the conduction and valence bands are widely separated in wavevector space [50]. In this case, the option that better correlates with the experimental data is the indirect transition (Figure12). From the interception of the linear correlation with the x axis, the value for the band gap (E_g) is 1.78 eV, by using the correlation from Figure 12.
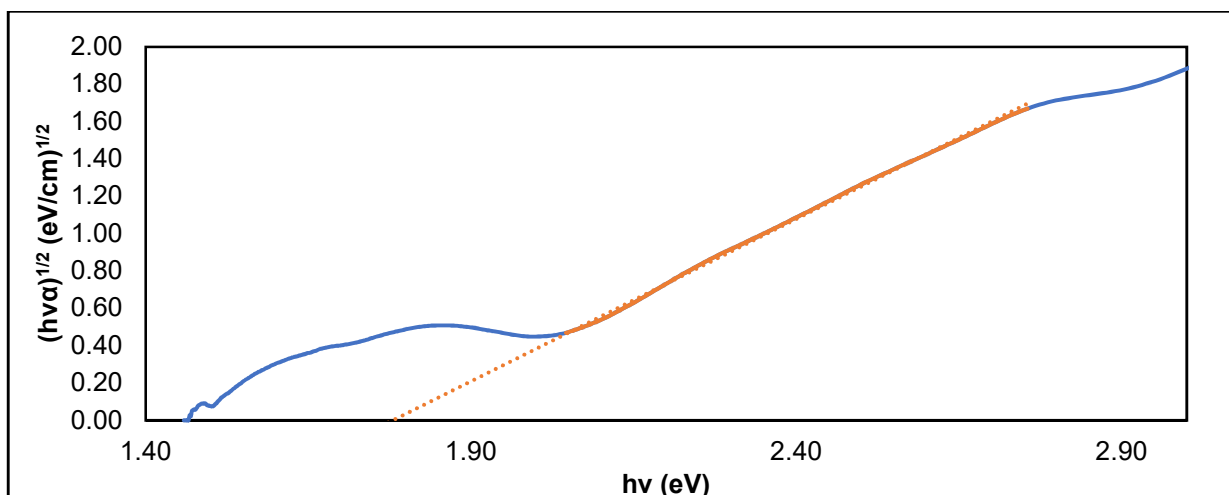
*Figure 12. Tauc's plot of Au$_{25}$(MHA)$_{18}$ – **Au1**- for absorption at day 0, with a correlation factor (R^2) of 0.999 and the expression $(\alpha h\nu)^{1/2} = 1.7393 h\nu - 3.0953$*

The value obtained for the band gap was applied to Jellium's equation (equation 8), in which E_F is the Fermi's energy and N the number of atoms. There is an anharmonicity factor (δ) for AuNCs with more than 10 atoms, which is between -0.4 eV and 0 eV [6, 51].

$$E_g = \frac{E_F}{N^{\frac{1}{3}} - \delta}$$

(8)

Being Fermi's energy for gold, 5.52 eV, the number of atoms obtained, using equation 8, is between 20 and 30, for δ between -0.4 eV and 0 eV, respectively. These values are according with the expected one, since these clusters should have 25 gold atoms, accordingly to the ESI mass spectra done by Yuan, X et al [26].

3.1.2.4.   Size by HR TEM

HR TEM was used to analyze the size of AuNCs, as well as their dispersion in the aqueous medium. The AuNCs were dispersed in the grid (Figure 13a). It shows stability in water, not aggregating easily.

The average size measured was (1.8±0.6) nm (Figure 13b). This size is higher than the presented by X. Yan and co-workers [52]. They obtained sizes below 1.5 nm, which is within the error associated to the measurements. The higher value may be due to the not well-defined limits of the AuNCs. Due to their small size, the contrast is not as high as for bigger gold particles. This means, the analysis and images result from a compromise between contrast and resolution. The AuNCs still show a size below 2 nm, which is according to the theoretical previsions. The HR TEM allows the visualization of the crystalline structure. The lattice has an average size of (0.16±0.04) nm. This value is similar to the one obtained by W. Zhang and co-workers [16].
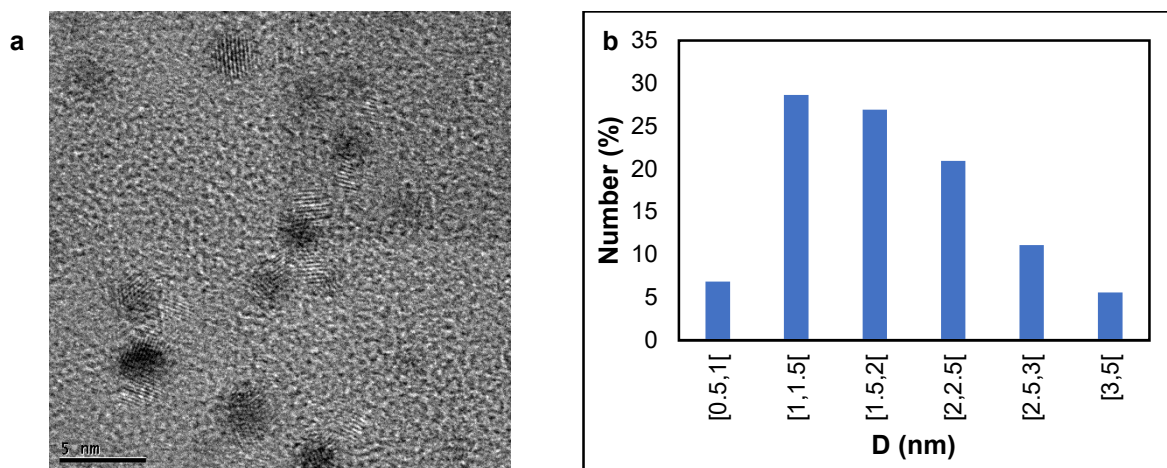
*Figure 13. a) HR TEM image of Au$_{25}$(MHA)$_{18}$ (**Au31**). b) Size distribution of Au$_{25}$(MHA)$_{18}$ (**Au31**) by HR TEM.*

3.1.3. Influence of NaBH4 (reducing agent) and MHA (ligand) concentration during synthesis in AuNCs size and optical properties

The mechanism behind the synthesis of AuNCs is not yet fully known, but strong evidences point for an equilibrium between etching by the excess of ligands and the reduction by the reducing agent, until it reaches an equilibrium [26]. To better comprehend these steps and their influence in the clusters formation, different combinations of MHA:Au and NaBH$_4$:Au ratios were studied. By changing the ratios between these 2 components and the gold salt, the size and stability of the AuNCs is affected. The amount of NaOH was kept constant throughout all the experiments since its effect was already study by Yuan, X. et al [26].

3.1.3.1. Influence of MHA:Au molar ratio

Starting by the molar ratio of MHA:Au, a change in the dispersions aspect is evident (Figure 14a). Between 4 and 6 of MHA:Au molar ratio, there is a loss of color going from brown to transparent, suggesting a change in size. The absorption spectra confirm this observation, since with the increase of MHA:Au the bands from Au$_{25}$(MHA)$_{18}$ disappear.

A decrease in the absorbance was observed with the increase of MHA: Au molar ratio (Figure 14b) accompanied by the disappearance of the bands at 450 nm and 670 nm. It indicated that by increasing the MHA:Au ratio, the final products change from Au$_{25}$(MHA)$_{18}$ to a mixture of sizes.

By increasing the amount of MHA, bands at higher wavelengths disappear in the emission spectrum, while the ones at other wavelengths show up as more intense (Figure 14c to f). As explained before (section 1.1.1), when the emission band is at a higher wavelength, the AuNCs are bigger. AuNCs result from an equilibrium reaction between the reduction from NaBH$_4$ and etching from MHA. By increasing the amount of MHA, the equilibrium is dislocated in the etching direction, which results in smaller particles. When the molar ratio between MHA:Au is about 2, the emission maximum is at 810 nm. When the ratio goes to 4, two new bands appear at 380 nm and 500 nm. These are two new smaller populations, which are present in the synthesis for MHA:Au=4 and 6. For the ratio MHA:Au=6, the population of larger size is not present anymore since the band at 810 nm is no longer present (Figure 14f). This results are according to the monolayer-thiol-

protected AuNPs model, which says that by increasing the Au: ligand ratio, more atoms of gold can be distributed on the Au-S interface, leading to smaller AuNCs [25].

*Figure 14.Dispersions visual aspect (a) and corresponding absorption spectra (b). Emission spectra with λ_{exc}=300 nm (c), λ_{exc}=350 nm, (d), λ_{exc}=450 nm (e) and λ_{exc}=650 nm (f). The molar ratio NaBH$_4$: Au was kept constant at 2.2 for all synthesis, varying MHA: Au molar ratio between 2 (blue, **Au31**), 4 (green, **Au35**) and 6 (orange, **Au36**).*

3.1.3.2. Influence of NaBH$_4$: Au molar ratio

By changing the amount of reducing agent, in the presence of a high amount of ligand, there is almost no change in the visual aspect, except for the ratio 0.75 (Figure 15a). This is slightly brown, which indicates the presence of AuNCs with about 25 atoms.

In terms of absorption (Figure 15b), no bands are visible, which indicates the presence of AuNCs with different sizes (no predominant population).

These observations are confirmed by the emission spectra of the different dispersions (Figure 15c and d). In all of them there are 2 populations, one with the maximum of emission at 380 nm and another at 500 nm. The major difference in these dispersions is the intensity of the bands, which is higher for NaBH$_4$:Au=0.5. In the dispersion with a ratio NaBH$_4$:Au of 0.75, there is another band at 810 nm too, confirming the presence of AuNCs with 25 atoms.

The presence of a different band at NaBH$_4$:Au=0.75 can be because in these ratios the populations are not stable but only metastable, evolving rapidly to a more stable population: Au$_{25}$(MHA)$_{18}$.

Since there is no change in the first two populations it is possible to conclude that at the molar ratio MHA: Au of 6, the size does not change with variation of NaBH$_4$: Au. This may be due to the large excess of MHA which shifts the reaction towards etching.

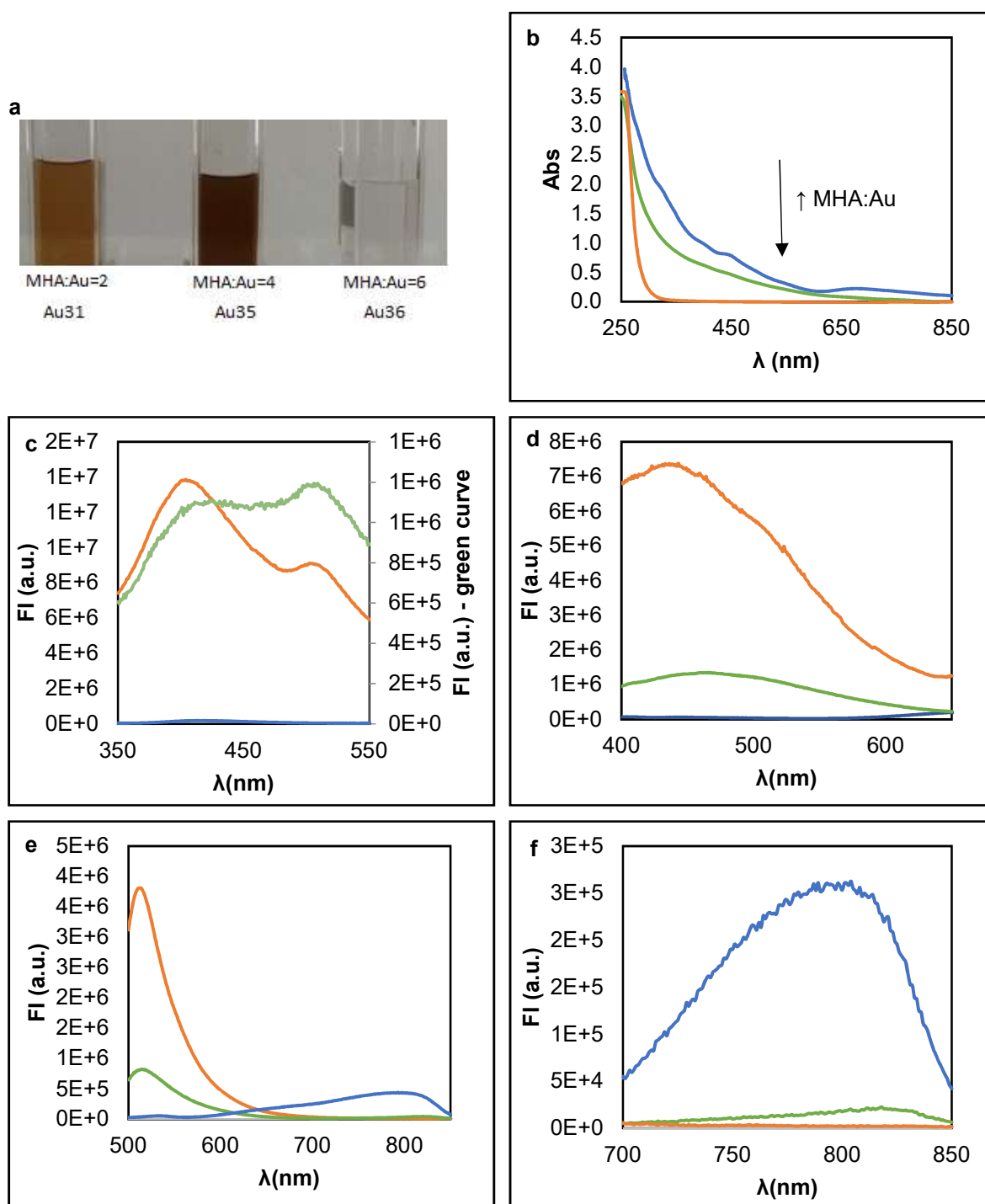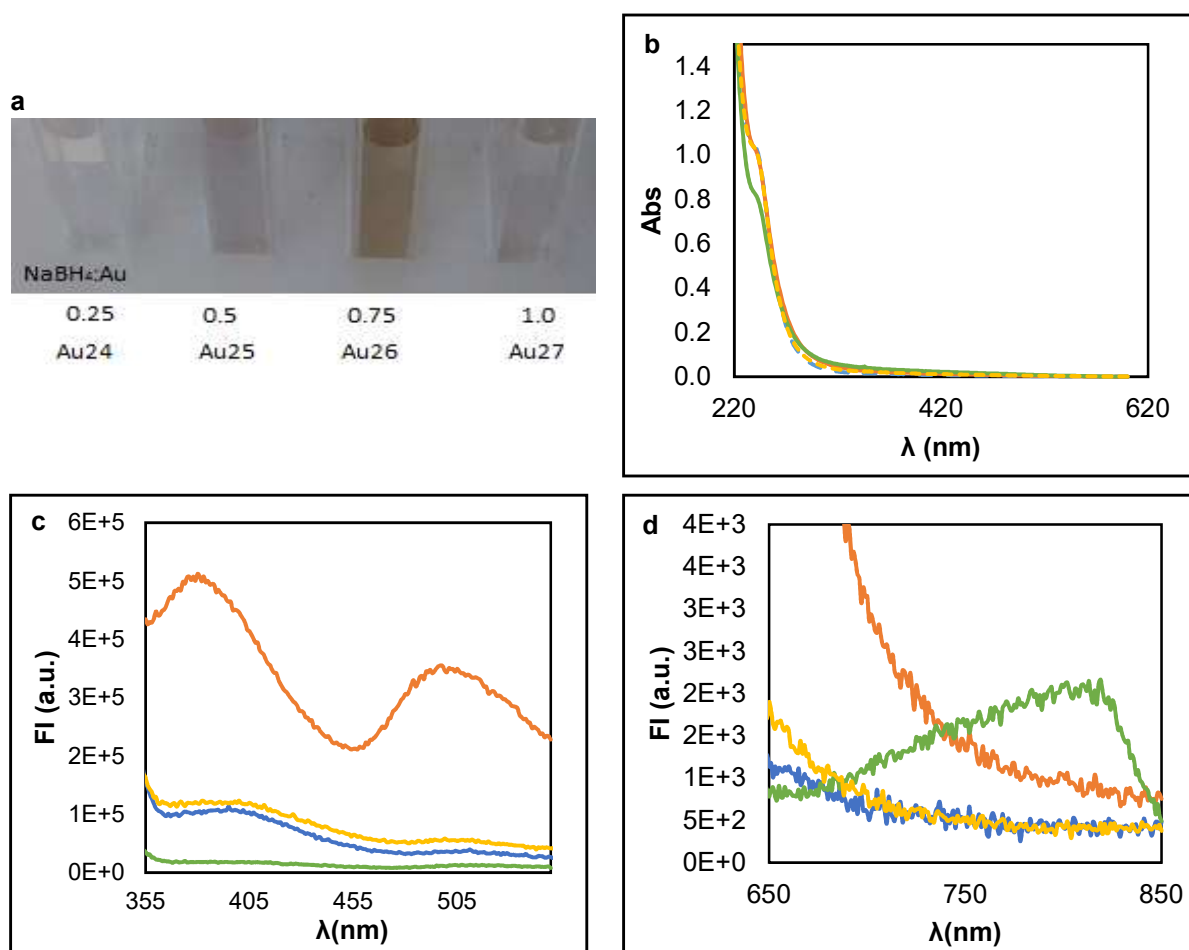*Figure 15. Dispersions visual aspect (a) and absorption spectra (b). Emission spectra with λ_{exc}=300 nm (c) and λ_{exc}=450 nm (d). The molar ratio MHA: Au was kept constant at 6 for all synthesis, varying NaBH$_4$: Au molar ratio between 0.25 (blue, **Au24**), 0.50 (orange, **Au25**), 0.75 (green, **Au26**) and 1.00 (yellow, **Au27**).*

3.1.4. Au$_5$/Au$_{11}$ characterization

3.1.4.1. Optical properties

From the previous experiments, where the molar ratio MHA:Au is 6 and NaBH$_4$:Au is 0.5 (synthesis **Au24** in Table 2), two populations are identified between 1 to 3 days after the synthesis. One population with an emission maximum of 380 nm and another population with emission at 500 nm (Figure 16b).

The excitation spectra of **Au24** show two maxima as well (Figure 16a), the first one corresponding to the Au$_5$ population and the second one to the A$_{11}$ population, the maximum of 310 nm and 435 nm respectively, according to the results from Jellium model.
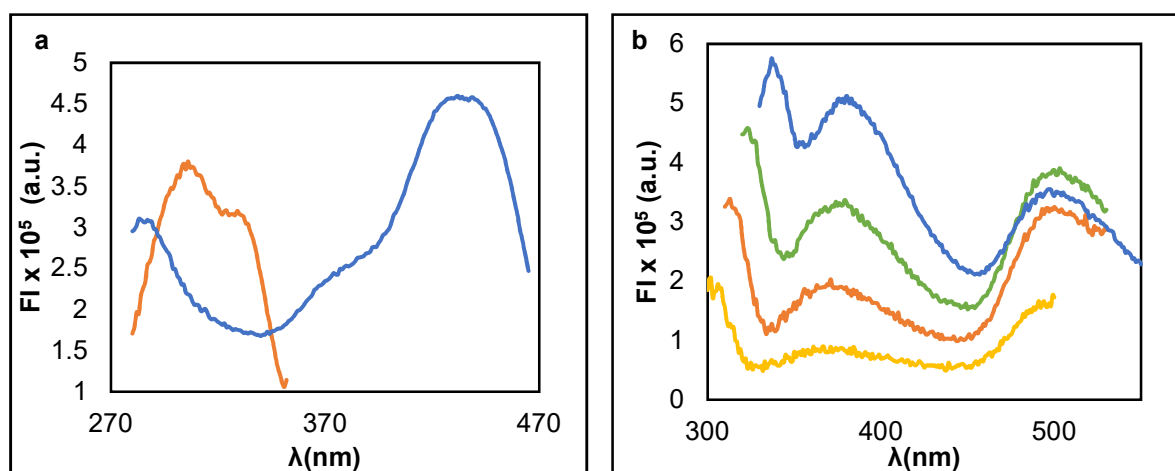
*Figure 16. For molar ratios of MHA: Au=6.0 and NaBH$_4$: Au=0.5 (**Au24**): a) Excitation spectra with λ_{em} 380 nm (orange) and 495 nm (blue). b) Emission spectra with λ_{exc} 270 nm (yellow), 280 nm (orange), 290 nm (green) and 300 nm (blue).*

3.1.4.2. Theoretical number of atoms – Jellium model

Applying Tauc's plot and Jellium model to this synthesis, an approximation of size can be calculated. According to Zheng's team [51], for small AuNCs it is possible to use the energy from the emission maximum without a big error associated to it, applying the Jellium equation (equation 8).

For the first band, at 380 nm, the population should have about 5 Au atoms, while the one at 500 nm should have 11 Au atoms.

3.1.4.3. Size by HR TEM

Due to their size, it was not possible to visualize Au$_5$/Au$_{11}$ (**Au43**) by HR TEM. Only after concentrating the AuNCs in another solvent (nBA and acetonitrile), which lead to their aggregation originating bigger AuNCs, with the average size of (1.3 ± 0.5) nm. The majority of the AuNCs has a diameter between 0.5 and 0.75 nm, being probably this the original diameter of the **Au43** in water.

3.1.5. Time evolution of optical properties: Au$_{25}$ vs Au$_5$ and Au$_{11}$

The AuNCs with 5 and 11 atoms are stable for 1 week, but after about 4 months they present new properties and aspect. From colorless, the samples turned brown, especially for higher amounts of reducing

agent (Figure 17 a and b). As mentioned before, the darker brownish color can be an indicator of the presence of $Au_{25}(MHA)_{18}$.

From the emission for $NaBH_4$:Au=0.25, the two previous population at 380 nm and 500 nm are not present, and in their place, there is a population at 440 nm (Figure 17c and d). For the other ratios of $NaBH_4$:Au, the population at 380 nm seems to have a decrease in its intensity, while the one at 500 nm increased. But overall, both maxima present a decrease in intensity, while a new band showed up at 810 nm (Figure 17e and f), another confirmation that AuNCs will tend to evolve with time to originate these Au_{25}. Some evidences point to the transformation of AuNCs with different sizes into Au_{25}, by addition of motifs of Au-thiol, or reaction between AuNCs with different sizes, by conserving the number of valence electron [24], which is according to the experimental results.
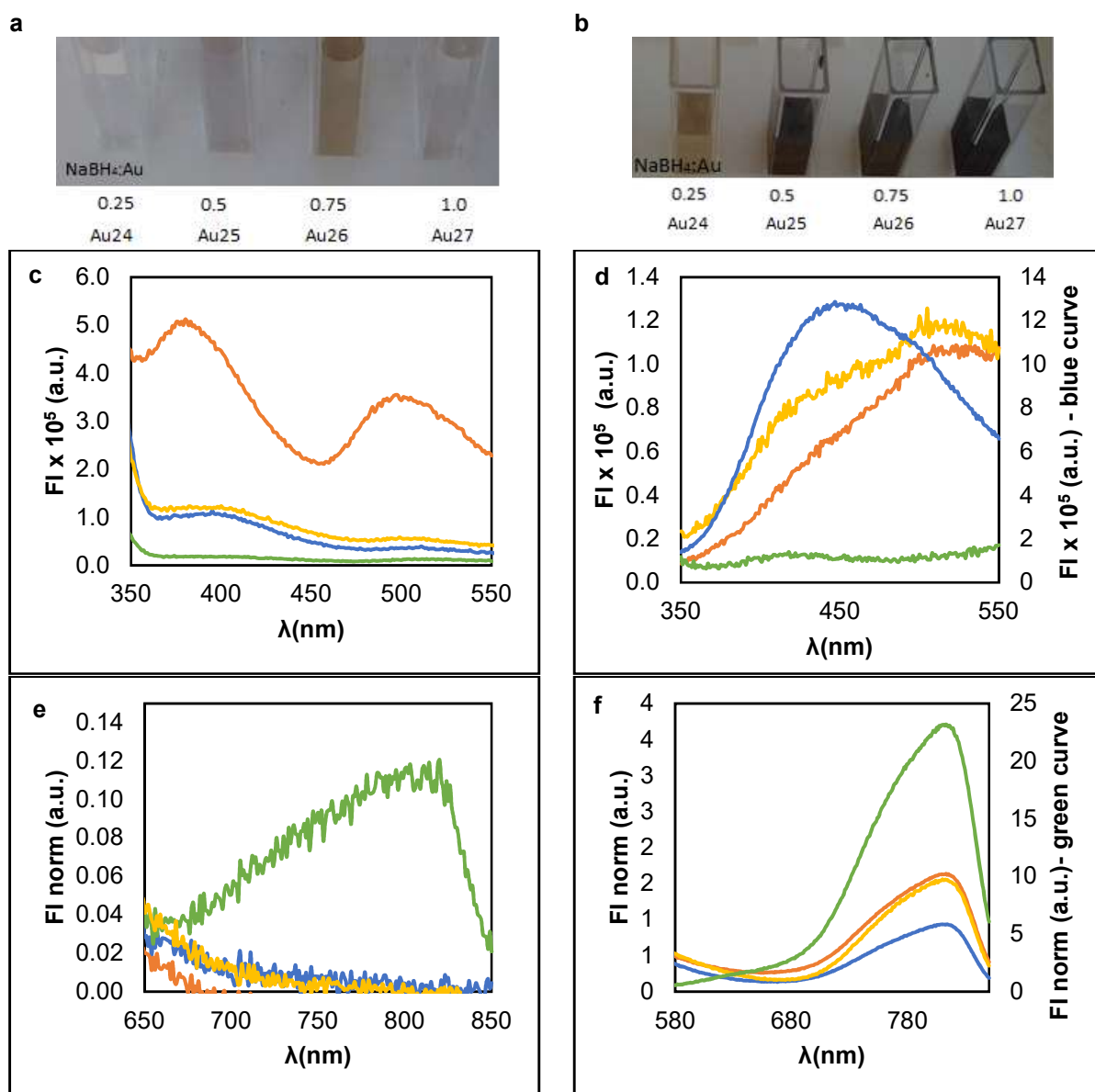
Figure 17. Visual aspect of dispersions with MHA: Au=6 and different $NaBH_4$: Au ratios 1 day after synthesis (a) and after 139 days after synthesis (b). Emission spectra after 1 day with λ_{exc}=300 nm (c) and 139 days with λ_{exc}=300 nm (d). Emission spectra after 1 day with λ_{exc}=450 nm (e) and after 139 days (f). The molar ratio MHA: Au kept constant at 6, varying $NaBH_4$: Au ratio between 0.25 (blue, **Au24**), 0.50 (orange, **Au25**), 0.75 (green, **Au26**) and 1.00 (yellow, **Au27**).

3.1.6. pH influence in AuNCs properties and behavior

The influence of pH during the synthesis, for this specific ligand -MHA, has been previously studied and optimized by X. Yuan et al [26], being the optimum pH about 12. However, when the ligands used are water soluble pH is a way to control the aggregation state, and so the size of the AuNCs. The most studied ligand is glutathione since it has 2 carboxyl, 1 amine and 1 thiol groups, with different pKas [24]. By changing the pH, glutathione changes its conformation originating different AuNCs with different charges. To explore this possibility with the MHA ligand, the pH was adjusted from pH= 12.2 to pH=2.3 after the AuNCs synthesis (**Au2**), using a solution of 1M HCl.

In Figure 18a, we can observe that the dispersion aspect slowly changes with pH decrease. From brown, it starts at pH=12.2 to have a darker color, until it turns black for pH 2.27 (precipitation). Since the pKa of MHA is 4.8 [53], the change of polarity and the deposition observed on the bottom was expected because the carboxyl group of MHA is completely protonated.

The emission maximum after the synthesis (pH=12.21) was at 511 nm, without any other band. After 14 days, there was a change in the AuNCs size, and it appeared two peaks at 403 nm and 777 nm. This change in size was not reversible, since the sample was subjected to ultrasounds, leading to an increase of the first maximum intensity and decrease of the second maximum intensity until a stabilization point. These were the initial conditions to start the study of the pH influence. Except for the sample at pH=2.27, the emission of all samples was analyzed (Figure 18b and c).

By decreasing the pH, both populations at 403 nm and 777 nm decreased in intensity, with a noticeable change of the first maximum from 403 nm to 430 nm. At pH=10.01, a new band appeared with an emission maximum at 637 nm (λ_{exc}=525 nm/550 nm). This observation indicates the increase in size of the AuNCs that results from a decrease in pH, since MHA is no longer soluble at this pH.

The change in size identified by the emission change, and the visual aggregation noticed for pH bellow 2.5, show a change in the AuNCs size with pH. Bigger AuNCs are obtained for lower p
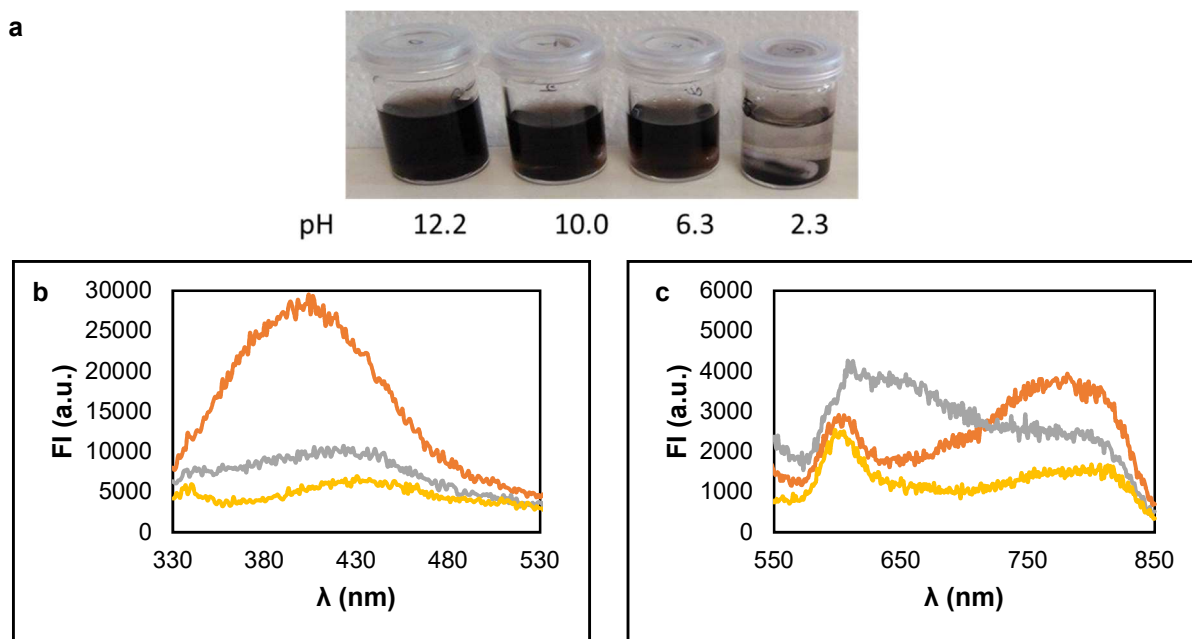
*Figure 18. AuNCs (**Au2**) aspect after adjusting pH after synthesis (a). Emission spectra after changing pH for pH = 12.21 (orange), pH=10.01 (grey) and pH=6.34 (yellow) for λ_{exc}=300 nm (b) λ_{exc}=500 nm (c).*

3.2. Miniemulsion polymerization

Miniemulsion polymerization is a technique widely studied for the incorporation of inorganic compounds into latex particles, being a good option to increase the stability of AuNCs. The polymerizations performed with this technique are presented in Table 3.

Table 3. Summary of miniemulsion main parameters and results.

Synthesis	Monomer	AuNCs synthesis	[AuNCs] in organic phase (mM)	Conversion (%)	D_h (nm)
ME1	Styrene (Sty)	**Au1**	0.560	70	63±4
ME2	Butyl methacrylate (BMA)	**Au2**	1.354	24	28±8

3.2.1. Miniemulsion incorporating AuNCs: styrene as monomer

The different steps of miniemulsion polymerization are explained in sections 1.2.1. The protocol was adapted from incorporating C_{70} [36], trying to keep the same concentration. The present miniemulsion is cationic instead of anionic [54] with styrene (Figure 19).
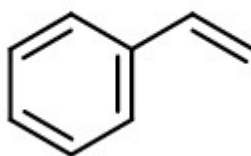
Figure 19. Styrene structure.

The concentration of AuNCs in the aqueous phase was calculated with the following assumptions: (i) all the gold salt is converted into AuNCs during the AuNCs synthesis; (ii) each mol of AuNCs corresponds to 25 mol of gold salt since each AuNCs has 25 atoms of gold. The concentration of AuNCs in the aqueous phase, following that assumptions, is 0.035 mM. To calculate the concentration in styrene, it was assumed that all the AuNCs migrate to the styrene. So, the concentration of AuNCs in styrene was 0.560 mM. The exact concentration of AuNCs in both media is smaller than the one estimated due to the approximation presented above, and the presence of some co-solvent (ethanol).

3.2.1.1. Aspect evolution of miniemulsion

After 30 min of magnetic stirring the emulsion was brownish (Figure 20a). But after the sonication, it got a milky color which indicate scattering from the miniemulsion.

During the polymerization, some AuNCs precipitated on the reactor walls. During this process, the dispersion become purple (Figure 20b). In the absence of AuNCs, polystyrene is white due to scattering. So, the change in color indicates the incorporation of gold.
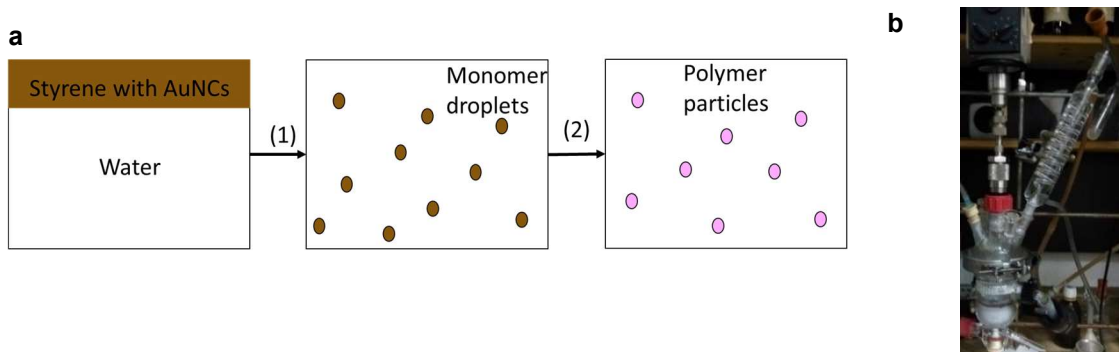
Figure 20. a) Miniemulsion polymerization with AuNCs in styrene phase: (1) sonication, (2) polymerization [28]. b) Three-necked round-bottom reactor with mixture after 8h of polymerization.

3.2.1.2. Optical properties

After freeze drying part of the sample **ME1** (polystyrene with AuNCs incorporated by miniemulsion polymerization), the powder was pressed to form pellets (Figure 21a). Commercial PS was also pressed to obtain a pellet. The emission of **ME1** in dispersion and in pellet was compared to the emission of commercial PS pellet. An emission band at 310 nm was observed in dispersion and in the pellet for **ME1** (Figure 21b). The band is the same present in the PS pellets, and it corresponds to the polystyrene excimer. This phenomenon occurs due to π-stacking resulting from the formation of dimers and multimers from the phenyl groups of PS [55]. To be able to detect the AuNCs, filters were used to cut the emission until different wavelengths such as 400 nm, 450 nm and 700 nm. This way, the band at 815 nm was detected in **ME1** like in the AuNCs in aqueous dispersion (Figure 21c). It confirms the presence of AuNCs in the polymer.
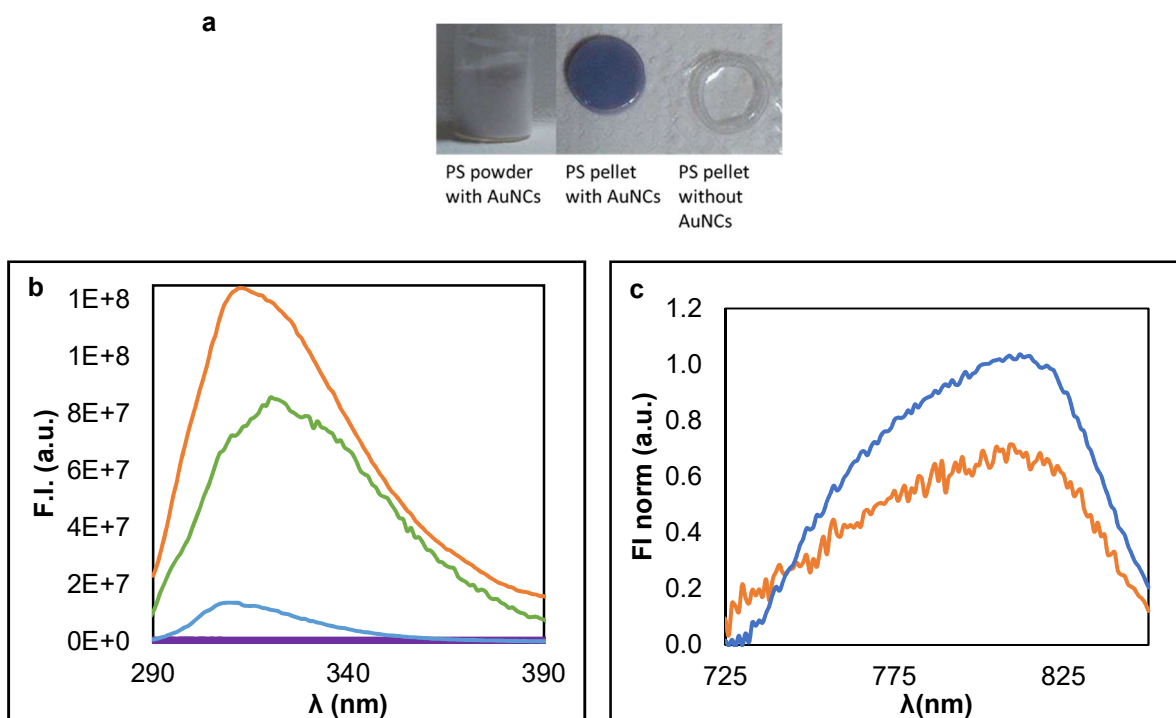
*Figure 21. a) PS incorporating AuNCs in powder after freeze drying (**ME1**), pellet PS incorporating AuNCs (**ME1**) and pellet of PS. b) Emission spectra with λ_{exc}=250 nm for AuNCs in aqueous dispersion (purple – **Au1**), PS with AuNCs in solution (blue – ME1), PS pellets with AuNCs (orange – ME1) and PS pellets (green). c) Emission spectra using λ_{exc}=380 nm (light blue), and λ_{exc}=650 nm (orange). Maximum at λ_{em}=812 nm.*

3.2.1.3. Polystyrene (PS) Nanoparticles with AuNCs

The polymer nanoparticles (PNP) size was determined by two techniques: dynamic light scattering (DLS) and transmission electron microscopy (TEM).

By TEM, it was possible to distinguish the morphology of the particles as round (Figure 22). But, due to the resolution it is not possible to confirm the presence of AuNCs inside PNPs. In terms of diameter, both methods give a similar result: about 60 nm (Table 4).
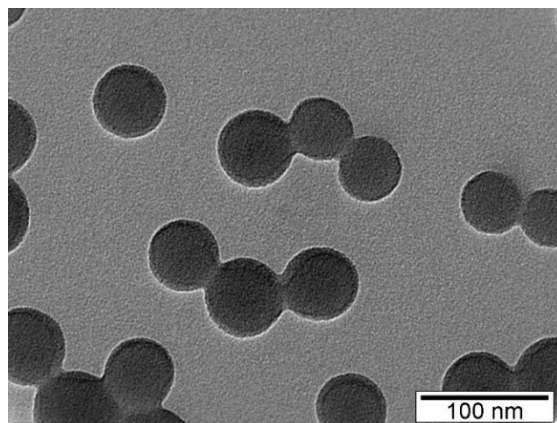
*Figure 22. TEM images of **ME1**.*

The solid content was 18% (Table 4), which means a conversion of 70%. It is very similar to the one obtained for the PNPs with C_{70} [36].

*Table 4. Diameter of **ME1** measured by DLS and TEM, and solid content of miniemulsion polymerization obtained.*

D_h (nm)	63±4
D_{TEM} (nm)	61±11
Solid Content (%)	18

The miniemulsion polymerization protocol was based on a protocol for an anionic surfactant [36]. To avoid screening CTAB (cationic surfactant) in the AuNCs, the **ME1** was converted to cationic miniemulsion. First, the concentration of AuNCs in styrene was kept similar to C_{70}. Aside from surfactant, a big difference is in the initiator: while KPS is water soluble, AIBN is oil soluble. So, the mechanism of radicals' formation and reaction with the monomer differ from one to the other, as explained in section 1.2.1.

In an article by Landfester [54], a comparison between anionic and cationic miniemulsion is made. The same surfactants and initiators that are used in the present work and the case of C_{70} are studied. Similar particles are obtained in both cases, slightly bigger in the case of anionic miniemulsion.

In the synthesis **ME1**, half of the amount of reagents were used, when compared with the anionic miniemulsion incorporating C_{70} [36]. But in terms of molar concentration the same values were used in all the reagents. So even though the initiator and surfactant are different, a similar size and solid content were obtained in both cases (Annexes IV).

3.2.2. Miniemulsion incorporating AuNCs: butyl methacrylate as monomer

Butyl methacrylate (Figure 23) is a monomer more soluble in water than styrene. But more importantly, this monomer does not have any kind of absorption or emission, and when polymerized does not present an excimer.
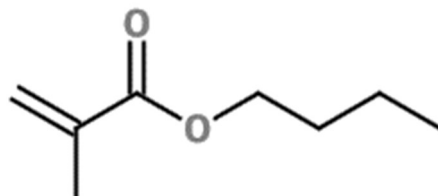
Figure 23. Structure of butyl methacrylate (BMA).

During the miniemulsion polymerization (**ME2**), the polymer solution became with a stronger purple color (Figure 24) than in the styrene polymerization (**ME1**). The purple color seems to indicate the presence of AuNPs, showing a higher amount in **ME2** than in **ME1**.

*Figure 24. Visual Aspect of reactional mixture during miniemulsion polymerization **ME2**.*

3.2.2.1. Optical properties

The AuNCs used in this polymerization correspond to **Au2**, which as mentioned before (Table 3), has emission maxima at 380 nm and 511 nm. By the absorption spectrum (Figure 25a), the presence of AuNPs was confirmed due to the presence of plasmonic band at 520 nm.

In terms of emission (Figure 25b), the bands previously identified in the AuNCs in dispersion are no longer detectable. Instead, a population with emission at 400 nm appears. This means that probably the population at 380 nm evolved to the one at 400 nm, while the one at 511 nm evolved to AuNPs without emission. This can be due to the increase in concentration and high temperature for a long period of time (8h at 65°C). It is also noticeable that these AuNCs are less stable than $Au_{25}(MHA)_{18}$, which in the same conditions kept their emission in the same wavelength as in aqueous dispersion.
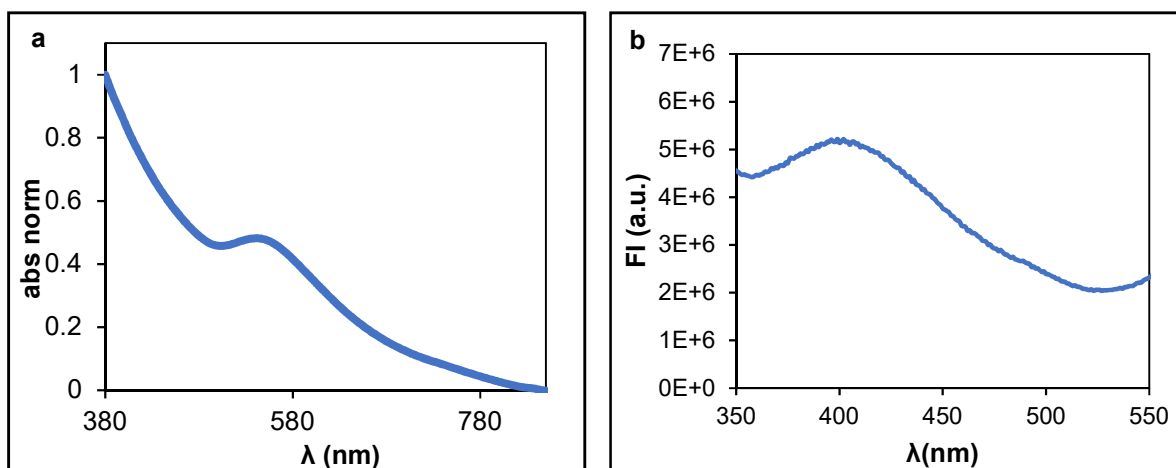
*Figure 25. a) Absorption spectrum of **ME2**. b) Emission spectrum of **ME2** using λ_{exc}=300 nm. It has emission maximum at λ_{em}=400 nm.*

3.2.2.2.   PBMA nanoparticles with AuNCs

The PNPs size of **ME2** was analyzed by the same methods as **ME1**: DLS and TEM. In the case of polystyrene, the Tg is 100°C, while for butyl methacrylate it is 20°C. This means that while for the polystyrene particle the TEM images are clear and the particles keep their integrity, in the case of poly (butyl methacrylate) the particles melted under the electron beam. So, as shown in Figure 26a, PNPs show a deformed morphology.
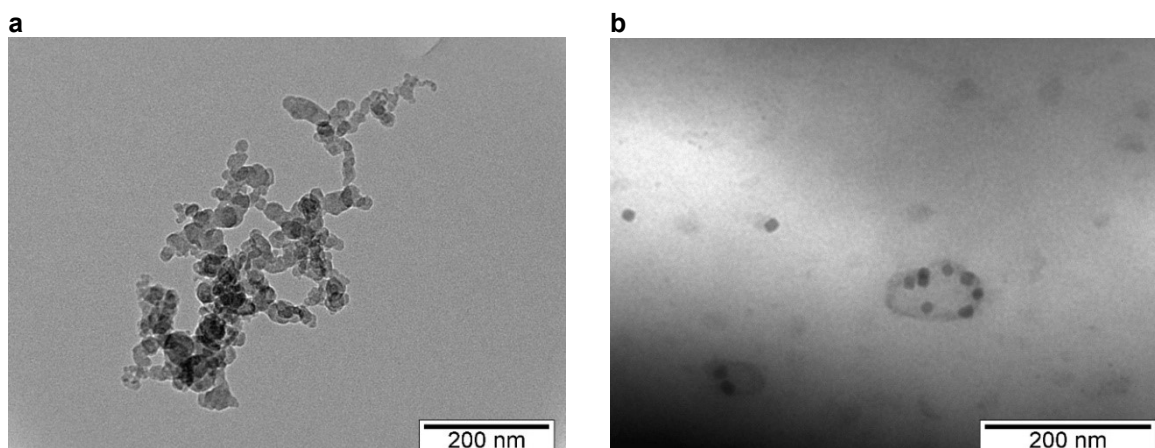
Figure 26. a) TEM image of ME2. b) TEM image of AuNPs inside polymer matrix of pBMA.

ME2 PNPs have a hydrodynamic diameter of (28±8) nm by DLS (Table 5). The value is half of the one for styrene, since the polymerization parameters were optimized for the styrene. This means that these particles have less scattering that the ones of PS. Since the PNPs melted during TEM, it not possible to measure a correct diameter.

Table 5. Hydrodynamic diameter of ME2 PNPs and solid content.

D_h (nm)	28±8
Solid content (%)	6.0

By TEM, was also possible to confirm the presence of AuNPs (Figure 26b), with about 15 nm. It is also important to notice that the particles seem to be incorporated inside bigger PNPs.

The conversion was 24%. It is much lower than in **ME1**. It shows that the conditions are not optimal for the BMA polymerization. But, even though the conditions used were not optimized, the polymerization proceed until a solid content of 6% (Table 5).

3.2.2.3.   pH influence in AuNCs optical properties after incorporation

After the phase transfer of AuNCs from aqueous phase to monomer and polymerization, the pH goes from 12.21 to 7.07. At this pH, after polymerization, the emission maximum was at 400 nm and by decreasing the pH below the pKa of MHA, the bands are exactly in the same place.

At pH ≈ 2, the AuNCs in aqueous dispersion tend to aggregate in the bottom leaving a clear aqueous phase. But, when incorporated into the particles, the purple color remains in the PNPs even after the pH change, turning slightly darker. This is an indication that most of the AuNCs are no longer in the water phase, but rather inside the PBMA particles where they are less affected by the pH change.
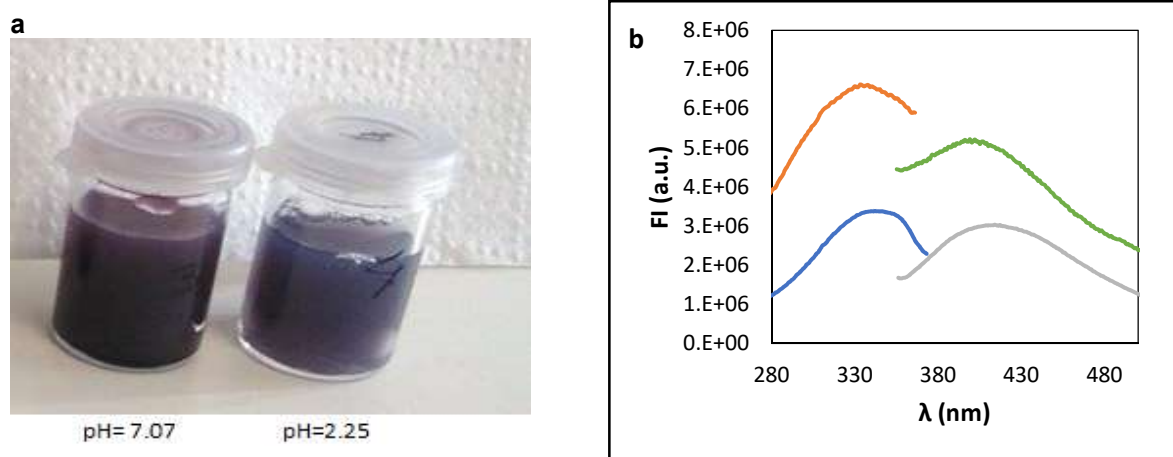
Figure 27. a) Visual aspect of miniemulsion (ME2) at pH=7.07 (left) and pH=2.25 (right). b) Emission spectra of miniemulsion (ME2) using λ_{exc}=320 nm (pH=2.25, grey) and λ_{exc}=300 nm (pH=7.07, green). Excitation spectra of ME2 at λ_{em}=414 nm (pH=2.25, blue) and λ_{em}=400 nm (pH=7.07, orange). The emission maximum is at 400 nm and the excitation maximum is at 340 nm.

These observations show that after the incorporation of the AuNCs into the PNPs, the changes in pH barely affect the optical properties of AuNCs and consequently their size. This observation shows good perspectives, since the incorporation of the AuNCs into PNPs seems to be successful, keeping the same maxima in different media.

3.3. PISA-RAFT

In the present work, the PISA-RAFT experiments used poly(N-acryloyl morpholine) (PNAM) as a hydrophilic macroCTA and nBA as hydrophobic monomer [30, 56]. The first experiments with this kind of system was reported by the Lyon laboratory (Bathfield, M. et al [56]) by dispersion polymerization: ethanol/water as solvent, temperature of 70°C and Mn(PNAM) as 38 100 g/mol. Particles with a core of about 120 nm and a shell thickness of 15 nm were obtained. Then PISA-RAFT was later optimized by D. Duret [30], who studied the influence of different parameters such as solvent, PNAM molecular weight or concentration of initiator through the ratio PNAM:ACPA (Table 6), on the particles size and polymerization kinetics. In his system, the conditions are water/acetonitrile as solvent, temperature of 80°C and Mn(PNAM) as 11 300 g/mol. The particles obtained had a size of about 50-60 nm.

Table 6. Parameters which influence PISA studied by D. Duret [30].

Parameter	Increase	Decrease
Ratio [macroCTA]/[initiator]	Slower kinetics	Faster kinetics Less control of polymerization
Ratio [monomer hydrophobe]/ [monomer hydrophilic]	More viscosity (self-assembly problems) Lower PDI	Smaller particles More particles Less induction period
Mn of macroCTA	Decrease of core size	Decrease of shell thickness
Solvent (% of acetonitrile)	Less induction period	PNAM is less soluble
Crosslinker (BDDA)	No influence on size of kinetics until 10% of [nBA]	

With the objective of producing hybrid particles (polymer particles incorporating AuNCs), different parameters of PISA with and without AuNCs were studied in the present work. It allowed to better understand the PISA mechanism (Figure 28) and the changes made by AuNCs. The PISA mechanism can be divided in two steps (Figure 28). First the beginning of polymerization in the continuous aqueous phase, in which nBA units are added to the PNAM chain. The second step consists in the self-assembly of the polymer chains, originating micelles.

Figure 28. PISA mechanism using PNAM as macroCTA and as monomer.

The summary of the main parameters and results are presented in Table 7.

Table 7. Summary of PISA main parameters and results.

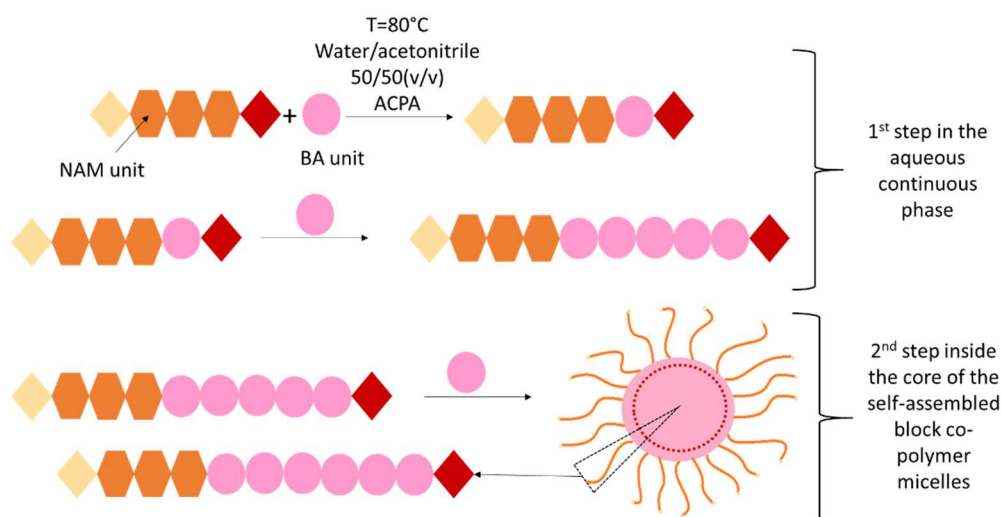| Exp.	Mn (PNAM) g/mol	pNAM: ACPA (molar)	nBA: PNAM (molar)	DP (PNAM)	T (°C)	[AuNCs] in organic phase (mM)	Time (h)	Cross-linker	Conversion (%)	D_h (nm)
PISA1	11 300	2.50	157	78.6	80	-	20	-	95	61±5
PISA2	10 300	2.50	157	71.5	80	-	20	-	91	55±3
PISA3	10 300	2.50	157	71.5	80	-	20	-	86	48.4±0.2
PISA4	10 300	2.50	157	71.5	80	0.140	20	-	84	26±2
PISA5	10 300	2.50	157	71.5	80	-	20	-	95	54±1
PISA6	10 300	2.50	157	71.5	80	0.140	20	-	92	29±2
PISA7	10 300	2.50	157	71.5	80	-	20	-	99	53±1
PISA8	10 300	2.50	157	71.5	80	0.140	20	-	71	25±1
PISA9	10 300	2.50	157	71.5	80	0.070	20	-	90	33±1
PISA10	10 300	2.50	157	71.5	80	0.035	20	-	87	42±4
PISA11	10 300	2.50	157	71.5	80	-	20	-	91	43.9±0.4
PISA12	10 300	2.50	157	71.5	80	0.140	20	-	84	27±1
PISA13	10 300	2.50	157	71.5	65	-	20	-	44	41±1
PISA14	10 300	0.62	157	71.5	65	-	20	-	96	37.5±0.0
PISA15	10 300	2.50	157	71.5	80	0.140	2	-	42	26.9±0.4
PISA16	10 300	1.25	157	71.5	65	-	20	-	74	46±1
PISA17	10 300	1.25	157	71.5	65	0.140	20	-	55	33.4±0.9
PISA18	10 300	1.25	157	71.5	65	-	6	-	33	37±1
PISA19	10 300	1.25	157	71.5	65	0.140	6	-	41	28.3±0.3
PISA20	10 300	2.50	79	71.5	80	0.140	2	-	35	27.1±3.3
PISA21	10 300	2.00	157	71.5	80	0.140	2	-	22	20±1
PISA22	10 300	2.50	157	71.5	80	0.070	2	-	45	34±1
PISA23	10 300	2.00	157	71.5	80	0.140	2	BDDA	57	31±2
PISA24	10 300	2.00	157	71.5	80	0.140	2	-	46	28±2
PISA25	10 300	2.00	157	71.5	80	0.070	2	-	48	34±1
PISA26	10 300	2.00	157	71.5	80	0.070	2	BDDA	53	32.0±0.4

In this section, RAFT solution polymerization was first used to synthesize a PNAM macroCTA. Then, after performing a reference PISA-RAFT without AuNCs in the conditions optimized by D. Duret [30], PISA-RAFT in the presence of AuNC was studied. Different parameters were optimized, such as degassing method, temperature and ACPA concentration, to obtain AuNC incorporating PNPs with a minimum destabilization of AuNCs.

3.3.1. Synthesis and characterization of PNAM

The PNAM synthesized is going to be used as macroCTA in the following PISA experiments, being the target Mw 12 000 g/mol with high purity. The reaction is stopped at 80% conversion to avoid side reactions and degradation of CTA. The different parameters have been optimize by A. Favier and his co-workers [30, 40, 57] (Figure 29).
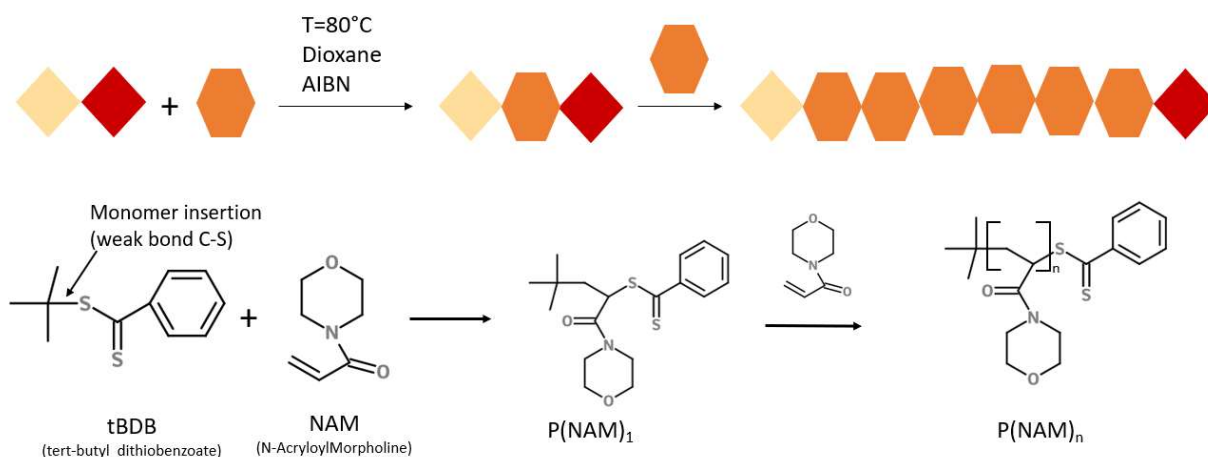
Figure 29. RAFT mechanism for PNAM polymerization

The polymerization of acrylates, like PNAM, is a difficult process, but it has been successfully done by RAFT with different monomers. In this project, NAM is the chosen monomer since PNAM presents certain advantages such as biocompatibility, solubility in different solvents (organic and aqueous solvents) and high molecular weight.

3.3.1.1. Visual aspect of reaction medium

The reaction medium changes aspect (color and viscosity) with the evolution of the reaction. The change from sharp pink to orange corresponds to the addition of monomer to the CTA during the addition-fragmentation step (Figure 29).

The color change occurs fast (Figure 30), being the color completely changed at 14% conversion (about 30min after the beginning of the reaction), which shows that the polymerization was already happening. This occurs due to the bond between the dithioester and the group connect to it, which change from tert-butyl to NAM. After this, only NAM is added to the chain keeping the color constant.
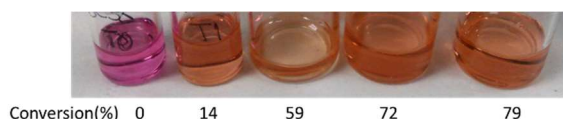
Figure 30. Visual aspect of RAFT polymerization.

3.3.1.2. Kinetics

The polymerization was stopped after 2h45min to have conversions around 80%. The conversion was calculated using ^{1}H NMR spectroscopy as explain in section 2.2.5 (Figure 31a).

In the first 30min, an induction period is identifiable, followed by 2 different periods (Figure 31b). First there is a period of fast polymerization, between 30 and 90min of reaction, followed by a slowing down until the 2h45. The higher conversion leads to an increase of viscosity, which at a certain point (about 70% conversion) results in slower kinetics.

The kinetics is similar to the reference experiment (performed by D. Duret [30]), confirming the reproducibility of the polymerization.
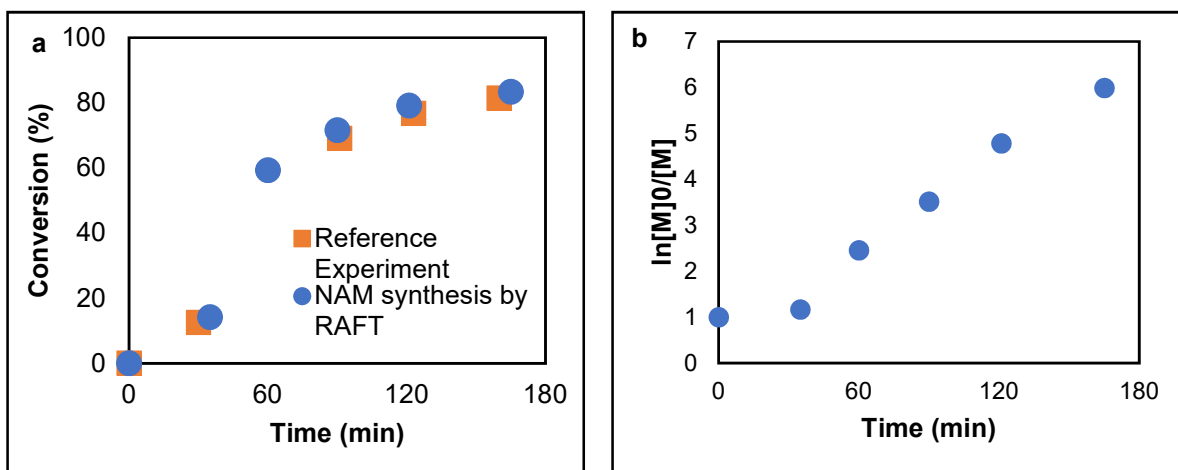
*Figure 31. a) NAM conversion as function of time with reference experiment (orange, experiment performed by D. Duret in the optimized conditions [30]) and **RAFT 1** (blue, PNAM synthetized in the present work). b) Ln (M_0/M) vs time for NAM polymerization at 80°C for **RAFT1**.*

3.3.1.3.   Molecular weight

The molecular weight (M_n) was analyzed after the purification of the different samples. The samples with small volumes (from 35 min to 2h) were purified by precipitation in diethyl ether and then dried after by vacuum. The absence of solvent (dioxane) or other impurities was checked by NMR.

M_n was analyzed by SEC-MALLS, showing a linear correlation with conversion (Figure 32). This shows that the polymerization is well controlled, which is supported by dispersities (Đ) close to 1. The final Mn value is 10 300 g/mol, close to 11 300 g/mol from the reference experiment.

The purified PNAM sample (79% conversion, 7.53 g) synthesized by RAFT exhibited the expected properties (M_n and PDI). It was then used for PISA-RAFT experiments.
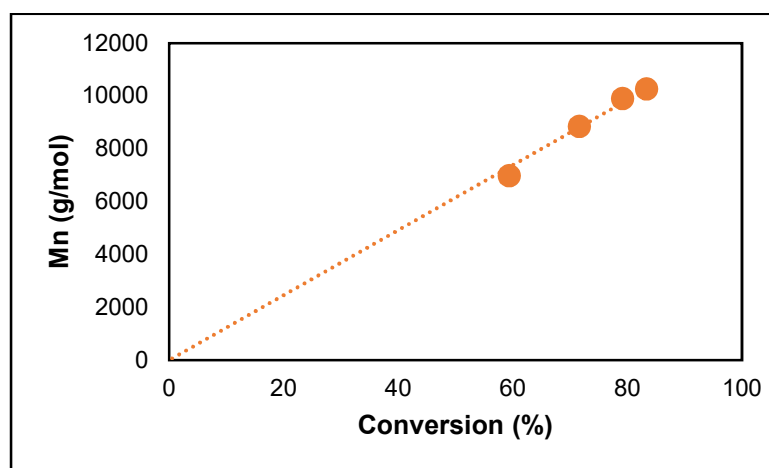
*Figure 32. Mn (PNAM) vs conversion (**RAFT1**). Mn determined by SEC/MALL. Conversion determined by ^{1}H NMR.*

3.3.2.   PISA-RAFT experiments without AuNCs

The PISA-RAFT condition were optimized and tested by D. Duret [30]. The main parameters were the molar ratios PNAM: ACPA, nBA: PNAM and the DP of PNAM. In the beginning of the project, the reproducibility

of the technique was tested using the original macroCTA synthesized by D. Duret (**PISA1**) and the one described in section 3.3.1 (**PISA 2**).

3.3.2.1. Visual aspect of reaction medium

The color of the reaction medium (Figure 33), as it happens in the synthesis of PNAM, indicated the evolution of the reaction. It starts with an orange color, meaning that the dithiobenzoate group is still attached to the NAM molecules (first part of Figure 28). As the addition of nBA starts, the color starts to change to salmon (first step of Figure 28), ending in a pink color as the nBA is being added to all macroCTA molecules (step 2 and 3 of Figure 28).
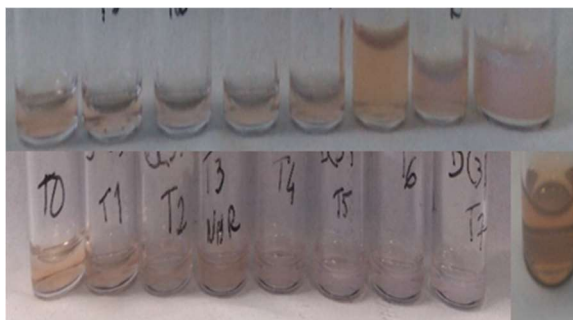
*Figure 33. Visual aspect evolution of PISA experiments: top - **PISA1**; bottom – **PISA 2**.*

In both experiments, the same color evolution is visible in both cases. The increase in milkyness (which is related to turbidity) with time is also visible, showing the formation of the micelles and sequent growth of the polymer nanoparticles (PNPs). The milkyness look a bit different from **PISA 1** to **PISA 2**, especially in the between the last 2 samples of **PISA2**, were the milkyness seems to decrease with conversion. This phenomenon is related with the storage conditions (section 3.3.4.4.)

3.3.2.2. Kinetics

The kinetics was followed by NMR (section 2.2.5.). **PISA 1**, with the macroCTA synthesized by D. Duret [30], and **PISA 2**, with macroCTA from section 3.3.1., were compared to experiment DD111 (**Ref. Exp**.) the one done by D. Duret [30].

In the 3 cases, the kinetics is similar which shows the reproducibility of the method (Figure 34). After 20h of reaction, the conversion of **PISA2** was 91% similar to 95% of **PISA1**. These values are slightly higher than the reference experiment (83% of conversion), but the final conversion can be changed by the entrance of oxygen or by the reaction medium volume.

As determined by D. Duret, when the solvent is 50/50 (v/v) acetonitrile/ water the induction period is about 30min. It is quite a small period because the presence of acetonitrile increases the solubility of the nBA in the aqueous continuous phase. Then there is a period until about 4h in which there is a fast rate of polymerization. After the formation of the micelles the acetonitrile will be inside the micelles too, which makes the nBA more diluted, favoring a lower the rate of polymerization compared to nBA bulk polymerization.
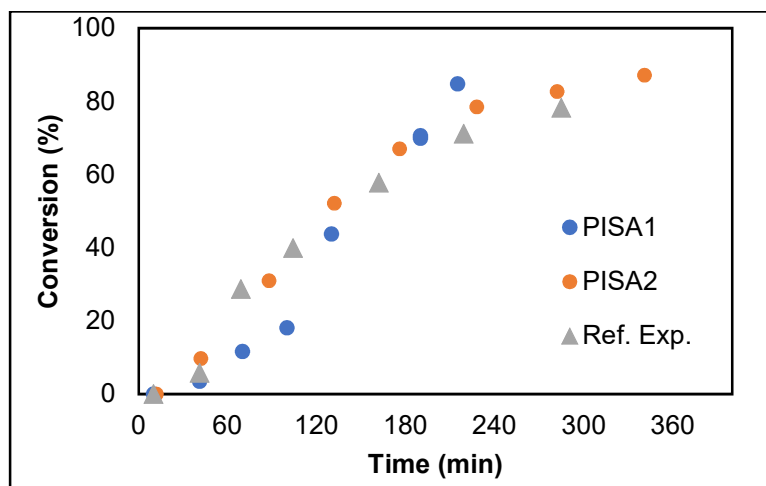
*Figure 34. Kinetics evolution of PISA polymerization (**Ref. Exp., PISA1 and PISA2**).*

3.3.2.3.   Particles size

DLS was used to study the dispersity and size of the particles, as well as their evolution with conversion (Figure 35). The trend is the same in both syntheses and reference experiment (**Ref. Exp**.). The final size (61±5) nm and (55±3) nm are similar, corresponding to synthesis using pNAM from D. Duret work (**PISA1**) and the one synthesized for the present work (**PISA2**). The particles have a similar size to **Ref. Exp.** which was 51 nm at 83% conversion.

For the next experiments, **PISA2** is going to be used as our new reference experiments, since **RAFT1** is the macroCTA used for the rest of the study.
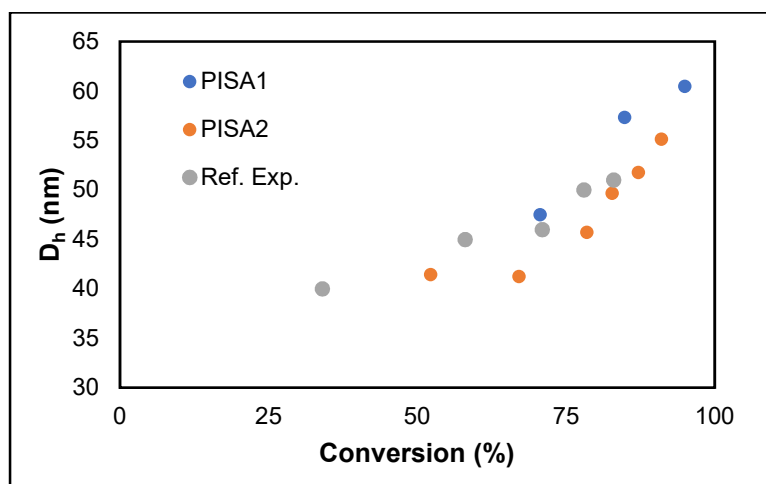
*Figure 35. DLS hydrodynamic diameter (D_h) vs conversion (**Ref. Exp. [30], PISA1, PISA2**).*

3.3.3. Phase Transfer of AuNCs from water to nBA

Phase transfer, as one of the intermediate steps, needs to be efficient and fast. For miniemulsion experiments the procedure used was similar to the one in reference [47]. A solution of CTAB in ethanol is added to the aqueous dispersion of AuNCs, followed by the addition of the monomer and stirred after. For miniemulsion, the phase transfer was fast and efficient (Figure 36).

For monomers like acrylates and methacrylates, the phase transfer was slower and less efficient. In addition, it could be better to avoid the use of ethanol which is known to induce transfer-to-solvent reaction during free radical polymerization processes. In order to minimize the number of external agents to the PISA-RAFT system (CTAB and ethanol), concentrations of surfactant and co-solvent were optimized.

Figure 36. Phase transfer of AuNCs between water and styrene (ME1).

3.3.3.1. Influence of surfactant amount

PISA-RAFT is a polymerization technique in which one of the advantages is the formation of PNPs without the use of surfactant. To minimize an influence of surfactant in PISA-RAFT after transferring the AuNCs, the amount of surfactant may be minimized. The effect of different concentrations of surfactant was then studied, using always CTAB as surfactant, starting by varying the amount of CTAB, using ethanol as a solvent and butyl acrylate (nBA) as a monomer (Table 8).

When the amount of CTAB is reduced to ¼, there is aggregation of AuNCs in the interface. This allows to conclude that CTAB is not only responsible for balancing the charge from MHA, but also helps with avoiding aggregation. It is determined from these experiments that an excess of CTAB is necessary to ensure the stability of the system.

Table 8. Influence of CTAB in phase separation.

Experiment	[CTAB] (M)	ethanol: Aqueous dispersion v/v
PT1T1	0.100	1
PT1T3	0.100	0.25

NaCl was added to the solution **PT1T3**, and the phase transfer was reversed making the AuNCs go back to the aqueous phase. The salt screens the MHA/CTAB interaction, making the process reversible.

To avoid the use of CTAB, changing pH was tested as an alternative method. For pH below 4, the AuNCs are no longer dispersed in water. So, by changing the pH to about 2 with strong stirring in the presence of a aqueous phase and a nBA phase, it was expected that the AuNCs may migrate to the nBA. But this was not observed, which may be due to the absence of a co-solvent.

3.3.3.2.   Influence of co-solvent

The co-solvent is soluble in both phases, to facilitate the migration of the AuNCs from the aqueous to the organic phases. In the case of nBA, a high amount of nBA was necessary when using ethanol, otherwise the nBA was completely soluble in the mixture water/ethanol. On the other hand, when the monomer was styrene, the solubility was lower, leading to a fast separation even for small amounts of styrene.

First, the role of the co-solvent was studied by reducing the amount of ethanol (Table 9). In the absence of ethanol, there wasn't a phase transfer at all (**PT1T5**), while in the presence of ethanol, even if it is in lower amount, there is always phase transfer of AuNCs from water to the monomer. This observation confirms that a co-solvent is essential to the phase transfer of AuNCs.
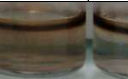
Table 9. Influence of ethanol in phase transfer.

Experiment	[CTAB] (M)	CTAB (mol)	ethanol: Aqueous dispersion v/v
PT1T1	0.100	0.0001	1
PT1T3	0.100	0.000025	0.25
PT1T4	0.268	0.0001	0.373
PT1T5	-	0.0001	0

Finally, to avoid the introduction of a new solvent in PISA-RAFT experiments, ethanol was substituted by acetonitrile. Different amounts of acetonitrile were tested (Table 10).

The objective was to obtain a good phase transfer with the minimum of acetonitrile possible. The images show that increasing the amount of acetonitrile lead to a better phase transfer with an optimum value in 80% acetonitrile/20% water. By gas chromatography (GC), the composition of the organic phase (top phase) was determined as being 49.7% nBA and 50.3% acetonitrile.

Table 10. Effect of acetonitrile (%v) in phase transfer and phase separation.

Experiment	PT2T5	PT2T6	PT2T7	PT2T8	PT2T9	PT2T10	PT2T11	PT2T12
% Acetonitrile (v)	50	55	60	65	70	75	80	85
Aspect								

3.3.3.3.   Dispersion of AuNCs in nBA

After transferring the AuNCs to the organic phase (nBA and acetonitrile), their stability was studied by absorption spectroscopy and HR TEM.

In terms of absorption (Figure 37), the bands are in the same place. The difference between the curves is due to the higher concentration of AuNCs in the organic phase than in water.
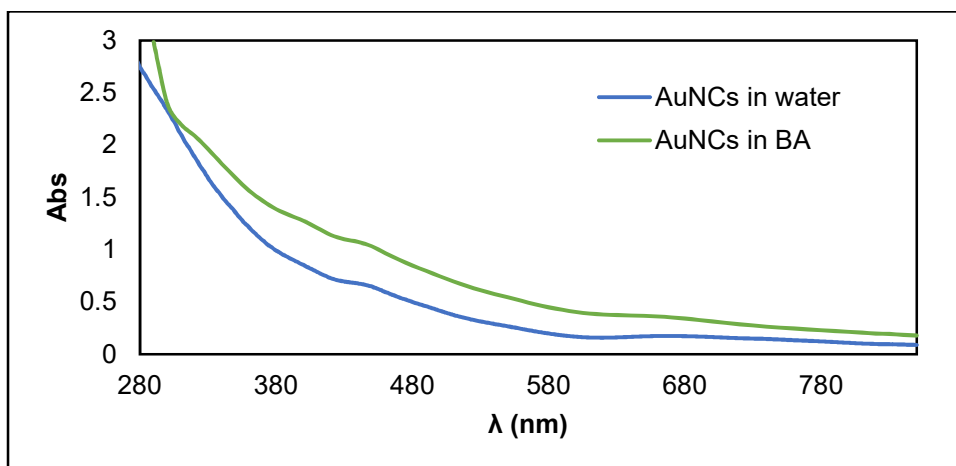
*Figure 37. Absorption spectra of Au$_{25}$(MHA)$_{18}$ (**Au40**) in water (blue) and nBA and acetonitrile(green).*

The size distribution of the AuNCs was analyzed by TEM (Figure 38a) and HRTEM (Figure 38b). In both cases, the AuNCs were randomly distributed on the grid (no aggregation). It shows that the AuNCs are stable in the organic phase with nBA and acetonitrile. In terms of size distribution (Figure 38c), the AuNCs present similar results using both techniques (HR TEM and TEM). The results presented are from HR TEM, since these are more accurate. The average size by TEM is (1.9±0.5) nm, while for HR TEM is (1.6±0.4) nm. Both results are similar to the ones obtained in water (1.8±0.6) nm. The AuNCs seem to be stable and well dispersed in the organic phase.
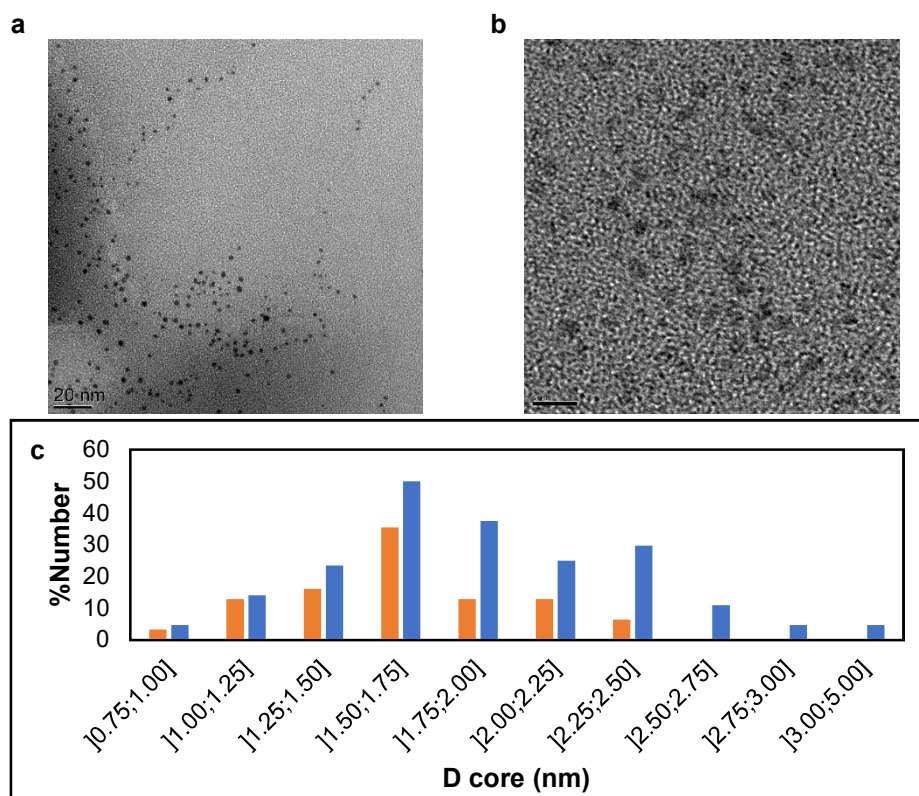
*Figure 38. TEM (a) and HR TEM (b) image of Au$_{25}$(MHA)$_{18}$ (**Au41**) in organic phase (nBA and acetonitrile). Size distribution by HR TEM (orange) and TEM (blue) of Au$_{25}$(MHA)$_{18}$ (**Au41**) in organic phase (nBA and acetonitrile (c)).*

3.3.4. PISA-RAFT experiments with AuNCs

To study the effect of AuNCs in PISA experiments, as well as their incorporation into the PNPs different parameters were studied, such as degassing methods, [AuNCs] in nBA, pNAM: ACPA ratio, temperature influence in different stages and presence of crosslinker.

The concentration of AuNCs in the aqueous phase was calculated with the following assumptions: (i) all the gold salt is converted into AuNCs during the AuNCs synthesis; (ii) each mol of AuNCs corresponds to 25 mol of gold salt since each AuNC has 25 atoms of gold. The concentration of AuNCs in the aqueous phase, following that assumptions, is 0.035 mM. To calculate the concentration in nBA, it was assumed that all the AuNCs migrate to the organic phase during phase transfer and that this one is 49.7% nBA in volume, being the rest acetonitrile (average value obtained by GC). Taking this assumptions into account, the concentration of AuNCs in organic phase (nBA and acetonitrile) is 0.140 mM. The exact concentration of AuNCs in both media is smaller than the one estimated due to the approximation presented above.

3.3.4.1. Comparison between PISA with and without AuNCs

3.3.4.1.1. Visual aspect of reaction medium

The AuNCs were transferred to the nBA phase using the technique discussed in section 3.3.3. In the beginning of the polymerization, the aspect was similar than the one without AuNCs, being the major difference the color of the nBA phase: instead of colorless it is dark brown (Figure 39). The degassing method used was freeze-pump-thaw, and during the defreezing some aggregates were noticeable. But they seem to disappear once the sample was at room temperature. During the polymerization, while the synthesis without AuNCs evolved from orange to pink, the one with AuNCs goes from orange/brown to purple. This color may be a first indicator of some aggregation of the AuNCs during the process.

It was observed during the reaction, that the transition from brown/orange to purple was gradual process, and the purple color intensity would increase with the time of reaction.
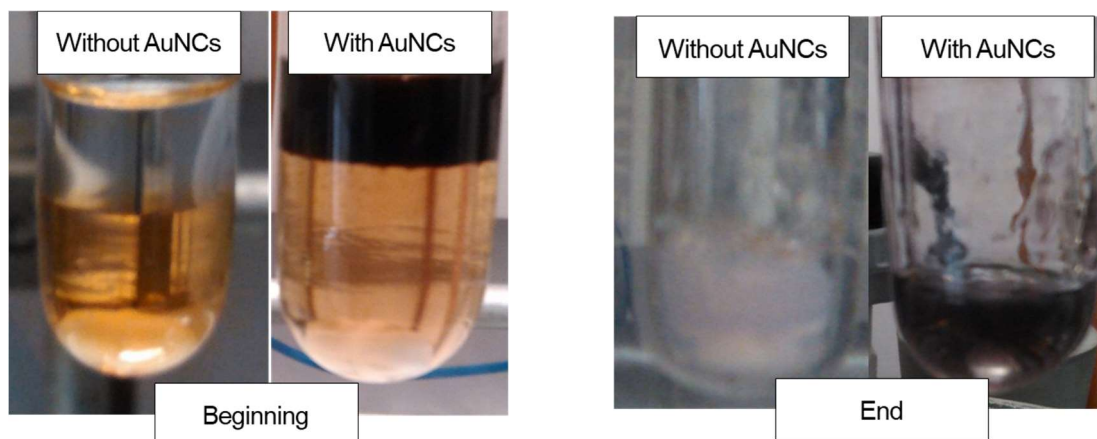
*Figure 39. Aspect evolution of PISA with AuNCs (**PISA3**) and without AuNCs (**PISA2**).*

3.3.4.1.2. Kinetics

The kinetics is studied by NMR by the methods explained in section 2.2.5. The kinetic in the presence of AuNCs seems to be slower (Figure 40). For **PISA3**, the composition of the organic phase containing nBA and AuNCs weren't precisely known. After GC analysis, the composition of the organic phase (acetonitrile and

nBa) was determined and it was concluded that an excess of 5% in volume of nBA was added to **PISA3.** This can be the reason for a lower conversion of nBA in the presence of AuNCs.

Both curves show similar evolution of kinetics, with the small induction period, followed by a period of fast rate of polymerization and last period in which the kinetics slows down. After 20h of reaction, the conversion with AuNCs was 84%, while the one without was 91%. Considering the uncertainty associated to the NMR measurements, the value can be considered similar.
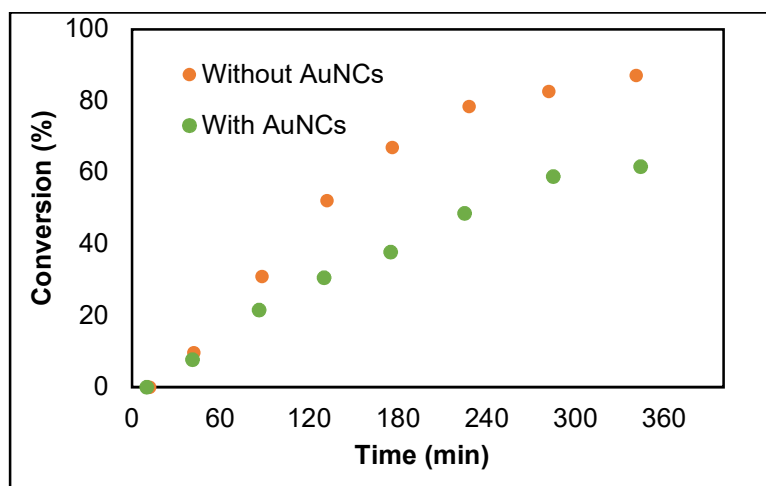
*Figure 40. Evolution of kinetics with time for PISA without AuNCs (**PISA 2**) and PISA with AuNCs (**PISA 3**).*

3.3.4.1.3. PNPs size

The PNPs are smaller in presence of AuNCs, which may contribute to the faster rate of polymerization near the end. It may be due to the presence of CTAB, which is in an 157% excess compared to MHA. It is also shown that while the size of the polymer particles increases with conversion for PISA-RAFT without AuNCs, in PISA-RAFT with AuNCs the size is approximately constant (Figure 41a).

The TEM results analyzed were the ones obtained with RuO_4 as contrast agent to increase the contrast of PNAM (shell). From TEM, it is possible to identify a core the PNPs without AuNCs (Figure 42d). The shell corresponds to the darker areas in the Figure 42d, but it is not possible to define the shell corresponding to one particle. The shell thickness is measured by measuring the space between three particles and considering that it corresponds to 3 cores and 6 times the shell thickness. In the PNPs synthesized with AuNCs (**PISA3**), the images weren't as clear as **PISA2**. So, it was only possible to measure the core of PNPs. For this reason, the diameter compared to the hydrodynamic (DLS) is the core diameter (TEM).

The final values obtained by TEM and DLS are similar. The size measured by TEM for the core of the particles is an accurate value, since the core does not change sizes from solution to dry on the grid. On the other hand, the corona (shell) thickness varies from solution to dry. While in DLS the measurements are made in solution where the shell is fully extended, obtaining the hydrodynamic diameter, in TEM the sample is dried in the grid, which can affect the disposition and size of polymer particles since the shell is collapsed. By DLS de size may be overestimated since it is the hydrodynamic diameter. On the other hand, by TEM, the shell thickness is underestimated for being dried.

The concentration of CTAB in the PISA-RAFT with AuNCs medium is about 14 mM, which is about 14 times the CMC of CTAB [54]. It is known that above CTAB CMC (1 mM) cylindrical CTAB micelles are formed, being not detected by TEM.

For the final sample (20h), the size distributions by DLS (Figure 42b) and TEM (Figure 42 c), which is also shown in Table 11 with the average values of diameter. The values from both methods are concordant.
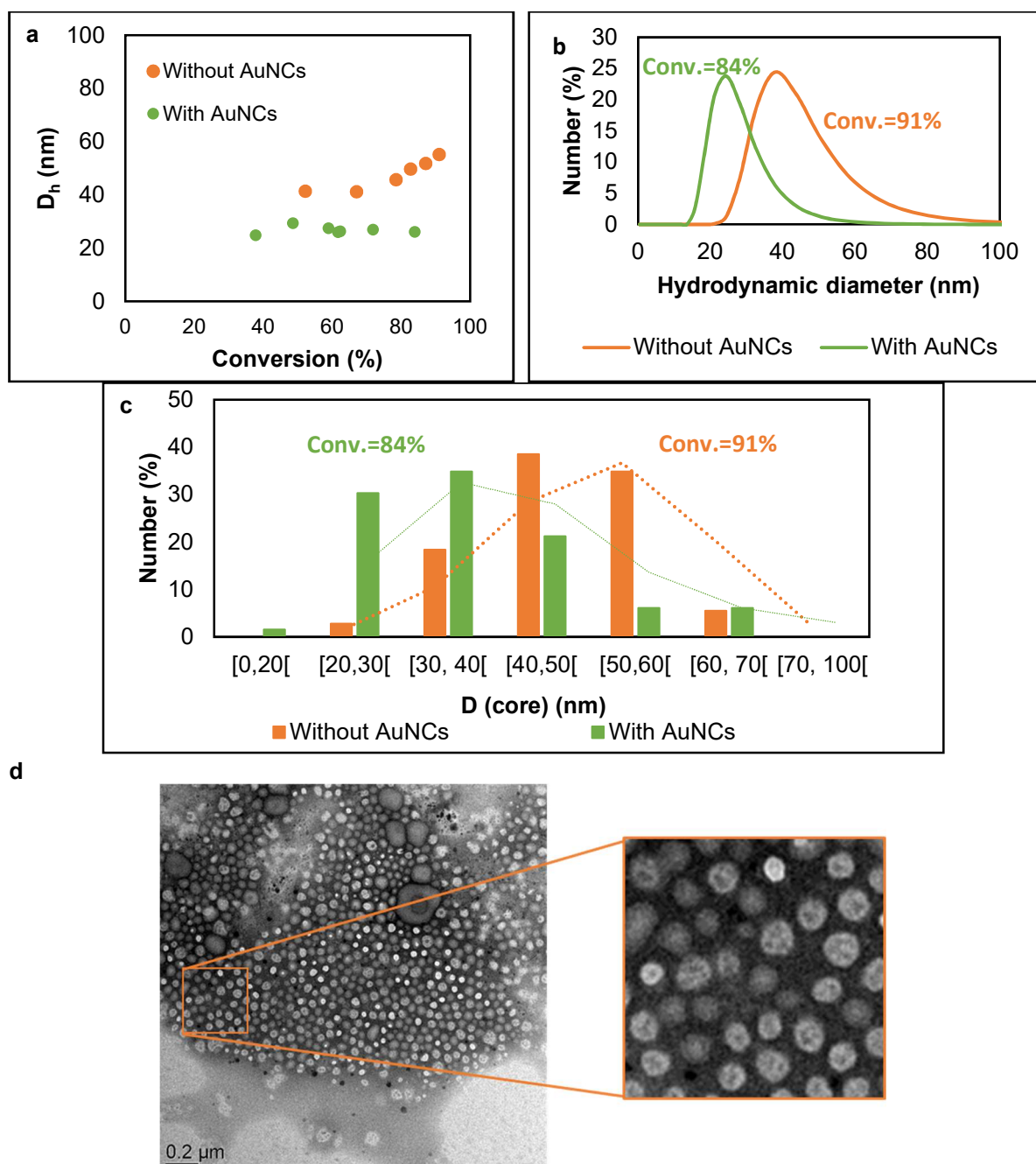
Figure 41. a) Evolution of DLS hydrodynamic diameter with conversion (**PISA 2** and **PISA 3**). b) Size distribution of DLS hydrodynamic diameter of PISA with (**PISA 3**) and without AuNCs (**PISA 2**). c) Size distribution of TEM core diameter of PISA with (**PISA 3**) and without AuNCs (**PISA 2**). d)TEM image of PISA without AuNCs (**PISA 2**) using contrast agent (RuO₄) with zoom in the PNPs (400 nm x 400 nm), where the PNPs core (light grey) and the shell (dark grey) are visible.

*Table 11. Comparison of the results obtained by TEM for PNPs with AuNCs (**PISA 3**) and without (**PISA 2**). *n.d. = not determined*

The results from PISA 3 were not clear, it was not possible to identify or measure the shell thickness.

Synthesis	PISA2	PISA3
Presence of AuNCs	No	Yes
D_h (nm, DLS)	55±3	26±2
Dcore (nm, TEM)	47±9	28±12
Dshell (nm, TEM)	6±3	n.d.*
D (nm, TEM)	54	-

3.3.4.1.4. Optical properties of PNPs

The optical properties of the PNPs with and without AuNCs were analyzed by absorption spectroscopy and fluorescence emission spectroscopy.

In the absorption spectrum, a band at 500 nm was detected in the samples without AuNCs (**PISA2**), which may be due the dithiobenzoate groups. For the sample with AuNCs (**PISA3**), the band is at 520 nm, characteristic wavelength for AuNPs. But since there is a band for the polymer (which is in higher concentration than the AuNCs), it is difficult to take conclusions about the AuNCs in the solution. The fluorescence spectra, in both cases, shows no bands at 815 nm, which is the emission wavelength for Au_{25} (the AuNCs used in the synthesis).

3.3.4.1.5. Conclusions

The presence of AuNCs in PISA seems to lead to slightly slower kinetics. The size of PNPs with AuNCs is smaller, obtaining similar results by TEM and DLS. As mentioned before, CTAB is in excess when compared with MHA. This leads to the hypothesis that CTAB acts as a surfactant in the micelles formation, and not only in the stabilization of AuNCs. The free CTAB, by acting as surfactant in a similar manner to miniemulsion polymerization, may stabilize more the particles, which leads to the formation of smaller micelles.

The presence of AuNCs in the PNPs cannot be observed by UV-Vis spectroscopy, since the polymer itself has a band at 500nm. But, together the change to purple in the end of the polymerization and the absence of emission in the fluorescence emission spectrum shows the evolution from AuNCs to AuNPs.

To assure that the AuNCs will not evolve to bigger sizes different parameters can be changed. The first one is the degassing method, to avoid the initial aggregation described before.

3.3.4.2. Influence of degassing method in AuNCs and PISA

Since some aggregation was detected during the freeze-pump-thaw degassing (Table 12), different deoxygenation methods were tried, to avoid it. The air bubbles, being hydrophobic, during the defreezing step may destabilize the AuNCs. The fast change of temperatures when the mixture is frozen by immersion in liquid nitrogen may also contribute to the destabilization.
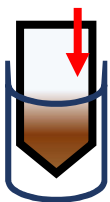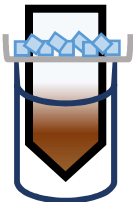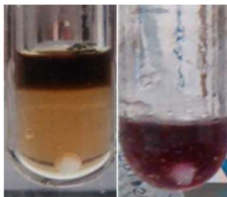
So, two other methods were tested to degas the mixture (see pros and cons in Table 12). In the argon flushing method, two different alternatives were used: with and without ice bath. With ice bath, there was no evaporation of the solvent. However, after a short period of time (5min), AuNCs aggregated at the interface between the aqueous phase and the monomer phase. It may be low temperature induced aggregation. Without the ice bath no aggregation was visible but there was a decrease of 13% in the liquid level (it can be evaporation of monomer and solvent). The third method, which is under argon with an ice condenser, avoids AuNCs

aggregation and most of evaporation. Argon (Ar) entrance is in the top of the tube and not close to the mixture, so we wanted to check that it is efficient to remove O_2 from the reactional mixture.

The solutions' color in the end of the reaction, with **method 1**, is darker and closer to black than the other ones which are closer to purple, more specifically plum.

While in the freeze-pump-thaw method there is a visible aggregation during the defrosting, in the argon flushing it is only evident when the solution is in the ice bath for about 5min, as mentioned before.

Table 12. Different degassing methods studied: pros, cons and solution aspect (after degassing, left, and at the end of polymerization, right) for freeze-pump-thaw, argon flushing and under argon with condenser.

Degassing method	Freeze-pump-thaw	Argon flushing	Under argon with ice condenser
Diagram	Liq. N$_2$		
Pros	✓ More efficient. ✓ No evaporation.	✓ No air bubbles.	✓ No air bubbles. ✓ No change in temperature.
Cons	✗ Big temperature gradient. ✗ Air bubbles. ↳ Visible aggregation.	✗ High evaporation of reaction medium in absence of ice bath. ✗ Visible aggregation of AuNCs in the presence of ice bath.	✗ Slight evaporation of reaction medium. ✗ Less efficient O_2 removal.
Aspect			
Synthesis	PISA 3 (Method 1)	PISA 6 (Method 2)	PISA 8 (Method 3)

3.3.4.2.1. Kinetics

A difference in term of kinetics was observed depending on the degassing method used (Figure 42). The rate of polymerization is faster using argon flushing (**method 2**) as degassing method, followed by under argon with ice condenser (**method 3**) and in last place freeze-pump-thaw (**method 1**). This order corresponds also to the evaporation during each method: **method 2** is the one with more evaporation of the mixture, while **method 1** is the one with less. This means that an increase in the evaporation of the mixture leads to a faster kinetics. According the studies made by D. Duret, by using only water instead of a mixture of water/acetonitrile of 50/50 (v/v), the rate of polymerization after the induction period is faster [30]. This suggests that what evaporates from the medium is mostly acetonitrile. After the formation of the micelles, there is less swelling (less acetonitrile), which allows the polymerization to procced in a faster way.

The final conversion after 20h is 84% using freeze-pump-thaw, 92% with Ar flushing and 71% under Ar with condenser. In the 3 cases there was polymerization with similar induction period. Since in PISA, the amount of initiator is lower than in conventional free radical polymerization to limit termination, the presence of O_2, even in low concentrations could have prevented polymerization or retarded it. But it is not the case, showing that the 3 methods successfully removed the O_2 from the medium.
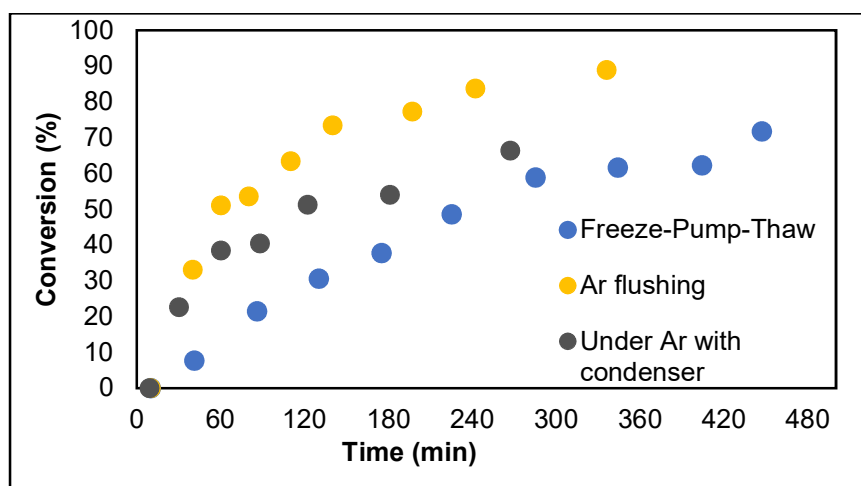
Figure 42. Kinetics in the presence of AuNCs according to the degassing method: freeze-pump-thaw (**PISA 3**), argon flushing (**PISA 6**) and under argon with condenser (**PISA 8**).

3.3.4.2.2. PNP size

In terms of size, measured by DLS, the evolution with conversion is the same (**method 1** – conversion=84%; **method 2**- conversion= 92%; **method 3** - conversion=71%). The size of the PNPs is constant for conversion between 50% to 80%, i.e., the size does not change with the increase in conversion between the values of 50% and 80% for conversion.
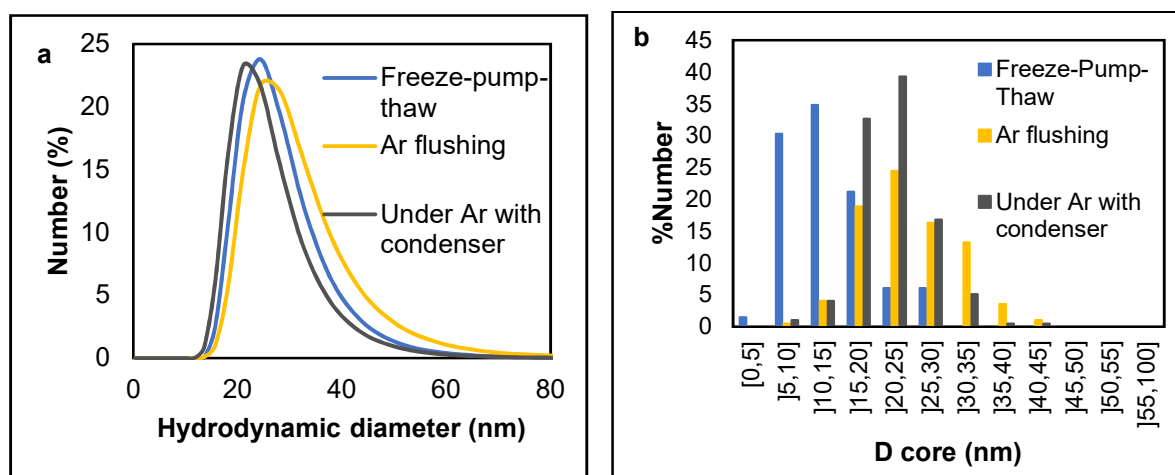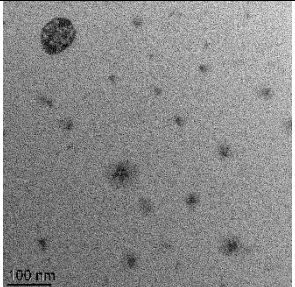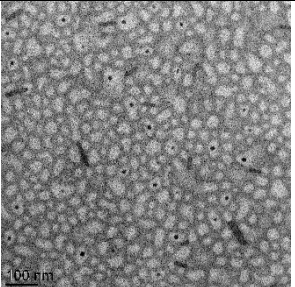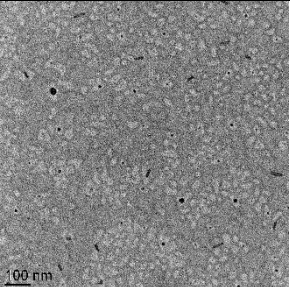
Figure 43. Size distribution obtained of PNPs with AuNCs according to the degassing method, freeze-pump-thaw (blue, **PISA 3**), argon flushing (yellow, **PISA 6**) and under argon with ice condenser (grey, **PISA 8**), after 20h of reaction by DLS (a) and TEM (b).

The distribution of sizes measured, by DLS (Figure 43a), is similar in the end of the 3 synthesis, being the average values in Table 13. These values are similar to the ones obtained by TEM. The size distribution of the particles measured by TEM shows a slight deviation in the results from DLS for the synthesis after freeze-pump-thaw, being the curve shifted to smaller values. The difference can be due to the low definition of the

particles in the images captured. For the other two methods, it shows a similar size distribution curve, which confirms the results from DLS (Figure 43a).

By TEM (Table 13), some AuNPs (bigger gold particles) are also visible in the synthesis after degassing by argon flushing and under argon with condenser. Both present average diameters of (12±4) nm. The AuNPs show similar sizes in both synthesis, and some of them seem to be located inside the PNPs. In the synthesis after degassing by freeze-pump-thaw, the images are less clear, being difficult to identify the gold nanoparticles.

Table 13. Average size of PNPs according to the degassing method used.

Degassing method	Freeze-pump-thaw	Argon flushing	Under argon with condenser
Aspect			
D_h (nm)	27±2	29±2	25±1
Dcore (nm)	28±12	24±7	22±5
D AuNPs (nm)	-	12±4	12±4
Synthesis	PISA 3	PISA 6	PISA 8

The PNPs with degassing by under argon with condenser were also analyzed by cryoTEM using copper grids covered with holey carbon film (these grids are used to visualize the particles in the holes without the noise from the carbon film). CryoTEM, as explain in section 2.2.1, allows to visualize the particles in the same conditions as in solution, allowing to measure the shell thickness without being collapsed from drying. Unfortunately, the particles mostly located on the carbon film (negatively charged) and not in the holes. This may be due to some positive charges at the surface of the particles that favor electrostatic interaction with the negatively charged carbon film. The average core diameter calculated is (22±7) nm. This size is the same as obtained by regular TEM. It was not however possible to measure the shell since the contrast was not good enough (due to the carbon film, which was similar in all TEM analysis).

3.3.4.2.3. Optical properties of PNPs

Both methods, UV-Vis absorption spectroscopy and fluorescence emission spectroscopy, were applied to the last sample (21h) of each one of the synthesis. In all of them, there was a band at 520 nm in the absorption spectra, which may be from the polymer or the AuNPs. But the absence of emission bands at any wavelength, especially at 810 nm, shows the absence of AuNCs or, at least, that the emission is weak and masked by PNPs scattering.

The hypothesis of the evolution from AuNCs to AuNPs is supported by the color change to purple as well as the detection of particles similar to AuNPs in the TEM analysis.

3.3.4.2.4. Conclusions

The three methods are efficient to deoxygenate the reaction medium. Freeze-pump-thaw is the method which allows better reproducibility and no evaporation, but it the one which destabilizes the AuNCs more. On the other hand, the experiment under argon with ice condenser is less aggressive for the AuNCs in terms of destabilization and the evaporation is low. So, the chosen method for the following studies is the one under argon with ice condenser, to avoid the AuNCs destabilization.

3.3.4.3.   Influence of [AuNCs] in nBA
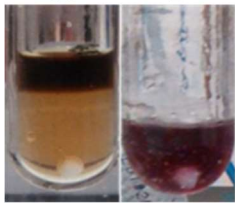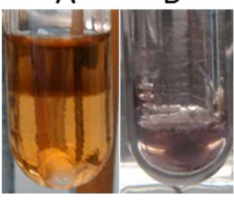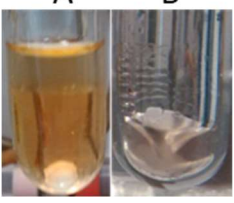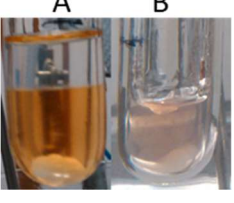
After setting-up an efficient deoxygenation method, the influence of concentrations of AuNCs in the nBA phase was studied. High AuNCs concentration may indeed favor the AuNCs aggregation into AuNPs. Lower AuNCs concentrations were then explored.

3.3.4.3.1. Visual aspect of reaction medium

The difference in concentration is visible in the color of the organic phase before the polymerization and after. At the beginning of polymerization, the brown color is lighter for lower AuNCs concentration as expected, as well as the purple color in the end of the polymerization (Table 14).

In terms of apparent viscosity there is no difference, but in terms of milkyness it seems to increase with the decrease of AuNCs concentration.

Table 14. Visual aspect evolution with time and AuNCs concentration, with A as the visual aspect at the beginning of PISA-RAFT and B at the end.

[AuNCs] (mM)	0.140	0.070	0.035	0
Synthesis	PISA 8	PISA 9	PISA 10	PISA 11

3.3.4.3.2. Kinetics

Kinetics are globally similar in the 4 cases: from without AuNCs to the [AuNCs] of 0.140 mM, even polymerization rate seems to increase at the beginning of the polymerization with the increase of AuNCs concentration (which may be due to CTAB acting as surfactant) (Figure 44).

These conclusions are different that the one obtained in section 3.3.4.1, where PISA with AuNCs seems to have slightly slower kinetics than PISA without AuNCs. As previously explained, the percentage of nBA in the organic phase containing AuNCs has a variation of 5%. The difference in the amount of nBA (monomer) can mean slight differences in the polymerization rate. Besides the difference in the amount of nBA, there is the slight evaporation during degassing under Ar with condenser which make the degassing hardly reproducible.

The influence of AuNCs and their concentration in the kinetics of PISA is thus not clear and does not show a clear trend, but independently of the AuNCs concentration PISA-RAFT occurs reaches between 70% and 90% after 20 h.
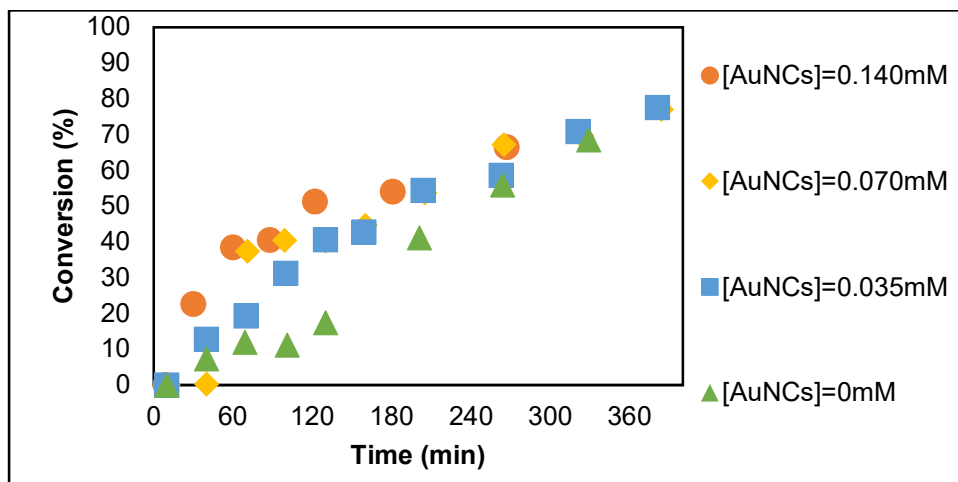
*Figure 44. Kinetics evolution with time and AuNCs concentration (**PISA8** to **11**).*

3.3.4.3.3. PNPs size

As observed in section 3.3.4.2., the presence of AuNCs leads to smaller PNPs and this decrease in size is related with the increase in [AuNCs] (Figure 45). This may be due to the AuNCs themselves with their anionic ligands but also to the presence of free CTAB with the AuNCs. An increase in the AuNCs concentration means an increase of the CTAB concentration as well. More surfactant allows the particles to be stabilized at smaller sizes.
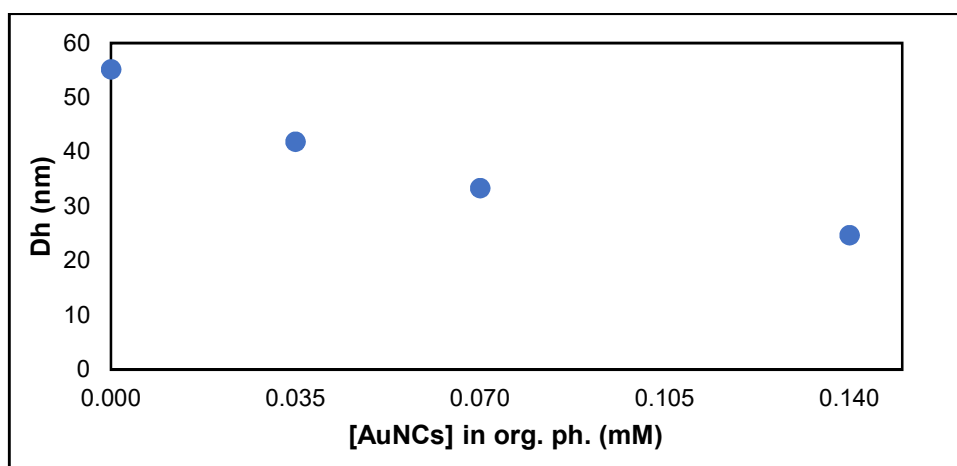
*Figure 45. Evolution of DLS hydrodynamic diameter with AuNCs concentration (**PISA 8** to **11**).*

The [AuNCs] of 0.140 mM and 0.070 mM were also analyzed by TEM (Table 15). In both cases, the average diameter coincides with the values measured by DLS, showing the same tendency of decreasing particles size by increasing [AuNCs]. But by TEM, it is also possible to identify gold nanoparticles (AuNPs) in the PNPs, with average diameters about 12 and 13 nm. It is however difficult to precisely estimate their proportion in the samples and to know if they are produced during the polymerization or during the sample preparation.

[AuNCs] (mM)	0.140	0.070	0.035	0.000
D_h (DLS, nm)	25 ±1	33±1	42±4	43.9±0.4
D core (TEM, nm)	22±5	28±6	-	-
D AuNPs (TEM, nm)	12±4	13±6	-	-
Sínteses	PISA 8	PISA 9	PISA 10	PISA 11

3.3.4.3.4. Optical properties

UV-vis absorption spectroscopy and fluorescence emission spectroscopy confirm the observations from TEM and visual aspect. From the absorption spectrum, a band at 520 nm was identified. Even though it can be the polymer band, the deviation of 20 nm with the rest of the previous analysis may indicate the presence of AuNPs (typical SPR band).

The absence of emission at any wavelength between 300 nm and 850 nm may be due the evolution of the AuNCs to AuNPs or to AuNCs which emit above 850 nm (more into IR). But, all the other analysis (TEM and UV-vis absorption) indicated the presence of AuNPs.

3.3.4.3.5. Conclusions

The concentration of AuNCs in the organic phase may influence the evolution to AuNPs, but it is not the main factor. Decrease of AuNCs concentration was tested, including concentration quite inferior to the one of the AuNCs in water, and after about 20h in the reaction medium at 80°C there is change in the properties of the gold compounds.

3.3.4.4. Influence of storage conditions

In the PISA with nBA as monomer, the particles do not have a frozen core. This means, that since the Tg of pBA is -54°C at room temperature, the core is still viscous and not hard or brittle. So, changes in the PNPs can happen after the synthesis during storage. The size of PNPs and aspect of PNP solutions was evaluated in 3 different cases: (i) storage at -20°C, (ii) effect of changing from -20°C to 4°C, and (iii) storage at 4°C vs storage at room T.

3.3.4.4.1. Storage at -20°C

After storing the sample at -20°C during a week, the milkyness of the sample increased. Milkyness corresponds to the scattering caused by the increase in size, appearing very clearly by eye when PNPs size is higher than 40 nm (Figure 46a).

The change in size is confirmed by DLS analyses, being from about 40 nm to 56 nm (Figure 46b).

By putting the PNPs at lower temperature, it seems they may fuse (and change their morphology) or evolve to a more stable conformation/size, which corresponds to bigger PNPs.
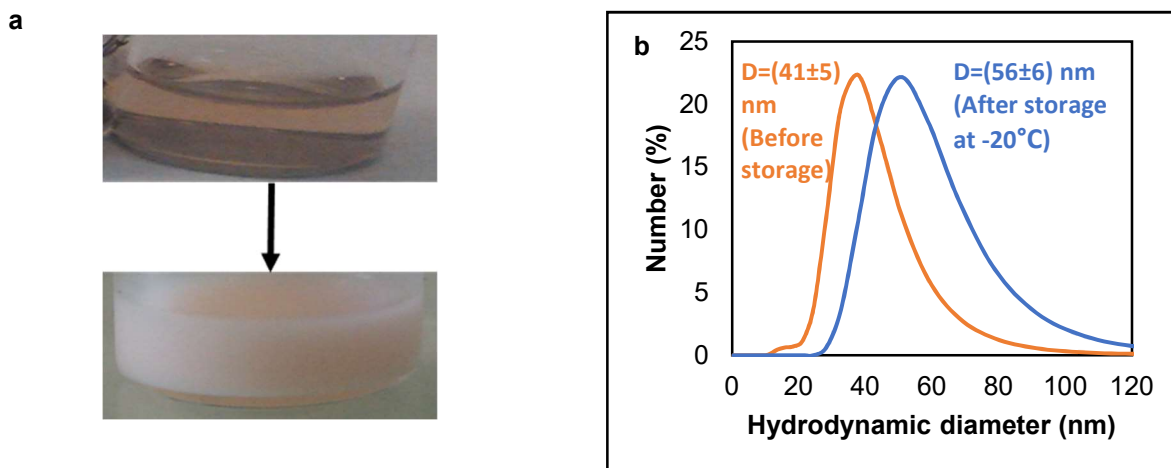
*Figure 46. a) Aspect change after being at -20°C for 7days (**PISA 2**). b) Size distribution (DLS) before and after storage at -20°C (**PISA 2**).*

3.3.4.4.2. From storage at -20°C to 4°C

After removing the particles from storing at -20°C and store them at 4°C, the aspect was kept constant and there wasn't any change in the milkyness of the solution.

In terms of hydrodynamic diameter, it is similar in both cases, showing that the PNPs size change with the storage at -20°C is not reversible (Figure 47).

By storing the particles at -20°C, they assume a size which is stable at higher temperatures, apparently reaching a stable, non-reversible state.
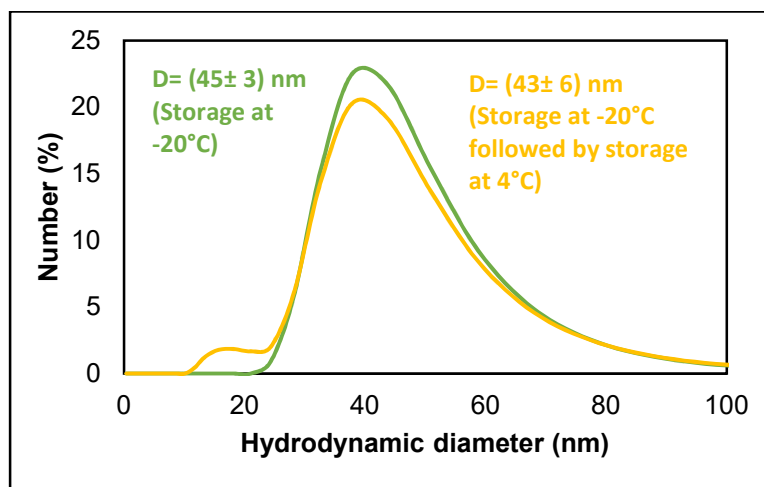
*Figure 47. Size distribution (DLS) of **PISA 4** after being storage a week at -20°C and after 1week at -20°C followed by a week at 4°C.*

3.3.4.4.3. Storage at 4°C vs storage at room T

Two samples from the same PISA-RAFT experiment at the same conversion were stored one at room T and the other at 4°C.

In both cases there wasn't difference in aspect or milkyness. The DLS hydrodynamic diameter was similar in both cases too (Figure 48). While lower temperatures as -20°C the PNPs seem to look for a more stable size, for temperatures between room T (about 25°C) and 4°C the particles seem to maintain their size,

To choose the storage conditions for the particles, it is important to account for the stability of the AuNCs at different temperatures. Through the degassing methods study, it was shown that the AuNCs are not stable at low temperatures. So, the storage adopted was at room temperature.
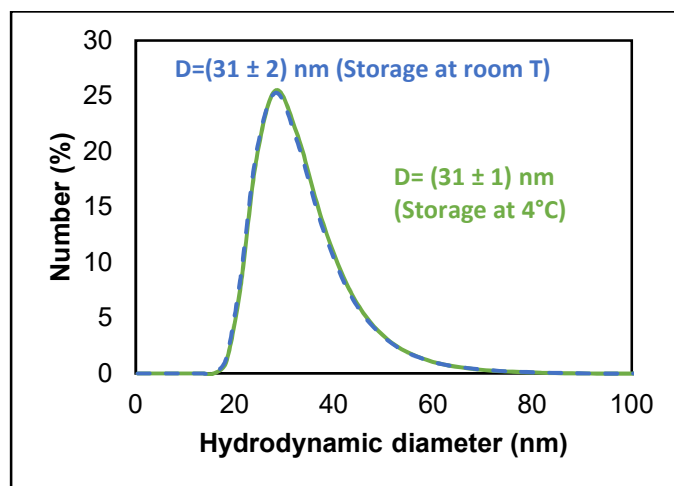
*Figure 48. Size distribution (DLS) of **PISA 10** after storage at room T and at 4°C.*

3.3.4.5.   Influence of temperature on Au$_{25}$(MHA)$_{18}$ stability

The stability of Au$_{25}$(MHA)$_{18}$ in function of temperature was studied by Chen and co-workers [58]. They showed that the AuNCs degrade after a few hours at temperatures higher than 40°C. To check the limit of time at 65°C and 80°C of the AuNCs, we studied their absorption and aspect after being at the mentioned temperatures

3.3.4.5.1. AuNCs in water

The AuNCs after the synthesis were divided into 3 samples: (i) left at room T after synthesis at 27°C, (ii) 6h at 65°C after synthesis at 27°C, and (iii) 3h at 80°C after synthesis at 27°C (Figure 49).
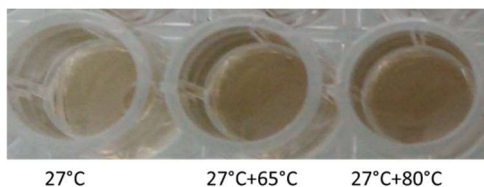
*Figure 49. Visual aspect of AuNCs aqueous dispersions after being exposed to different temperatures (**Au40**): room temperature, 65°C for 6h and 80°C for 2h (from left to right).*

In terms of aspect, the brown color turns slightly darker after the AuNCs being exposed to higher temperatures (Figure 49).

In the absorption spectra (Figure 50), there is a shift to the right after the exposure to high temperatures. Similar phenomena has been observed by Chen during the AuNCs synthesis, which is associated with the increase in the reaction yield [58]. Since 27°C is lower than the optimal temperature for the synthesis (40°C), the reaction is slower and with lower yield.

The 2 bands characteristic of Au$_{25}$(MHA)$_{18}$ are less defined after exposure to high temperatures, which can indicate the beginning of a degradation of the AuNCs due to temperature.
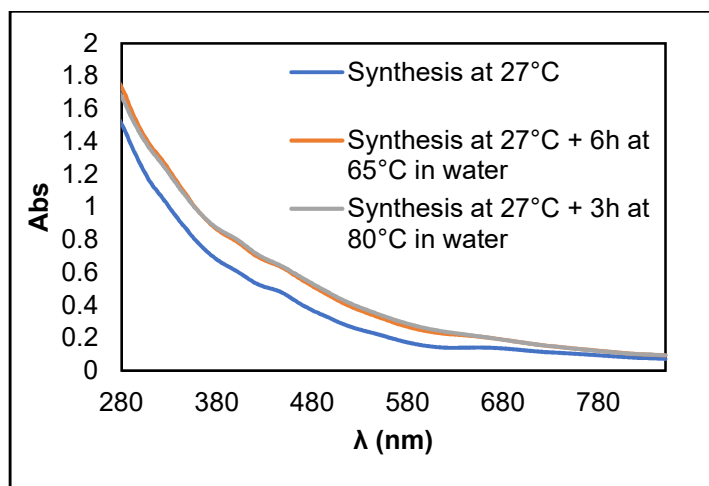
*Figure 50. Absorption spectra of aqueous dispersion of AuNCs after being exposed to different temperatures (**Au40**).*

3.3.4.5.2. AuNCs in nBA

The AuNCs after they are transferred to nBA were divided into 3 samples: (i) left at room temperature, (ii) 6h at 65°C, and (iii) 3h at 80°C (Figure 51).
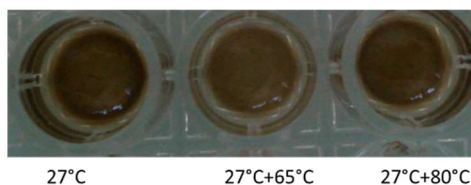
*Figure 51. Visual aspect of AuNCs organic dispersions after being exposed to different temperatures (**Au40**): room temperature, 65°C for 6h and 80°C for 2h (from left to right).*

In terms of aspect, there is no visual deposition of any particles on the bottom of the wells. As opposed to the change in the AuNCs in water, by heating the dispersions, the color seems to turn slightly lighter.

In terms of absorption (Figure 52), there is no shift in the curves, contrary to what was observed AuNCs dispersion. This indicates that the AuNCs dispersion does not evolve, which can be due to the absence of some of the reagents from the aqueous medium. However, if not shifting, the bands characteristic of $Au_{25}(MHA)_{18}$ almost completely disappeared, indicating a faster degradation than in water. It may be caused by the higher AuNCs concentration in nBA than in water, facilitating aggregation and degradation at high temperature.

After observing the changes in the optical properties of the AuNCs with temperature, the time and temperature of reaction are studied to avoid the formation of AuNPs during the PISA synthesis.
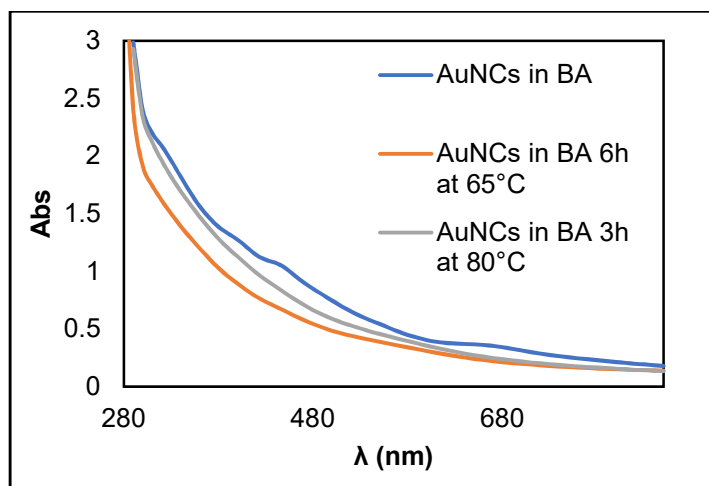
*Figure 52. Absorption spectra of dispersion of AuNCs in nBA and acetonitrile after being exposed to different temperatures (**Au40**).*

3.3.4.6. Influence of temperature and initiator concentration in PISA-RAFT

Since AuNCs seem susceptible to degradation/aggregation when exposed to temperatures higher than 60°C for several hours, it was explored if satisfactory PISA-RAFT experiments could be run not at 80°C for 20h as before. Other options were study: at a lower temperature (65°C) at various initiator concentrations and compared to similar reference experiment at 80°C.

3.3.4.6.1. Influence of Temperature in PISA-RAFT (80°C vs 65°)

Compared to PISA-RAFT at 80°C, only a slight visual difference is observed (Figure 53). The PISA at 65°C, after the 6h, shows a more salmon coloration instead of the pink ton from PISA at 80°C, probably because polymerization rate is slower. The most important point is after 6h, but the polymerization was studied for 20h to check if there is a stabilization in the particles evolution in terms of visual aspect, conversion and particle size, or if it is stabilized like at 80°C.
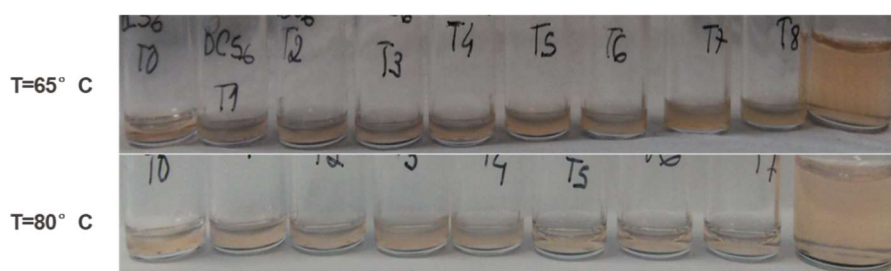
Figure 53. Visual aspect of PISA at 65°C (PISA 13) and at 80°C (PISA 12).

In terms of kinetics (Figure 54a), PISA-RAFT at 65°C was slower than at 80°C as expected. Only 44% conversion was obtained after 20h, instead of 91% at 80°C due to the slower initiator decomposition.

In terms of PNPs size, at comparable conversion (for instance between 10 and 15%), similar PNPs hydrodynamic diameter (about 27 nm) are obtained. It seems that temperature does not influence the particles size (Figure 54b).
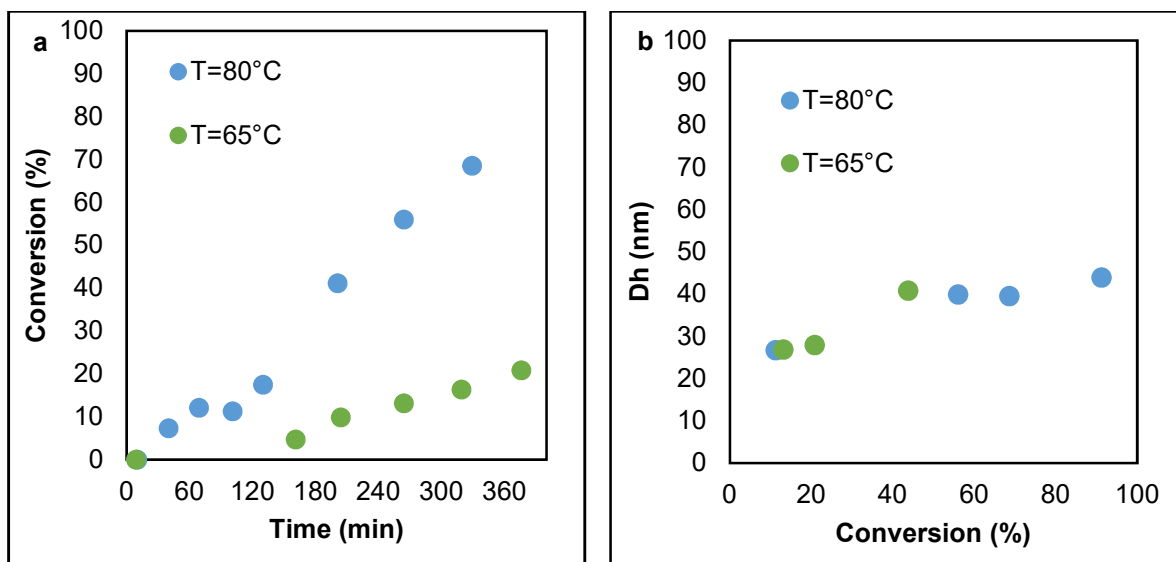
*Figure 54.. a) Kinetics of PISA-RAFT at 65°C (**PISA 13**) and at 80°C (**PISA 12**). b) Particle size of PISA-RAFT at 65°C (**PISA 13**) and at 80°C (**PISA 12**).*

3.3.4.6.2. Increase of Initiator concentration at 65°C

As the objective was run PISA-RAFT at 65°C for no more than 6h, ACPA (initiator) concentration was increased to increase the polymerization rate and to obtain higher monomer conversions.

In terms of visual aspect, there is a significant difference between the PISA-RAFT experiments when decreasing the PNAM:ACPA ratio from 2.5 to 1.25 to 0.62 (Figure 55). Milkyness and discoloration (loss of pink/salmon color intensity) of reaction medium increased with the increase of ACPA initial concentration, indicating respectively an increase in PNPs size and a degradation of the dithioester polymer chain-ends (necessary for an efficient RAFT process).
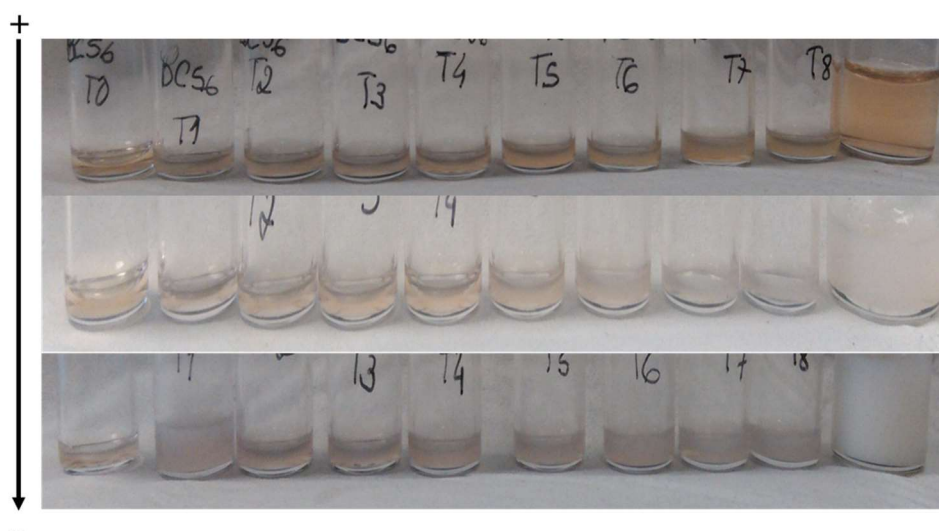
Figure 55. Visual aspect evolution with PNAM: ACPA ratio and conversion (PISA 13, PISA 14 and PISA 16).

In terms of kinetics (Figure 56a), as expected, the rate of polymerization increased with the increase of APCA concentration (decrease of PNAM:ACPA molar ratio). After 6h reaction, the conversion was 56% for

[ACPA]=2.6 mM (PNAM:ACPA=0.62), 26% for [ACPA]=1.3 mM (PNAM:ACPA=1.25) and 11% for [ACPA]=0.7 mM (PNAM:ACPA=2.5).

The PNPs sizes were between 25 nm and 50 nm, depending on the ACPA:PNAM ratio (Figure 56b). Besides the difference in size, increasing the ACPA initiator concentration led to the appearance of a new particle population with diameters between 180 nm and 250 nm. Its proportion in number was quite low (0.2% for PNAM:ACPA=1.25 and 0.3% for PNAM:ACPA=0.62) but tended to increase with ACPA initial concentration. This is in agreement the increased milkyness that was observed (Figure 55) and suggest a loss of control about the PNP synthesis.
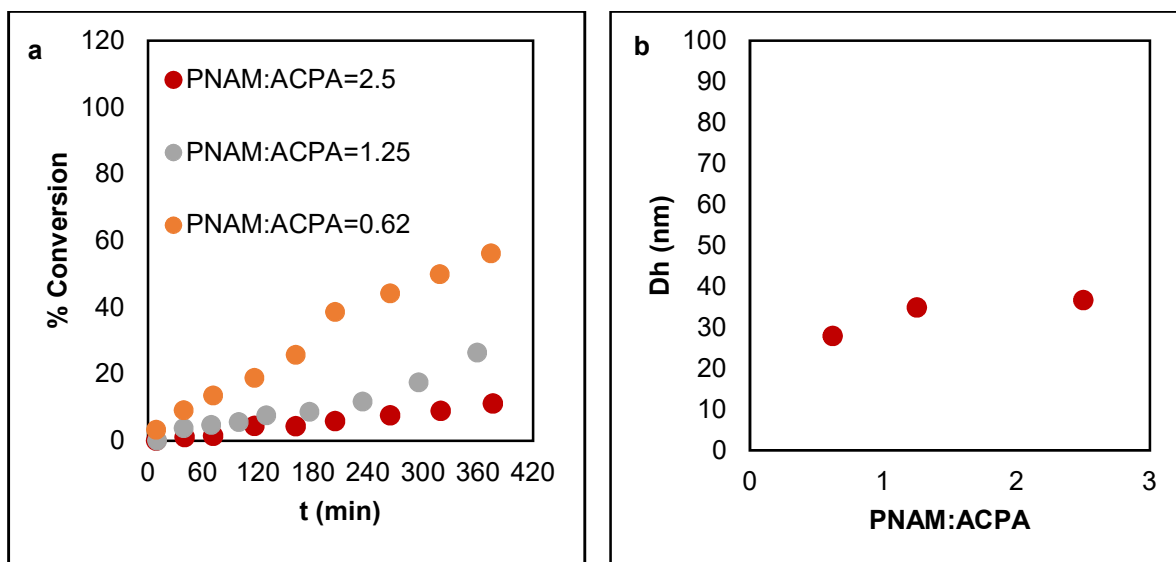
*Figure 56. a) Kinetics of PISA-RAFT by changing PNAM: ACPA ratio (**PISA 13, PISA 14** and **PISA 16**). b) Particle size of PISA-RAFT by changing PNAM: ACPA ratio after 6h of reaction (**PISA 13, PISA 14** and **PISA 16**).*

The increase of ACPA initiator thus led to an increased polymerization rate. However, at the same time, the resulting increased radical concentration favored a loss of control of particle synthesis (involving dithioester degradation and production of pBA homopolymer chains without PNAM stabilizing block). The best compromise appeared to be [ACPA]=1.3 mM (PNAM:ACPA=1.25) for a good conversion after 6h polymerization (26%) while limiting this control loss. It was selected for the rest of the study

3.3.4.7.   Optimized parameters for PISA-RAFT with AuNCs

The aim is to assure that the AuNCs keep their properties and PISA-RAFT proceeds in a reproducible and controlled way.

After studying the effect of temperature in the AuNCs and in PISA-RAFT, separately, it was explored if satisfactory PISA-RAFT with AuNCs experiments could be run not at 80°C for 20h as before. Two other options were study:

(i)   PISA-RAFT with AuNCs at 80°C for 2h with PNAM: ACPA=2.5;

(ii)   PISA-RAFT with AuNCs at 65°C for 6h with PNAM: ACPA=1.25.

3.3.4.7.1. Visual aspect of reaction medium

The visual aspect of both syntheses was similar in the beginning, but the sample after 6h at 65°C is more turbid than the one at 80°C after 2h (Figure 57). After leaving the samples to rest for a few hours, 2 phases appear in both cases, due the partial conversion of nBA that phase separated.

While the samples from **PISA15** present a dark brown phase on top and the a more salmon aqueous bottom phase, with sedimentation of dark particles, the sample from **PISA19** has a light brown aqueous phase with a darker brown top phase of dark brown and no sedimentation. It seems that the AuNCs are more stable when PISA-RAFT is conducted at 65°C (**PISA19**).

*Figure 57. Visual aspect of PISA-RAFT with AuNCs at 80°C for 2h and PNAM: ACPA=2.5 (**PISA 15**) and at 65°C for 6h and PNAM: ACPA=1.25 (**PISA 19**).*

3.3.4.7.2. Kinetics

Polymerization rate was faster at 80°C with PNAM: ACPA=2.5 than at 65°C with PNAM:ACPA=1.25 (41% conversion after 6h) (Figure 58). The conversion at 80°C after 2h (46% conversion) was however similar to the conversion at 65°C after 6h.

The advantage of the synthesis at 80°C is the possibility to achieve the same conversion in a smaller period of time. However, a higher temperature may also favor a faster AuNCs degradation rate.

*Figure 58. Kinetics of PISA-RAFT with AuNCs at 80°C for 2h and PNAM: ACPA=2.5 (**PISA 15**) and at 65°C for 6h and PNAM: ACPA=1.25 (**PISA 19**).*

3.3.4.7.3. PNPs size

The hydrodynamic diameter for the particles were similar at 80°C after 2h is (26.8±0.4) nm and at 65°C after 6h is (28.3±0.3) nm (Figure 59). But while at 80°C there is only one population, there was two at 65°C. The second population has about (166±21) nm, and this population represents about 0.3% in number. This bigger population seems responsible for the increase in the solution turbidity mentioned before.

*Figure 59. Particle size distribution (DLS) of PISA-RAFT with AuNCs at 80°C for 2h and PNAM: ACPA=2.5 (**PISA 15**) and at 65°C for 6h and PNAM: ACPA=1.25 (**PISA 19**).*

TEM gave similar results, being the core and shell thickness of the particles measured as in section 3.3.4 (Table 16). However slightly smaller diameters were obtained compared to TEM (Figure 60). This can be due to the fact that PNP are dried on the TEM grid, leading to a hydrophilic shell collapse whereas DLS hydrodynamic diameters are measured in solution.

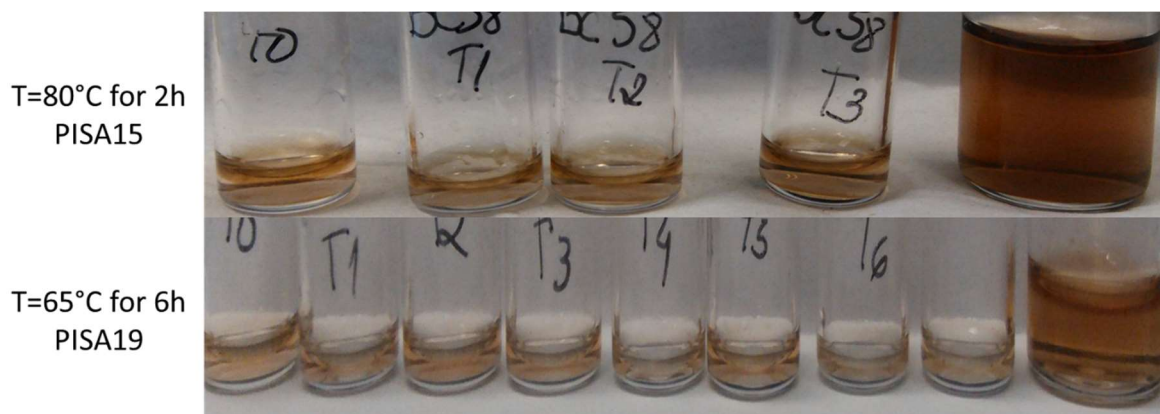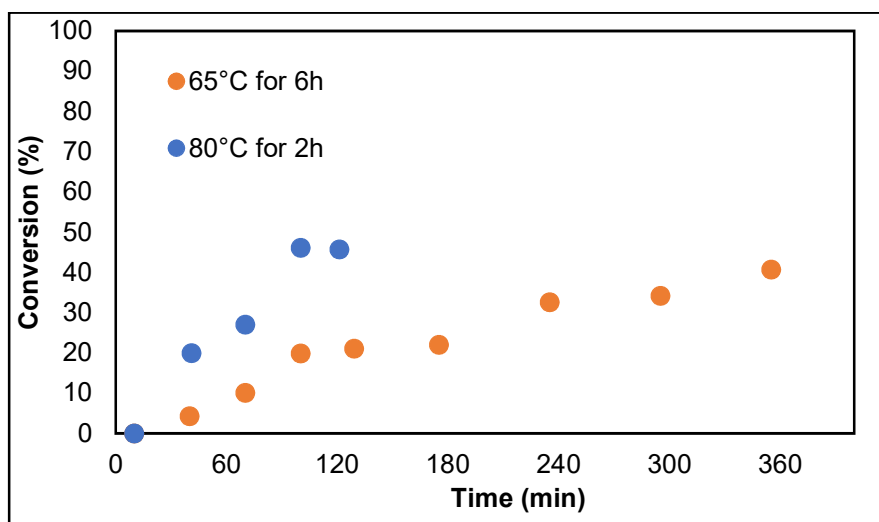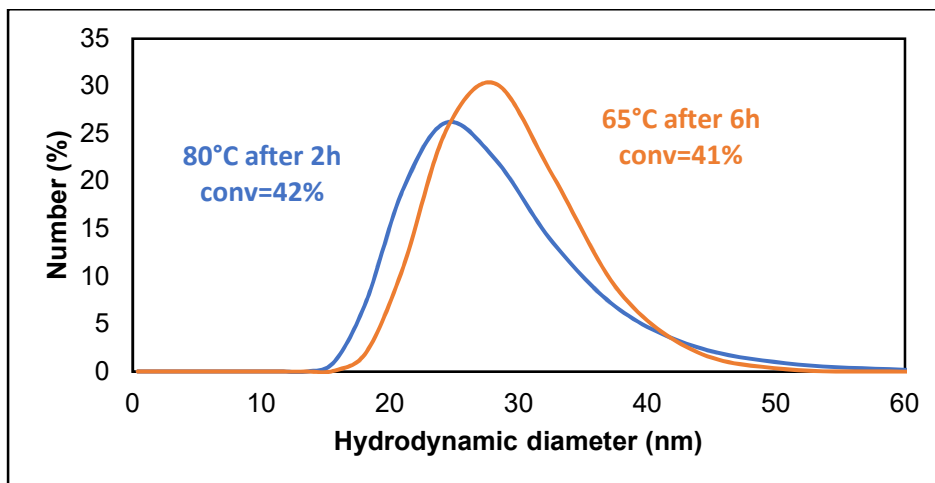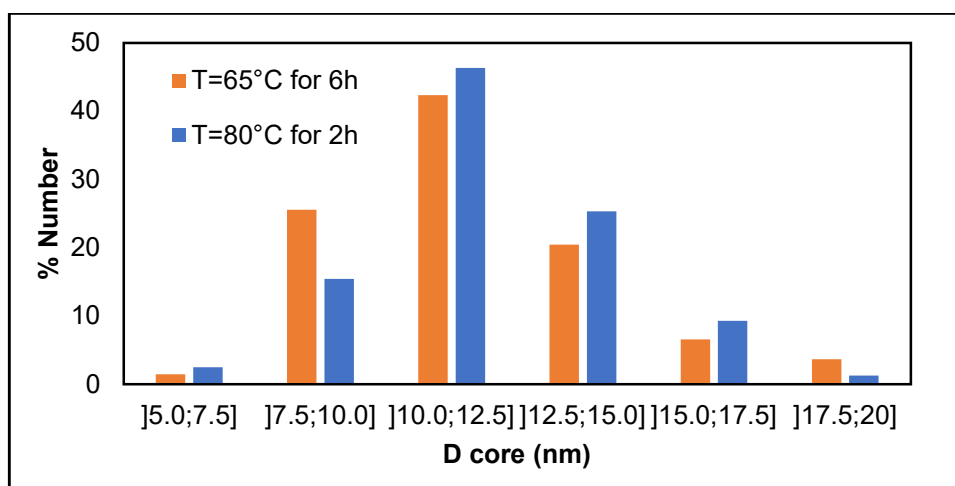*Figure 60. Particle size distribution (DLS) of PISA-RAFT with AuNCs at 80°C for 2h and PNAM: ACPA=2.5 (**PISA 15**) and at 65°C for 6h and PNAM: ACPA=1.25 (**PISA 19**).*

Table 16. Comparison between average results by TEM and by DLS.

	D core (TEM, nm)	Shell thickness (TEM, nm)	D (TEM, nm)	D_h (DLS, nm)
With AuNCs @ 80°C	12±2	4±1	20	26.8±0.4
With AuNCs @ 65°C	9±3	4±1	17	28.3±0.3

For the experiment at 80°C for 2h, the supernatant top phase, corresponding to the remaining nBA monomer not polymerized, was characterized by HR TEM to study AuNCs degradation (Figure 61a).

The AuNCs appeared well dispersed in the organic phase, even after being at 80°C with strong stirring during PISA-RAFT. In terms of size (Figure 61b), the average diameter is (1.8±0.5) nm, similar to the size previously measured in nBA (organic phase) and in water (before PISA-RAFT). It shows that the AuNCs seem not degraded (at least in the monomer phase) during 2h at 80°C.
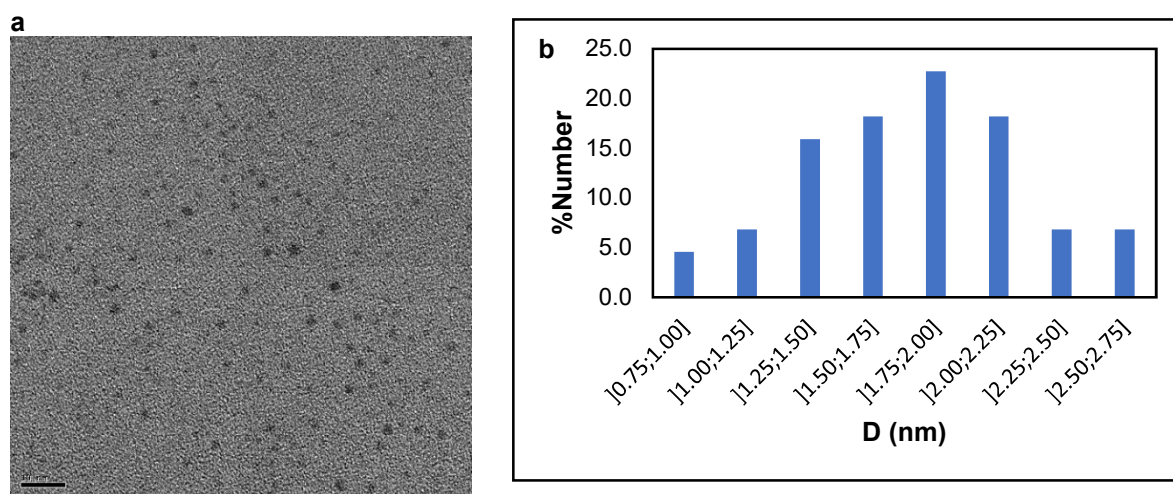
*Figure 61. a) HR TEM image of Au$_{25}$(MHA)$_{18}$ organic phase (top phase) of PISA-RAFT at 2h at 80°C with high stirring velocity (**PISA 15**). b) Size distribution by HR TEM of Au$_{25}$(MHA)$_{18}$ organic phase (top phase) of PISA-RAFT at 2h at 80°C with high stirring velocity (**PISA 15**).*

3.3.4.7.4. Optical properties of hybrid particles by PISA-RAFT with Au$_{25}$(MHA)$_{18}$

The fluorescence emission spectra were acquired in the same conditions for both cases:

(iii)   PISA-RAFT with AuNCs at 80°C for 2h with PNAM: ACPA=2.5;

(iv)   PISA-RAFT with AuNCs at 65°C for 6h with PNAM: ACPA=1.25.

The spectra show the presence of AuNCs in the aqueous phase of PISA-RAFT in both cases, with emission maximum at 815 nm. It also shows that the aqueous phase PISA-RAFT at 65°C has more intensity than at 80°C (Figure 62). Difference in the fluorescence intensity may indicate that there is more AuNCs degradation for 2 h at 80°C than for 6 h at 65°C. In the future it would thus be interested to further improve PISA-RAFT PNPs synthesis at temperatures similar or lower than 65°C (maintaining PNPs synthesis control, favoring high conversion in short polymerization times).

To confirm the fine location of the AuNCs inside or outside the PNPs further analyses are needed. The location of the AuNCs was not confirmed by TEM or HR TEM, but size exclusion techniques can be later applied to obtain such answers. But these results open good perspectives to future work.
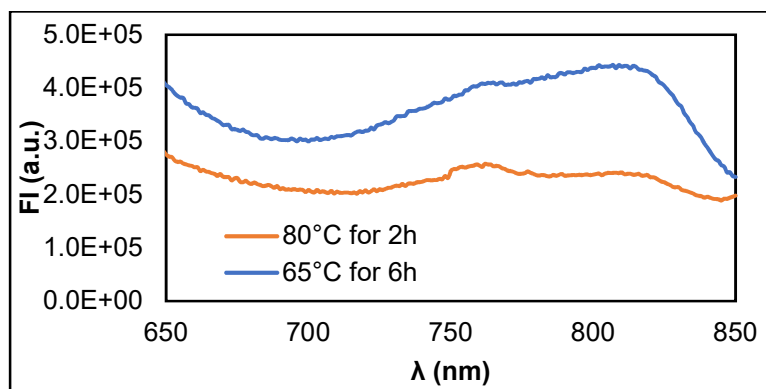
*Figure 62. Fluorescent emission spectra of PISA-RAFT with AuNCs at 80°C for 2h and PNAM: ACPA=2.5 (**PISA 15**) and at 65°C for 6h and PNAM: ACPA=1.25 (**PISA 19**), with λ_{exc}=450 nm.*

3.3.4.8. Study of parameters to increase PISA-RAFT kinetics at 80°C

As it seems that low PISA-RAFT polymerization time limit AuNCs degradation, it would be valuable to find means to increase PISA-RAFT kinetics. The system ''80°C for 2h'' was selected to study/test different solutions. Increasing the ACPA concentration, decreasing the nBA:PNAM ratio and decreasing the [AuNCs] in nBA. Briefly, those experiments did not bring much improvement in terms of kinetics and more generally on the final particles (see Annexes V and VI).

3.3.4.9. Influence of AuNCs type: from Au_{25} to Au_5 and Au_{11}

PISA-RAFT was also performed in the presence of Au_5 and Au_{11} (section 3.1.4.), not only to check the stability of these smaller AuNCs, but to see if the influence in PISA-RAFT was different than the Au_{25} in terms kinetics and particle size. The conditions chosen for the synthesis were 80°C for 2h with PNAM:ACPA=2.5. These conditions were chosen since there is a higher control of polymerization.

Due to stability issues, the concentration of AuNCs in organic phase (nBa and acetonitrile) had to be decreased to 0.070Mm (calculated according to section 3.3.4). At higher concentration the AuNCs properties change rapidly, identified by the change in color from transparent to brown.

3.3.4.9.1. Visual aspect of reaction medium

The visual aspect of the PISA-RAFT medium differs (Figure 63). Using the Au_{25}, the medium is brown and have two phases, as described in the previous sections. With the Au_5 and Au_{11}, the medium keeps the salmon color and there is no phase separation after 2h.
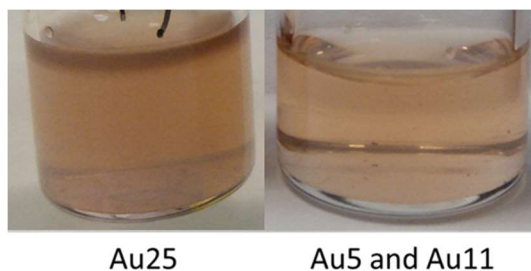
*Figure 63. Visual aspect of PISA with AuNCs solutions after 2h at 80°C, varying the size of AuNCs (**PISA 22** and **PISA 25**).*

3.3.4.9.2. Kinetics

The polymerization rate is similar for the PISA-RAFT with Au_{25} and with Au_5 and Au_{11} (Figure 64). It suggests that the size of the AuNCs does not influence the kinetics of PISA-RAFT. The final conversion, after 2h, is 45% for Au_{25} and 48% for Au_5 and Au_{11}.
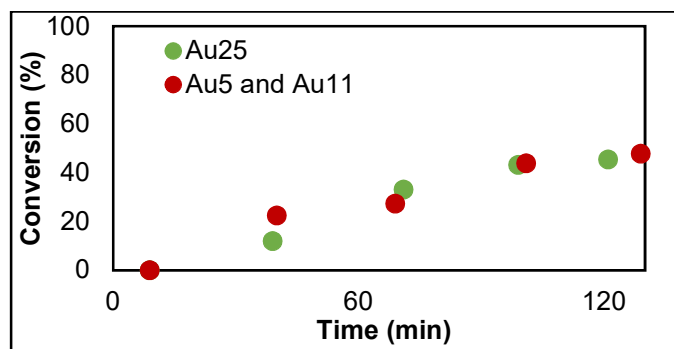
*Figure 64. Kinetics of PISA with AuNCs solutions after 2h at 80°C, varying the size of AuNCs (**PISA 22** and **PISA 25**).*

3.3.4.9.3. PNPs size

The particles size, using the Au_{25} with 45% conversion, is (34±1) nm. For the PNPs incorporating Au_5 and A_{11}, the size is (34±1) nm for 48% of conversion. Both syntheses led to similar average size and size distribution (Figure 65). The size of the AuNCs does not influence significantly the size of the PNPs.
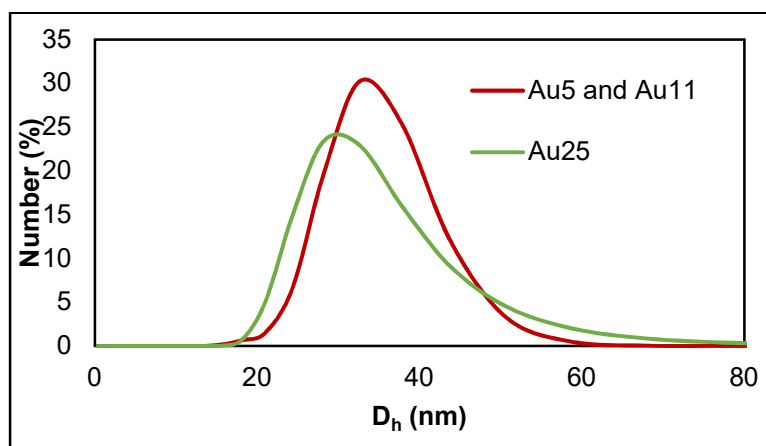
*Figure 65. Size distribution (DLS) of PISA-RAFT with AuNCs solutions after 2h at 80°C, varying the size of AuNCs (**PISA 22** and **PISA 25**).*

3.3.4.9.4. Optical properties

The Au_5/Au_{11} are expected to have to emission bands (380 nm and 500 nm). By analyzing samples of PNPs by PISA-RAFT without AuNCs and with AuNCs from both sizes, 2 bands in that region are detected with maximum at 445 nm and 540 nm (Figure 66a). The band has about 8 times more intensity in the polymer without AuNCs than with AuNCs. The excitation spectra with emission wavelength of 450 nm, have a maximum at about 400 nm (Figure 66b).

The bands apparently correspond to the polymer, and since they are located in the same region as the Au_5/Au_{11} with high intensity, it is not possible to confirm the presence or absence of the AuNCs. These results are surprising, and further investigation is needed to make more precise conclusions.
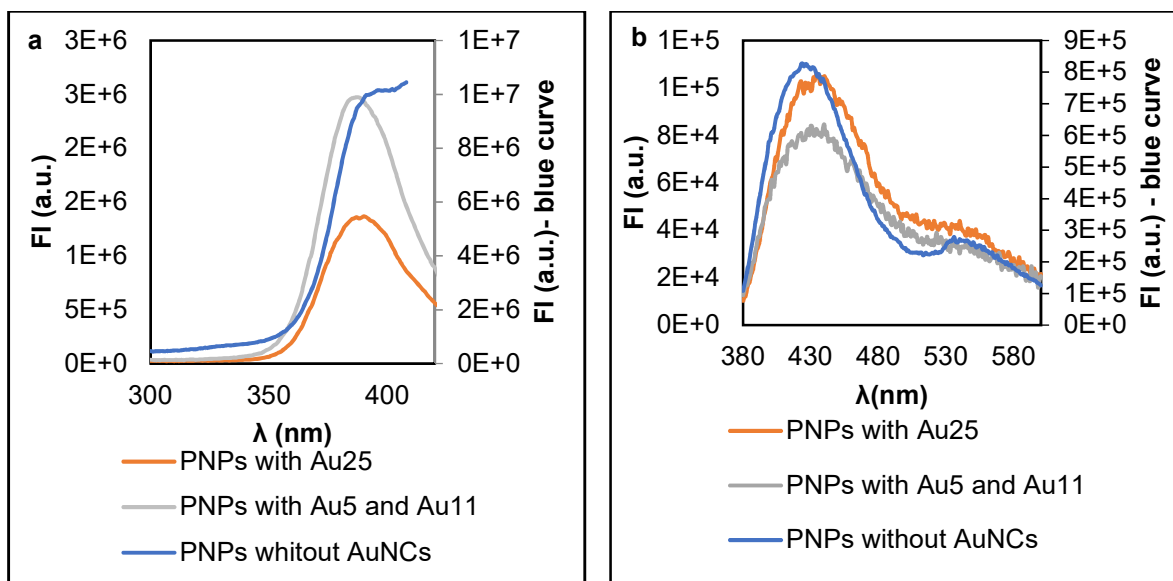
*Figure 66. Excitation spectra with λ_{em}=450 nm (a) and emission spectra with λ_{exc}=350 nm (b) of polymer nanoparticles (**PISA18**), polymer nanoparticles with Au_{25}(**PISA19**) and polymer with Au5 and Au11 (**PISA 25**).*

3.3.4.9.5. Conclusions

The kinetics is similar in both cases, but in the presence of Au_5 and Au_{11}, after the 2h there was only one phase, while for $Au_{25}(MHA)_{18}$ there was two phases. It suggests that the smaller AuNCs lead to a faster stabilization of the polymerization medium. The bond between ligand and gold, in smaller AuNCs, is less strong, which can lead to less MHA attached to the AuNCs. Consequently, more CTAB was free to act as surfactant in the micelles of PISA-RAFT. On the other hand, the fact that similar PNPs size was obtained suggests that the free CTAB concentration in both cases is the same. So, it was not the excess of CTAB that lead to the faster stabilization of nBA in the aqueous phase. It may be due to the properties of the smaller AuNCs. To confirm it further studies are needed.

In terms of optical properties, it was not possible to make conclusive observations.

3.3.4.10. Synthesis of core-crosslinked PNPs

In the incorporation of inorganic solids into polymer particles, crosslinkers can be used to better stabilize the PNPs and inorganic they incorporate. BDDA crosslinker was then used to synthesize core-crosslinked PNPs incorporating AuNCs (polymerization parameters were 80°C for 2h with smaller (Au_5 and Au_{11}) and bigger ($Au_{25}(MHA)_{18}$) AuNCs). 1,4-butanediol diacrylate (BDDA) has previously been used successfully by D. Duret in PISA-RAFT without AuNCs (no influence in terms of kinetics or particle size [30]).

3.3.4.10.1. Visual aspect of reaction medium

In the presence of crosslinker for PISA-RAFT incorporating $Au_{25}(MHA)_{18}$ (Figure 67a), the solution acquires a darker color, even after the phase occur. This is not fully understood at this stage, but it may be due an increase of concentration of AuNCs in the aqueous medium encapsulated in the PNPs or due to a change in the AuNCs properties conferring them a darker color.

While without crosslinker, with time there is some sedimentation of AuNCs in the bottom, in the presence of crosslinker there is no sedimentation, which may be correlated with the difference in color. The

absence of sedimentation and darker color seem to indicate a higher concentration of AuNCs in the PISA-RAFT aqueous phase.

After the PISA-RAFT incorporating Au_5 and Au_{11}, the reaction medium is slightly more turbid than for the synthesis without crosslinker (Figure 67b). No color change is witnessed since the AuNCs remains transparent in both syntheses.
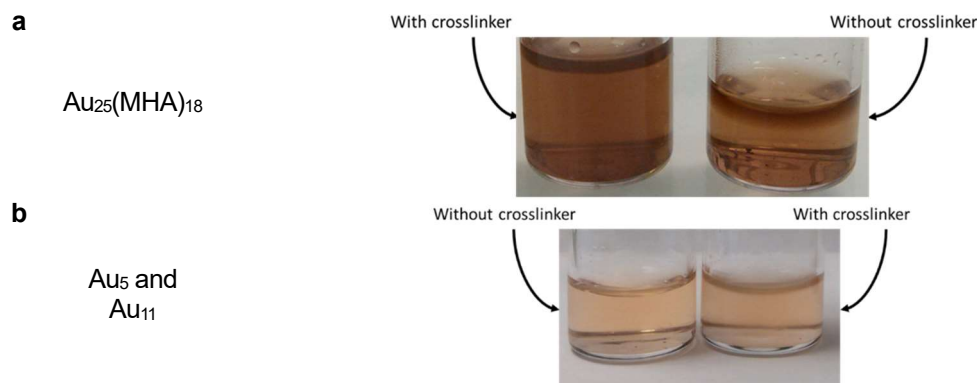
*Figure 67. a) Visual aspect of PISA-RAFT with $Au_{25}(MHA)_{18}$ solutions after 2h at 80°C, varying the presence of crosslinker (BDDA) (**PISA 23** and **PISA 24**). b) Visual aspect of PISA-RAFT with $Au_{25}(MHA)_{18}$ solutions after 2h at 80°C, varying the presence of crosslinker (BDDA) (**PISA 25** and **PISA 26**)*

3.3.4.10.2. Kinetics

The results show no influence of the crosslinker in the kinetics (Figure 68), which is in agreement with the results of D. Duret [30]. The final conversion is 56% with crosslinker and 46% without crosslinker for PISA-RAFT incorporating $Au_{25}(MHA)_{18}$, and 53% with crosslinker and 48% without crosslinker for PISA-RAFT incorporating Au_5 and Au_{11}. The difference can be justified by a sampling problem in the synthesis without crosslinker, since after the sample at 100min, there is a stabilization and the conversion does not change more.
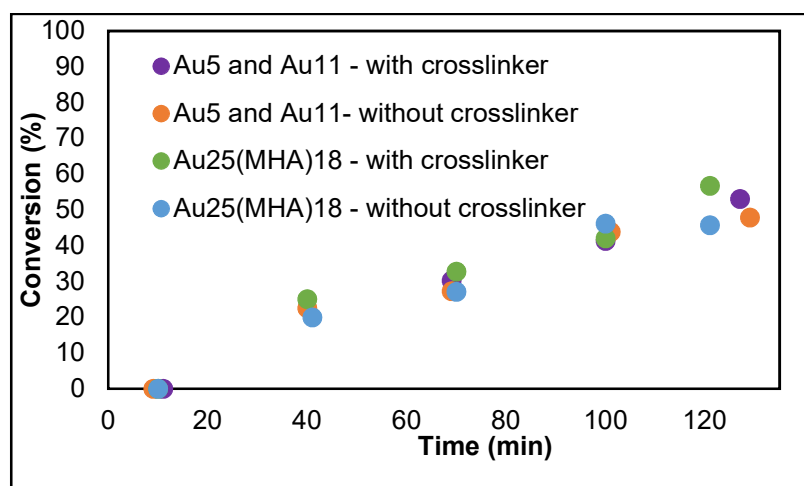
*Figure 68. Kinetics of PISA-RAFT with AuNCs solutions after 2h at 80°C, varying the presence of crosslinker (BDDA) and the AuNCs size (**PISA 23** to **PISA 26**).*

3.3.4.10.3. PNPs size

In terms of size, without crosslinker it is (28±2) nm and with crosslinker it is (31±2) nm, for PISA-RAFT incorporating $Au_{25}(MHA)_{18}$. For the PISA-RAFT incorporating Au_5 and Au_{11}, the PNPs with crosslinker have

(32.0±0.4) nm, while without have (34±1) nm. It seems that the presence of crosslinker does not influence PNPs size neither the size distribution (Figure 69), but further tests are needed to confirm such conclusion.
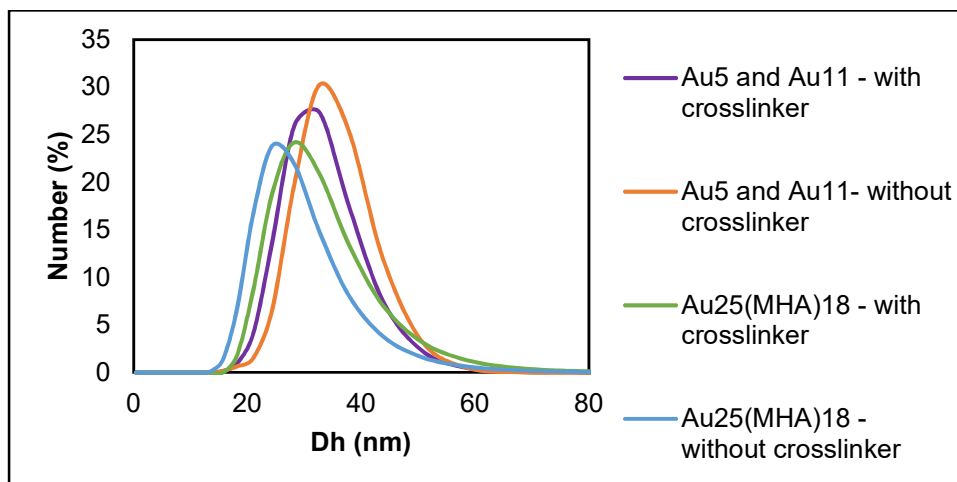
*Figure 69. Size distribution of PISA-RAFT with AuNCs solutions after 2h at 80°C, varying the presence of crosslinker (BDDA) and AuNCs size (**PISA 23** to **PISA 26**).*

3.3.4.10.4.   Optical properties

In terms of optical properties, there was no fluorescence emission in the presence of crosslinker, for $Au_{25}(MHA)_{18}$. But this happens with all the PISA-RAFT incorporating the AuNCs of a certain synthesis (**Au 42**). The issue is probably the AuNCs synthesis and not the effect of the crosslinker. Further test is needed to confirm the optical properties of PNPs with AuNCs in the presence of crosslinker.

For the smaller AuNCs (Au_5 and Au_{11}), it is not possible to evaluate the emission of the AuNCs in the PNPs due to the polymer emission.

4. Conclusions and Outlook

The objective of the project was to stabilize AuNCs through incorporation into polymer nanoparticles (PNPs) by miniemulsion polymerization and PISA-RAFT. It starts by the study of AuNCs in terms of size, optical properties and stability.

$Au_{25}(MHA)_{18}$ were studied, proving gold clusters with 25 atoms are one of the most stable (keep their optical properties for a period of about 90 days). They were characterized in terms of optical properties by UV-Vis spectroscopy and fluorescence spectroscopy. The two bands in the UV-Vis absorption spectrum characteristic of $Au_{25}(SR)_{18}$ were identified, being at 440 nm and 670 nm. In terms of fluorescence emission, the maximum emission was at 810 nm, for excitation wavelengths from 450 nm to 650 nm. These wavelengths (emission and excitation) correspond to the near-IR window for biological tissue (therapeutic window). $Au_{25}(MHA)_{18}$ optical properties are indicated for biological applications, such as bioimaging. The size was determined by HR TEM as being (1.8±0.6) nm, which is according to the size determined by other researchers in $Au_{25}(SR)_{18}$.

Au_5/Au_{11} were synthesized by modification of the MHA:Au and $NaBH_4$:Au from $Au_{25}(MHA)_{18}$. In terms of optical properties, it was not possible to determine the UV-Vis absorption spectrum, which can be due to the presence of multiple populations (AuNCs with different sizes) or to the low concentration of AuNCs (which is below the equipment detection capacity). Fluorescence emission and excitation spectroscopy showed two populations, one emitting at 380 nm and another at 500 nm. The number of atoms of each population was determined using the Jellium equation (equation 8). This method is an indirect method, with different approximations. The value can be confirmed by other methods such as ESI mass in future studies. The size was studied by HR TEM. But since they are smaller, it was not possible to determine the exact value. The stability of Au_5/Au_{11} is lower than $Au_{25}(MHA)_{18}$, keeping their properties for about one week. To improve the stability of Au_5/Au_{11} parameter, such as pH, temperature, gold salt concentration, can be improved.

The study of MHA:Au and $NaBH_4$:Au molar ratios, keeping the gold salt concentration constant, improved the understanding of the AuNCs synthesis. The increase in the ratio of MHA:Au leads to the formation and stabilization of smaller AuNCs. On the other hand, changing $NaBH_4$:Au ratio didn't lead to clear conclusions, because the MHA:Au was too high. To better study this parameter, a lower MHA:Au ratio should be employed. These conclusions were according the idea that the reaction consist in an equilibrium between reduction and etching. The MHA (ligand) concentration shift the reaction to etching (smaller particles), while the $NaBH_4$ (reducing agent) shift to the reduction of gold (bigger particles). To a more complete understanding of AuNCs synthesis, other parameters can be studied, such as the concentration of gold salt and the use of different gold salts. Parameters such as temperature and pH have already been studied and optimized for the present synthesis of $Au_{25}(MHA)_{18}$ [26, 58], and can be studied to optimize the synthesis of the smaller AuNCs.

Two syntheses were performed by miniemulsion polymerization using different monomers: styrene and butyl methacrylate. The polymerization with styrene was successfully done with a conversion of 70% obtaining particles of about 60 nm of diameter. To improve the encapsulation of the AuNCs, avoiding their evolution to AuNPs, some parameters such as reaction time and temperature could be optimized as in the synthesis by PISA-RAFT. AuNCs seem to be stable in styrene and in polystyrene, but this polymer shows the presence of an excimer which can mask the AuNCs emission. To avoid that, the polymerization was done using butyl methacrylate as monomer. The conversion obtained was lower, about 24%, and the particles diameter

was about 30 nm. The difference of stability of the AuNCs from one polymerization to the other can be related to the stability of the AuNCs, since different kind of AuNCs were used, or due to the monomer used. In any case, the miniemulsion polymerization parameters (the concentration of monomer, hexadecane, initiator and CTAB) should be optimize in the case of butyl methacrylate to obtain higher conversion. Even without optimizing the miniemulsion polymerization for BMA, it seems that the AuNCs are inside the PBMA particles. Miniemulsion polymerizations was successfully used to encapsulate and stabilize AuNCs.

PISA-RAFT experiments in the presence of AuNCs were conducted in the conditions present in Table 14. They were based on previous optimizations performed by D. Duret for PISA-RAFT without AuNCs [30]. 27 nm PNPs in the presence of AuNCs were successfully obtained at 80°C. Compared with the same PISA-RAFT without AuNCs, polymerization kinetics was similar, but PNPs size was about two times smaller.

Table 17. Parameters from PISA-RAFT in the presence of AuNCs.

Monomer	Butyl acrylate (nBA)
macroCTA	PNAM
Initiator	ACPA
PNAM:ACPA (molar)	2.5
nBA:PNAM (molar)	157
Temperature (°C)	80

The decrease of AuNCs concentration from 0.140 mM to 0 mM, leads to a decrease of the PNPs size from 25 nm to 45 nm, not having a major influence in kinetics. It can be due to the presence of CTAB acting as surfactant or because the AuNCs themselves may act as a surfactant.

As PISA-RAFT is a quite recent technique, optimization of several different parameters had to be studied for the AuNCs incorporation into the PNPs, such as AuNCs phase transfer and stability in nBA, degassing methods, storage temperature, crosslinker, AuNCs size, polymerization temperature and duration, and PNAM:ACPA ratio.

Transferring the AuNCs to nBA was optimized to increase the efficiency of the process and reduce the interference in the PISA-RAFT. The co-solvent used was acetonitrile, which is one of the PISA-RAFT solvents. The amount of CTAB (ionic phase transfer agent) and acetonitrile (co-solvent) were optimized (minimum amount possible to obtain efficient phase transfer and separation). The optimized solution of CTAB has a concentration of 100 mM in 80% (v) acetonitrile and 20% (v) water. After the phase transfer, the organic phase with the AuNCs is 49.7% (v) nBA and 50.3% (v) acetonitrile as determined by gas chromatography.

The stability of the $Au_{25}(MHA)_{18}$ in the organic phase was analyzed by HR TEM and TEM. With both techniques, the size measured for the AuNCs was about the same as in water (about 1.8 nm) and they were well dispersed on the grid, not showing signs of aggregation. The $Au_{25}(MHA)_{18}$ are stable in nBA and acetonitrile with concentrations higher than in water.

Since generally used deoxygenation technique leads to destabilization of the AuNCs in the nBA phase (favored by low temperature and gas bubbles), a new methodology was set-up. Performing the deoxygenation of the initial polymerization medium by Argon flushing in the presence of a vapor condenser appeared as the best compromise since deoxygenation is efficient while avoiding AuNCs destabilization.

In terms of storage conditions, it was determined that the particles with a nBA core tend to evolve to bigger particles when store at -20°C undergoing an irreversible process. To avoid any change in size of morphology, the PNPs were stored at room temperature for this study.

The crosslinker, at 80°C for 2h, didn't interfere with kinetics of PNPs size. Further studies are required to conclude the effect in AuNCs encapsulation and stabilization. It seems to lead to a darker polymerization medium, each can be due to a higher concentration of AuNCs in the medium or to a change in their properties, and avoid the sedimentation of AuNCs.

The use of AuNCs with different sized seems not influence the polymerization, since the kinetics and particles size remain the same. The advantage of using the $Au_{25}(MHA)_{18}$ is their higher stability during phase transfer. For the incorporation of the small AuNCs, the phase transfer should be optimized.

The PNP produced by PISA-RAFT at 80°C after 20h unfortunately did not show the characteristic fluorescence emission of the AuNC. This was attributed to a destabilization of the AuNC after exposition for a long period of time at 80°C. For this reason, 2 different approaches using $Au_{25}(MHA)_{18}$ were explored to obtain fluorescent PNPs: (i) lowering polymerization temperature from 80°C to 65°C for 6h; and (ii) keeping the temperature at 80°C, but reducing the polymerization time to 2h. Different parameters were varied to obtain satisfactory nBA conversion while limiting AuNC degradation (ACPA initiator concentration (PNAM:ACPA ratio), nBA:PNAM ratio). Similar final conversion (~45%) and PNP size (~27 nm) were obtained in both cases.

Fluorescence emission analyses showed that PNPs produced by the 2 approaches emit fluorescence at a wavelength corresponding to the one of the AuNCs. In addition, it appeared that the PNPs produced at 65°C exhibit a higher fluorescence intensity. These very important results thus validated our hypotheses and provided very interesting and promising guidelines to further improvements in the future.

Both miniemulsion and PISA-RAFT polymerization techniques were thus successfully used to encapsulate AuNCs. HR TEM and TEM were used in order to confirm the location of the AuNCs inside the core of the PNPs. But due to the low PNPs size and the limits of the techniques, the first analyses did not provide yet convincing results. In future works, the location and organization of the AuNCs in PNPs could be studied by size exclusion techniques after the purification of PNPs for instance by ultrafiltration. The percentage of AuNCs inside and out of the PNPs can also be investigated.

Different parameters in PISA can also be evaluated in future projects to work at lower temperature (avoid AuNCs decomposition) such as different initiators, CTA and to increase PNPs size (facilitate PNPs study), such as size of PNAM chain, the amount of BA, and the type of hydrophobic monomer (easy to visualize PNPs by TEM, compatibility with AuNCs.

The phase transfer in future work can be optimized by trying different surfactants (biocompatible). Another option is the synthesis of AuNCs in different solvents, avoiding at all the use of surfactant.

The simplification of the process by doing one pot-synthesis of AuNCs and PNPs, by both polymerization techniques, have also interest for future work.

References

1. Hutchings, G.J., M. Brust, and H. Schmidbaur, *Gold - an introductory perspective*. Chemical Society Reviews, 2008. **37**(9): p. 1759-1765.
2. Mingos, D.M.P., *Gold Clusters, Colloids and Nanoparticles I*2014: Springer International Publishing.
3. Faraday, M., *The Bakerian Lecture: Experimental Relations of Gold (and Other Metals) to Light*. Philosophical Transactions of the Royal Society of London, 1857. **147**: p. 145-181.
4. Buceta, D., et al., *Metallic Clusters: Theoretical Background, Properties and Synthesis in Microemulsions*. Catalysts, 2014. **4**(4): p. 356-374.
5. Jin, R.C., *Quantum sized, thiolate-protected gold nanoclusters*. Nanoscale, 2010. **2**(3): p. 343-362.
6. S. G., B., *Síntesis, caracterización y propiedades fluorescentes de clústeres cuánticos subnanométricos*, in *Departamento de Química-Física*2012, Universidade de Santiago de Compostela: Facultad de Química. p. 173.
7. Romão Dias, A., *Ligação Química*. 2th ed2006: IST Press.
8. Zheng, Y., et al., *Recent advances in biomedical applications of fluorescent gold nanoclusters*. Advances in Colloid and Interface Science, 2017. **242**: p. 1-16.
9. Yu, Y.Y., et al., *Dendrimer-like core cross-linked micelle stabilized ultra-small gold nanoclusters as a robust catalyst for aerobic oxidation of alpha-hydroxy ketones in water*. Green Chemistry, 2016. **18**(12): p. 3647-3655.
10. Yasukawa, T., H. Miyamura, and S. Kobayashi, *Simple Homopolymer-incarcerated Gold Nanoclusters Prepared by Self-assembled Encapsulation with Aluminum Reagents as Crosslinkers: Catalysts for Aerobic Oxidation Reactions*. Chemistry Letters, 2015. **44**(1): p. 50-52.
11. Miyamura, H. and S. Kobayashi, *Tandem Oxidative Processes Catalyzed by Polymer-Incarcerated Multimetallic Nanoclusters with Molecular Oxygen*. Accounts of Chemical Research, 2014. **47**(4): p. 1054-1066.
12. Fang, J., et al., *The support effect on the size and catalytic activity of thiolated Au-25 nanoclusters as precatalysts*. Nanoscale, 2015. **7**(14): p. 6325-6333.
13. Snow, A.W., M.G. Ancona, and D. Park, *Nanodimensionally Driven Analyte Response Reversal in Gold Nanocluster Chemiresistor Sensing*. Langmuir, 2012. **28**(44): p. 15438-15443.
14. Ancona, M.G., et al., *Analyte kinetics in a nanocluster-based chemiresistor: A case study*. Sensors and Actuators B-Chemical, 2013. **177**: p. 936-946.
15. Yu, Y., et al., *Scalable and Precise Synthesis of Thiolated Au10-12, Au-15, Au-18, and Au-25 Nanoclusters via pH Controlled CO Reduction*. Chemistry of Materials, 2013. **25**(6): p. 946-952.
16. Zhang, W., et al., *Supramolecular Self-Assembly Bioinspired Synthesis of Luminescent Gold Nanocluster-Embedded Peptide Nanofibers for Temperature Sensing and Cellular Imaging*. Bioconjugate Chemistry, 2017. **28**(9): p. 2224-2229.
17. Chen, Y., et al., *Near-Infrared Emitting Gold Cluster–Poly(acrylic acid) Hybrid Nanogels*. ACS Macro Letters, 2014. **3**(1): p. 74-76.
18. Li, J.J., et al., *Nanomaterial-based activatable imaging probes: from design to biological applications*. Chemical Society Reviews, 2015. **44**(21): p. 7855-7880.
19. Yahia-Ammar, A., et al., *Self-Assembled Gold Nanoclusters for Bright Fluorescence Imaging and Enhanced Drug Delivery*. Acs Nano, 2016. **10**(2): p. 2591-2599.
20. Chen, D., et al., *Amphiphilic Polymeric Nanocarriers with Luminescent Gold Nanoclusters for Concurrent Bioimaging and Controlled Drug Release*. Advanced Functional Materials, 2013. **23**(35): p. 4324-4331.
21. Sahoo, A.K., et al., *Simultaneous RGB Emitting Au Nanoclusters in Chitosan Nanoparticles for Anticancer Gene Theranostics*. Acs Applied Materials & Interfaces, 2014. **6**(1): p. 712-724.
22. Wu, X.T., et al., *Multifunctional spherical gold nanocluster aggregate@polyacrylic acid@mesoporous silica nanoparticles for combined cancer dual-modal imaging and chemo-therapy*. Journal of Materials Chemistry B, 2015. **3**(12): p. 2421-2425.
23. Brust, M., et al., *Synthesis of thiol-derivatised gold nanoparticles in a two-phase Liquid-Liquid system*. Journal of the Chemical Society, Chemical Communications, 1994(7): p. 801-802.
24. Goswami, N., et al., *Mechanistic exploration and controlled synthesis of precise thiolate-gold nanoclusters*. Coordination Chemistry Reviews, 2016. **329**: p. 1-15.
25. Chen, T., et al., *Synthesis of thiolate-protected Au nanoparticles revisited: U-shape trend between the size of nanoparticles and thiol-to-Au ratio*. Chemical Communications, 2016. **52**(61): p. 9522-9525.
26. Yuan, X., et al., *Balancing the Rate of Cluster Growth and Etching for Gram- Scale Synthesis of Thiolate- Protected Au25 Nanoclusters with Atomic Precision*. Angewandte Chemie-International Edition, 2014. **53**(18): p. 4623-4627.
27. Carotenuto, G., S. De Nicola, and L. Nicolais, *Fluorescent Thiol-Derivatized Gold Clusters Embedded in Polymers*. Advances in Materials Science and Engineering, 2013. **2013**: p. 6.
28. Landfester, K., *Miniemulsions for Nanoparticle Synthesis*, in *Colloid Chemistry II*, M. Antonietti, Editor 2003, Springer Berlin Heidelberg: Berlin, Heidelberg. p. 75-123.
29. Schork, F.J., et al., *Miniemulsion Polymerization*, in *Polymer Particles: -/-*, M. Okubo, Editor 2005, Springer Berlin Heidelberg: Berlin, Heidelberg. p. 129-255.
30. Duret, D., *Développement de sondes polymères fluorescentes à propriétés de ciblage améliorées pour des applications en imagerie cellulaire et en oncologie*, in *INSA Lyon*2016.
31. Asua, J.M., *Miniemulsion polymerization*. Progress in Polymer Science, 2002. **27**(7): p. 1283-1346.
32. van Herk, A.M., *Historical Overview of (Mini)emulsion Polymerizations and Preparation of Hybrid Latex Particles*, in *Hybrid Latex Particles: Preparation with (Mini)emulsion Polymerization*, A.M. van Herk and K. Landfester, Editors. 2010, Springer Berlin Heidelberg: Berlin, Heidelberg. p. 1-18.
33. Ando, K. and H. Kawaguchi, *High-performance fluorescent particles prepared via miniemulsion polymerization*. Journal of Colloid and Interface Science, 2005. **285**(2): p. 619-626.
34. Lelu, S., et al., *Encapsulation of an organic phthalocyanine blue pigment into polystyrene latex particles using a miniemulsion polymerization*. Polymer International, 2003. **52**(4): p. 542-547.
35. Tronc, F., et al., *Fluorescent polymer particles by emulsion and miniemulsion polymerization*. Journal of Polymer Science Part a-Polymer Chemistry, 2003. **41**(6): p. 766-778.
36. Augusto, V., et al., *Oxygen-proof fluorescence temperature sensing with pristine C-70 encapsulated in polymer nanoparticles*. Journal of Materials Chemistry, 2010. **20**(6): p. 1192-1197.
37. Crespy, D. and K. Landfester, *Miniemulsion polymerization as a versatile tool for the synthesis of functionalized polymers*. Beilstein Journal of Organic Chemistry, 2010. **6**: p. 1132-1148.

38. Warren, N.J. and S.P. Armes, *Polymerization-Induced Self-Assembly of Block Copolymer Nano-objects via RAFT Aqueous Dispersion Polymerization.* Journal of the American Chemical Society, 2014. **136**(29): p. 10174-10185.

39. Tritschler, U., et al., *50th Anniversary Perspective: Functional Nanoparticles from the Solution Self-Assembly of Block Copolymers.* Macromolecules, 2017. **50**(9): p. 3439-3463.

40. Favier, A., M.T. Charreyre, and C. Pichot, *A detailed kinetic study of the RAFT polymerization of a bi-substituted acrylamide derivative: influence of experimental parameters.* Polymer, 2004. **45**(26): p. 8661-8674.

41. Charleux, B., et al., *Polymerization-Induced Self-Assembly: From Soluble Macromolecules to Block Copolymer Nano-Objects in One Step.* Macromolecules, 2012. **45**(17): p. 6753-6765.

42. Rieger, J., *Guidelines for the Synthesis of Block Copolymer Particles of Various Morphologies by RAFT Dispersion Polymerization.* Macromolecular Rapid Communications, 2015. **36**(16): p. 1458-1471.

43. Favier, A., et al., *Study of the RAFT Polymerization of a Water-Soluble Bisubstituted Acrylamide Derivative. 1. Influence of the Dithioester Structure.* Macromolecules, 2002. **35**(22): p. 8271-8280.

44. *The Transmission Electron Microscope.* 2017 13-10-2017]; Available from: https://www.nobelprize.org/educational/physics/microscopes/tem/.

45. Williams, D.B. and C.B. Carter, *Transmission Electron Microscopy - A Textbook for Materials Science.* Vol. 2. 2009: Springer.

46. *Dynamic light scattering - common terms defined* 2011, Malvern Instruments Limited.

47. Yao, Q.F., et al., *Introducing Amphiphilicity to Noble Metal Nanoclusters via Phase-Transfer Driven Ion-Pairing Reaction.* Journal of the American Chemical Society, 2015. **137**(5): p. 2128-2136.

48. Tauc, J., Grigorov.R, and A. Vancu, *OPTICAL PROPERTIES AND ELECTRONIC STRUCTURE OF AMORPHOUS GERMANIUM.* Journal of the Physical Society of Japan, 1966. **S 21**: p. 123-&.

49. Polozkov, R.G., et al., *New applications of the jellium model for the study of atomic clusters*, in *International Conference on Dynamics of Systems on the Nanoscale*2013, Iop Publishing Ltd: Bristol.

50. Kittel, C., *Introduction to Solid State Physics.* 8th edition ed2005: John Wiley & Sons, Inc.

51. Zheng, J., C.W. Zhang, and R.M. Dickson, *Highly fluorescent, water-soluble, size-tunable gold quantum dots.* Physical Review Letters, 2004. **93**(7).

52. Yuan, X., et al., *Insights into the effect of surface ligands on the optical properties of thiolated Au25 nanoclusters.* Chemical Communications, 2016. **52**(30): p. 5234-5237.

53. Preston, T.C., et al., *Role of Hydrogen Bonding in the pH-Dependent Aggregation of Colloidal Gold Particles Bearing Solution-Facing Carboxylic Acid Groups.* The Journal of Physical Chemistry C, 2009. **113**(32): p. 14236-14244.

54. Landfester, K., et al., *Miniemulsion polymerization with cationic and nonionic surfactants: A very efficient use of surfactants for heterophase polymerization.* Macromolecules, 1999. **32**(8): p. 2679-2683.

55. Kuo, A., *Fluorescence Resulting from π-stacking in Polystyrene Solutions.* ChemM, 2011.

56. Bathfield, M., et al., *Sub-micrometer sized hairy latex particles synthesized by dispersion polymerization using hydrophilic macromolecular RAFT agents.* Macromolecular Rapid Communications, 2007. **28**(15): p. 1540-1545.

57. Favier, A., et al., *Study of the RAFT polymerization of a water-soluble bisubstituted acrylamide derivative. 1. Influence of the dithioester structure.* Macromolecules, 2002. **35**(22): p. 8271-8280.

58. Chen, T., et al., *Heating or Cooling: Temperature Effects on the Synthesis of Atomically Precise Gold Nanoclusters.* The Journal of Physical Chemistry C, 2017. **121**(20): p. 10743-10751.

Annexes

I.   SEC-MALLS results relatively to final PNAM

The SEC-MALLS analysis was made to all the samples of PNAM polymerization (**RAFT1**). In all of them, the dispersity is close to 1 and the molecular weight shows a linear evolution, being the values presented on Table 18.

Table 18. Evolution of Mn and dispersity during RAFT polymerization of PNAM (RAFT1).

Mn (g/mol)	Dispersity	Sample
6986	1.042	RAFT1T2
8853	1.040	RAFT1T3
9901	1.037	RAFT1T4
10270	1.050	RAFT1T5

In Figure 70, it represents the SEC spectra of the sample RAFT1T5.
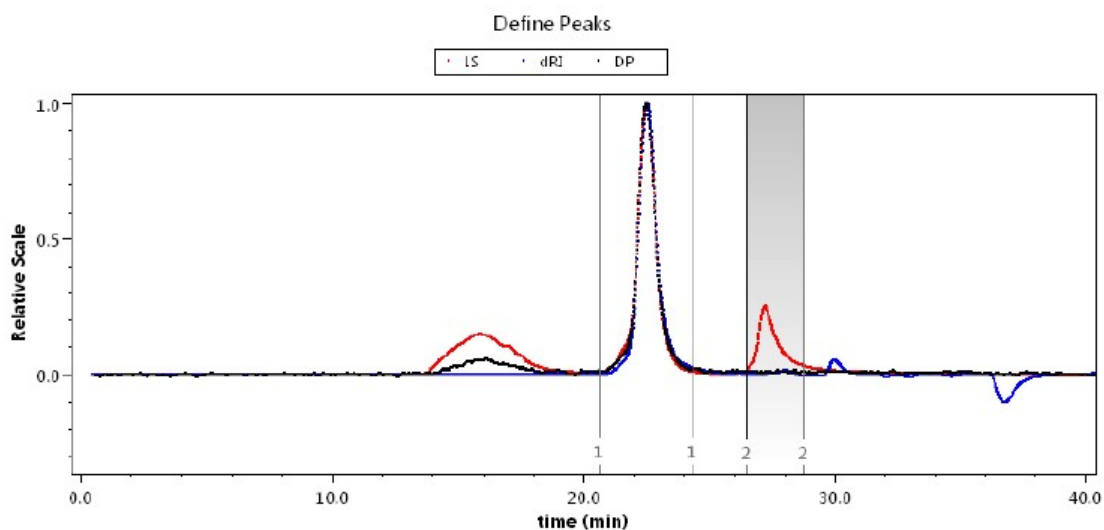
Figure 70. SEC results for PNAM with Mn of 10 300 g/mol after purification.

II.   GC results relatively to phase transfer of AuNCs to nBA

In Figure 71 it is present the weight composition (represented by area%) from the organic phase after transferring the AuNCs to nBA and acetonitrile. This is the composition after optimization of the system.
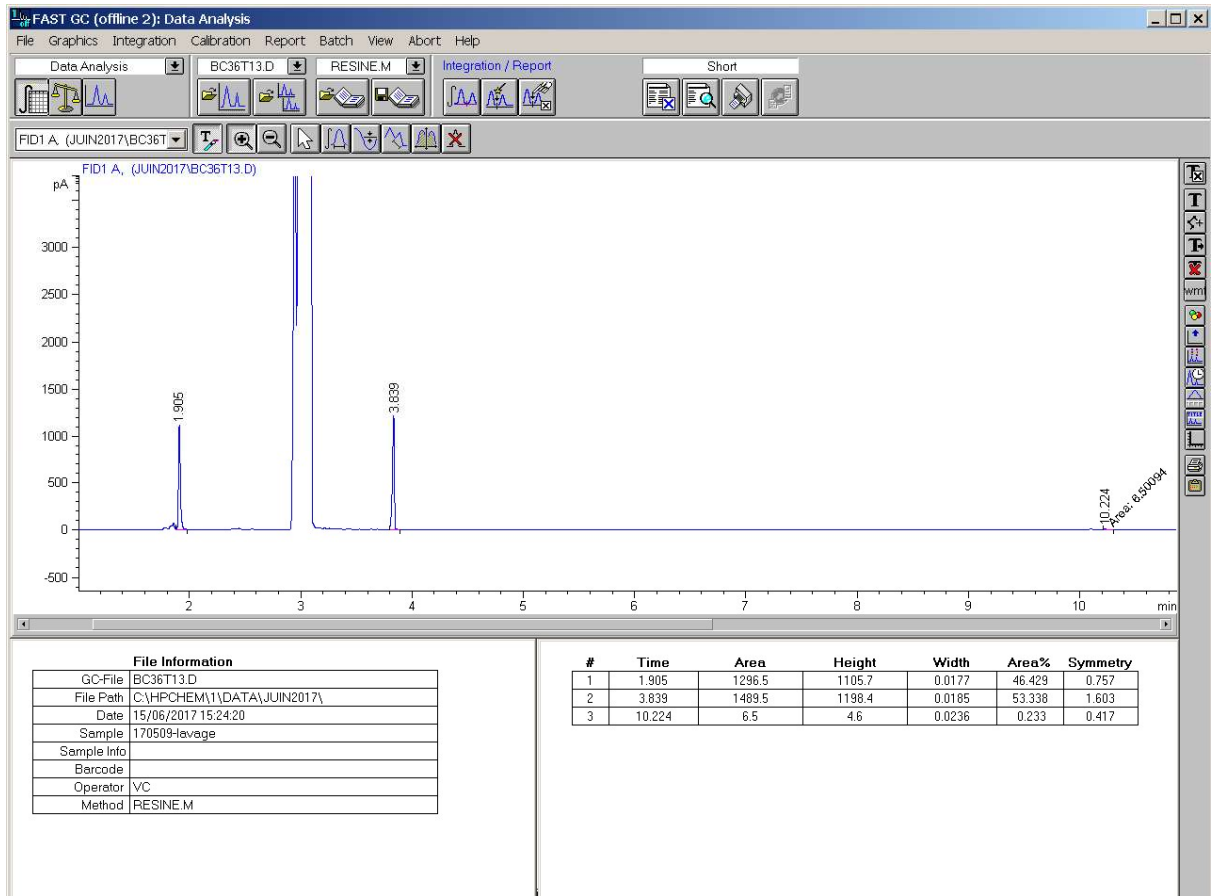
*Figure 71. GC spectrum of organic phase from **PT2T13**. It is the organic phase after optimizing the system, where the elution time of 10.2 min corresponds to the CTAB, 3.8 min corresponds to nBA and 1.9 min to acetonitrile.*

III.   ¹H NMR evolution of PISA-RAFT synthesis

The 1H NMR spectra for the different samples from **PISA 2** are presented from Figure 72 to 80.
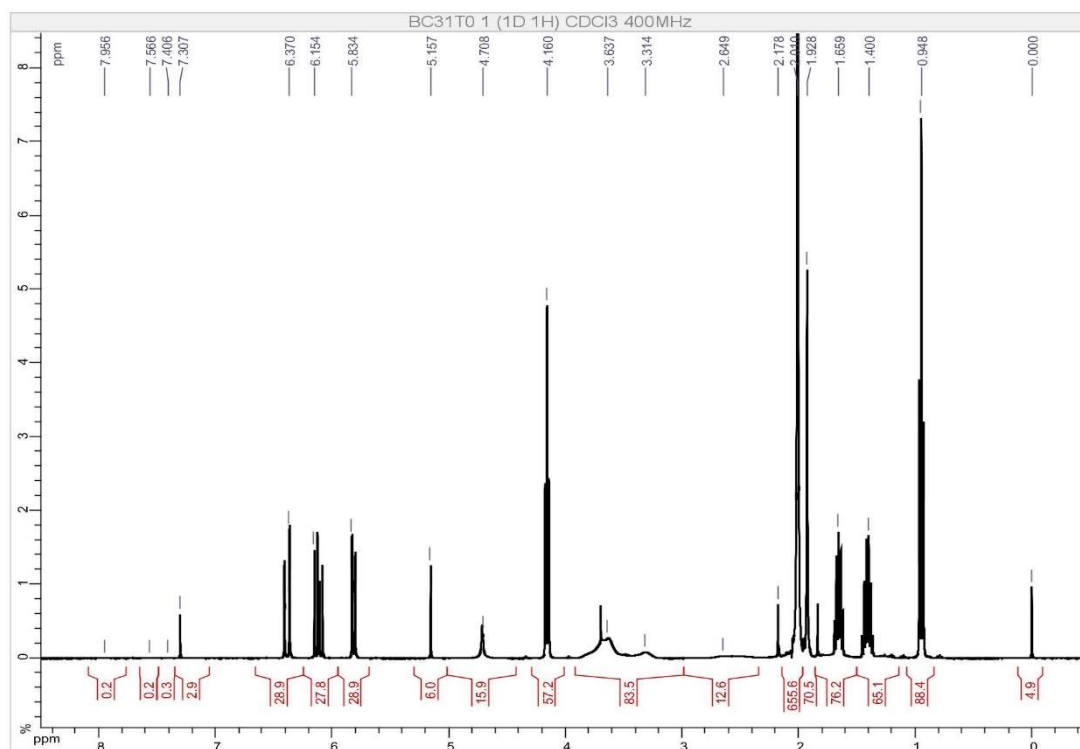
*Figure 72. ¹H NMR **of PISA2T0** (sample before the polymerization starts).*
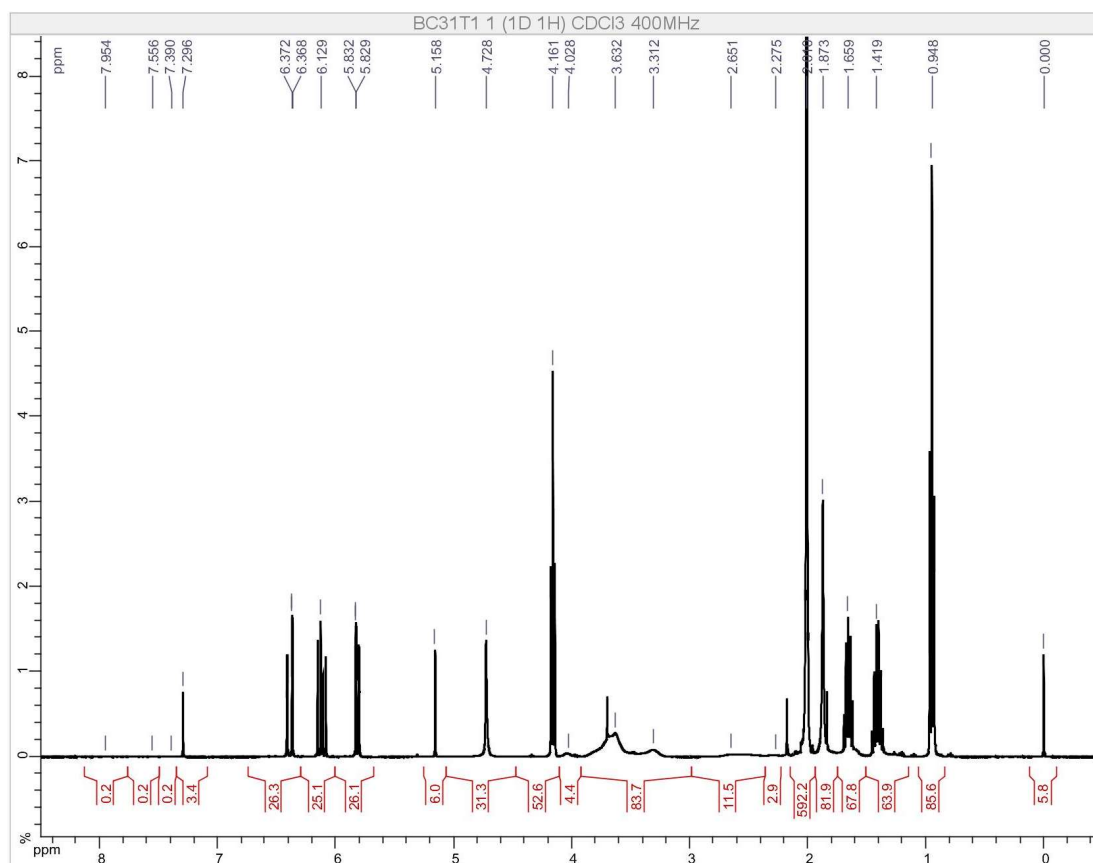
*Figure 73. ¹H NMR of **PISA2T1**.*
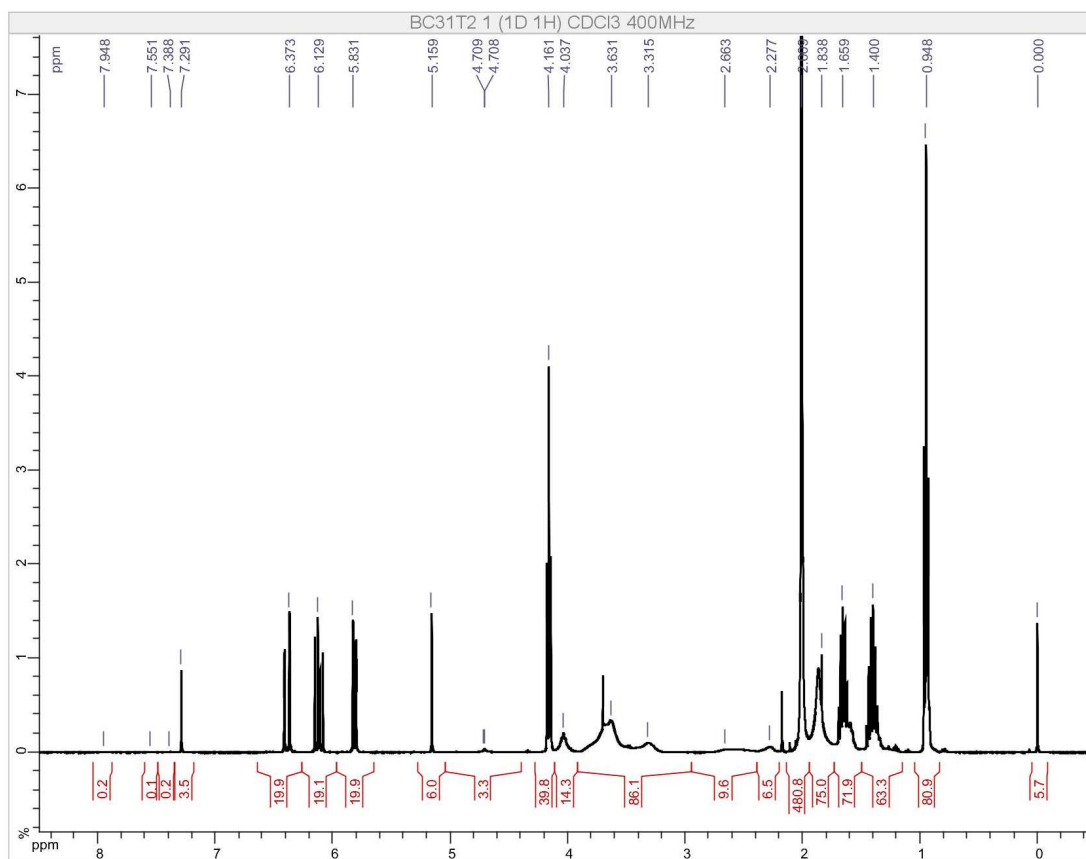
*Figure 74. ¹H NMR of **PISA2T2**.*
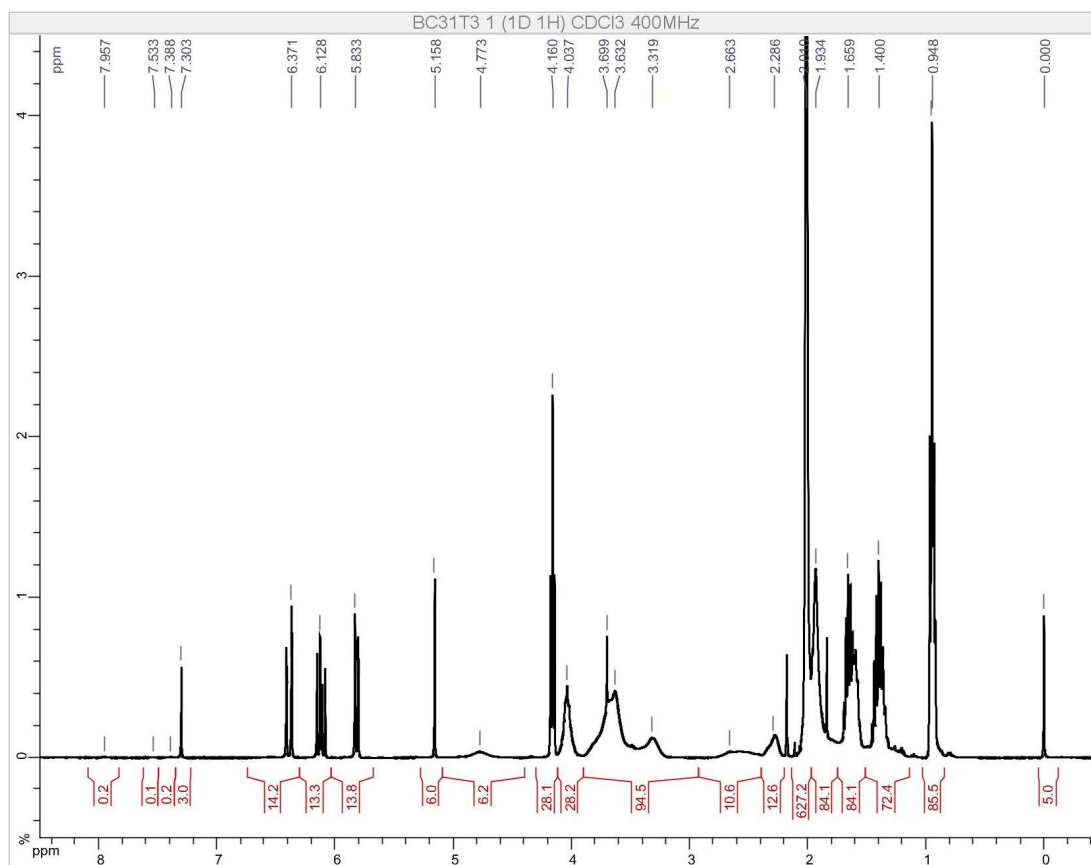
*Figure 75. ¹H NMR of **PISA2T3**.*
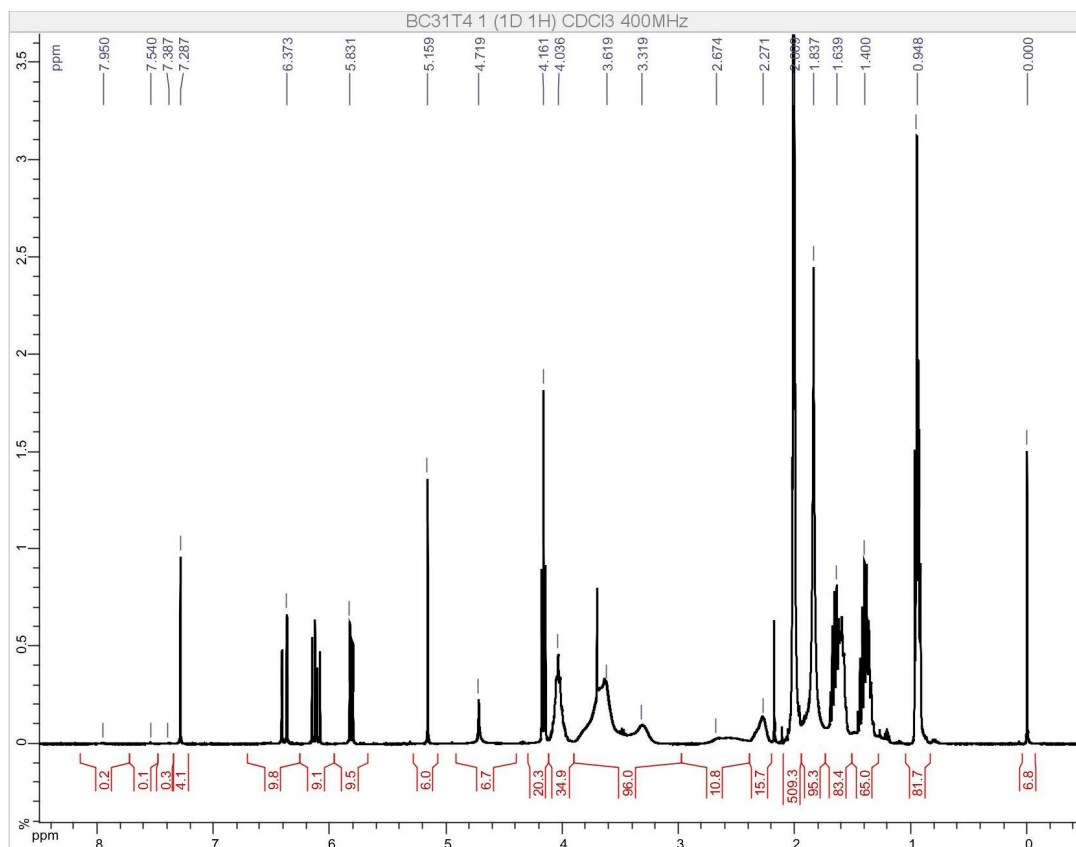
Figure 76. ^{1}H NMR of **PISA2T4**.
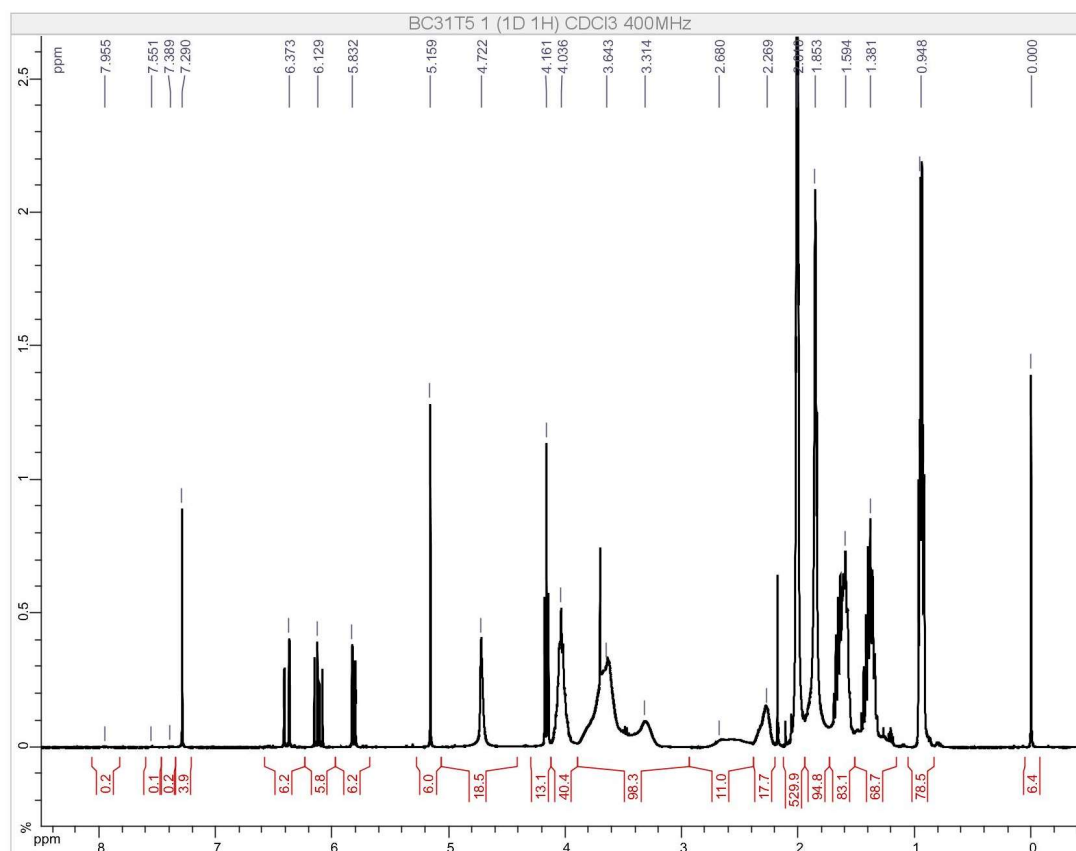
Figure 77. ^{1}H NMR of **PISA2T5**.
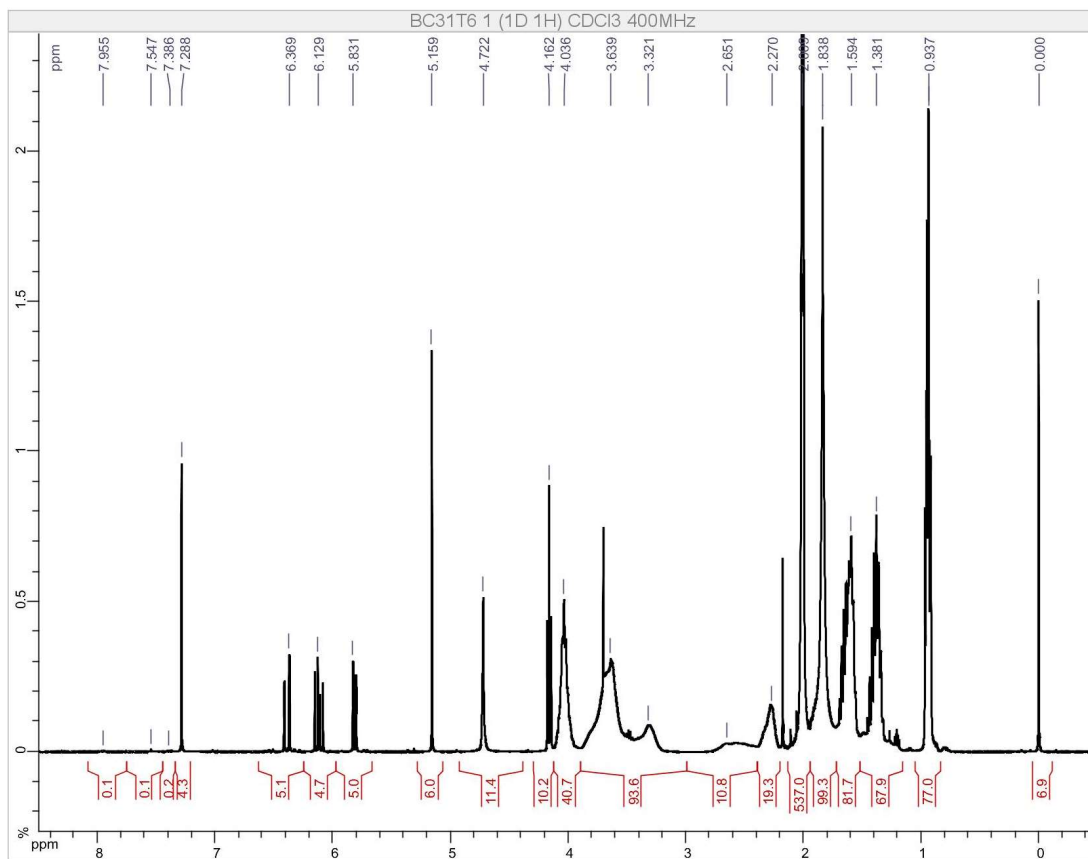
*Figure 78. ¹H NMR of **PISA2T6**.*
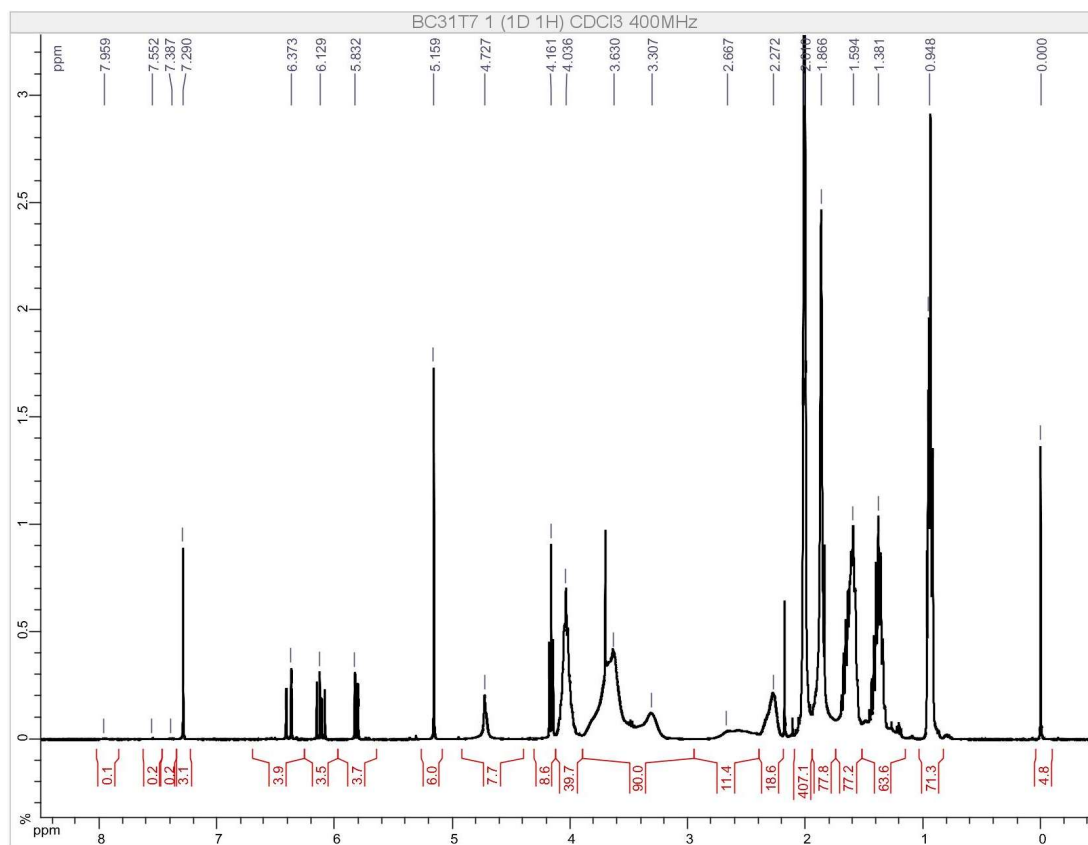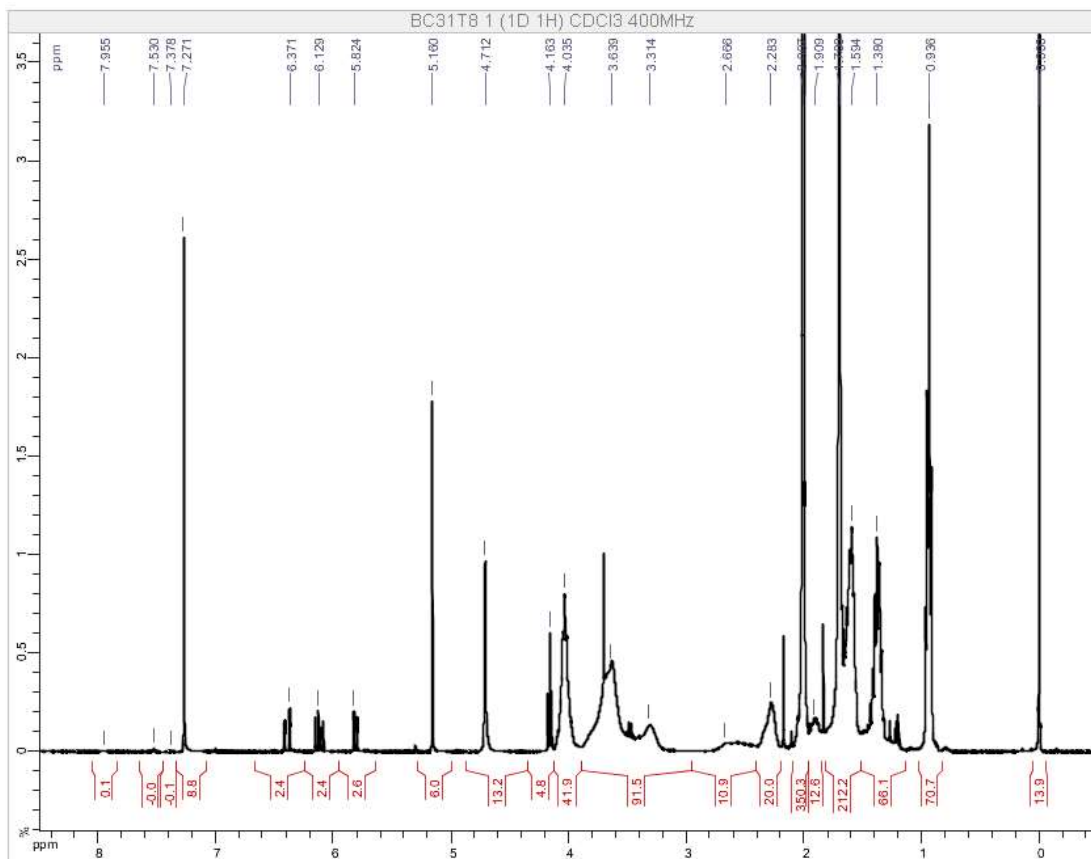

*Figure 79. ¹H NMR of **PISA2T7**.*

Figure 80. *1H NMR of **PISA2T8** (final samples from polymerization).*

IV. Comparison between miniemulsion polymerization incorporating C$_{70}$ and AuNCs

Table 19. Comparison between miniemulsion incorporating C$_{70}$ and AuNCs (ME1).

	C$_{70}$	ME1
C$_{70}$/AuNCs (g)	0.093	0.020
Sty (mol)	0.173	0.089
DVB (mol)	6.99×10^{-4}	3.61×10^{-4}
hexadecane (mol)	0.002	0.001
SDS (mol)	0.002	-
CTAB (mol)	-	0.001
H2O (mol)	2.963	1.518
Initiator (mol)	0.00050	0.00026
Initiator	KPS	AIBN
R$_{H}$(nm)	60.000	60.460 (TEM)
%SC	20-22	18
Surfactant (mol/nm^2)	2.54×10^{-25}	2.54×10^{-25}
Hexadecane (mol/nm^2)	2.68×10^{-25}	2.73×10^{-25}
[SDS]/[CTAB] (M)	0.038	0.037
CMC (SDS/CTAB) (mM)	8.2	1.0
Surfactant	SDS	CTAB

V.   Study of parameters to increase PISA-RAFT kinetics at 80°C

i.   PNAM: ACPA

The amount of ACPA initiator was increased, changing the ratio PNAM:ACPA from 2.5 to 2 to increase polymerization kinetics while limiting the downside, the loss of PISA-RAFT control (section 3.3.4.7.) .

Visual aspect of reaction medium

In terms of visual aspect, there wasn't a big difference between the 2 experiments (Figure 81). In both of them, after a few hours, there was a brown top phase and the aqueous phase has a salmon color with a slight brown color. Also, in both cases there was aggregates in the bottom after a few hours.
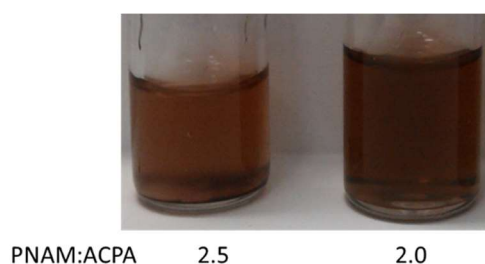

PNAM:ACPA   2.5   2.0

*Figure 81. Visual aspect of PISA-RAFT with AuNCs solutions after 2h at 80°C, varying the PNAM: ACPA ratio (**PISA 15** and **PISA 20**).*

Kinetics

In terms of kinetics, surprisingly there was not a major difference (Figure 82). However, it agrees with, D. Duret results for in PISA without AuNCs. The final conversion after 2h is also similar: 41% for PNAM:ACPA=2.5 and 35% for PNAM:ACPA=2.0. Due to the 5% error from the NMR measurements, it can be assumed that these values are the same. In terms kinetics, there is thus no advantage in using the ratio 2.0 instead of 2.5.
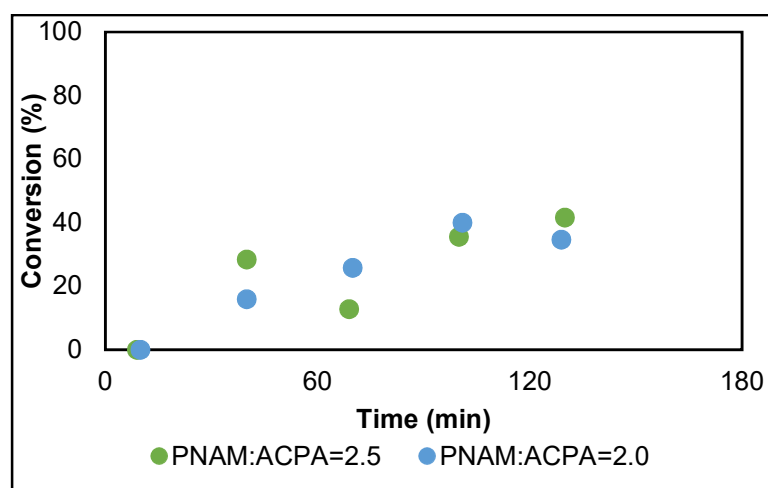

*Figure 82. Kinetics evolution of PISA-RAFT with AuNCs solutions after 2h at 80°C, varying the PNAM: ACPA ratio (**PISA 15** and **PISA 20**).*

PNPs size

In terms of PNPs size there is a no difference either, for the PNAM:ACPA=2.5 is 26.8±0.4nm, while for PNAM:ACPA=2.0 is 28.0±1.7 nm. Both samples have similar size distribution, showing that this change does not influence the PNPs size (Figure 83).
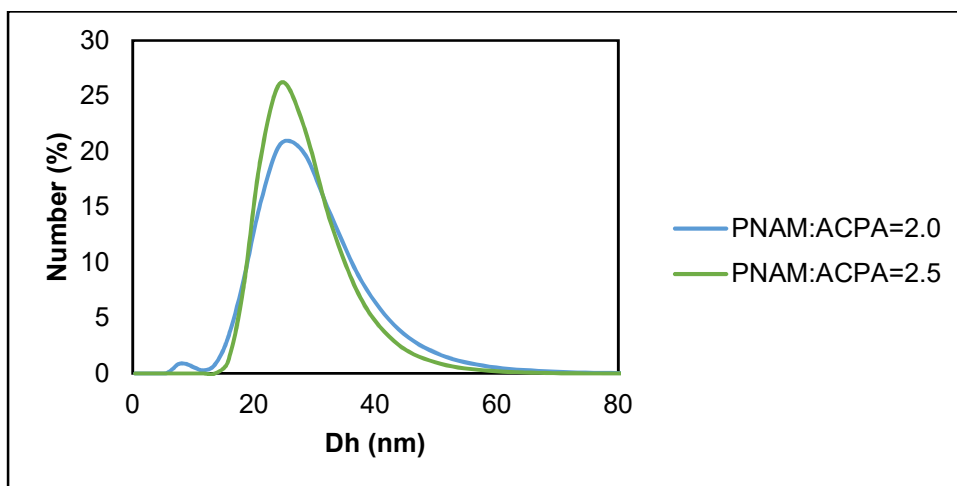
*Figure 83. Size distribution (DLS) of PISA-RAFT with AuNCs solutions after 2h at 80°C, varying the PNAM: ACPA ratio (**PISA 15** and **PISA 20**).*

Optical properties

The decrease of the ratio PNMA:ACPA seems to slightly decrease the fluorescence emission intensity. But more tests were needed to confirm such conclusion. Both have the same emission maximum: 810nm (Figure 84).
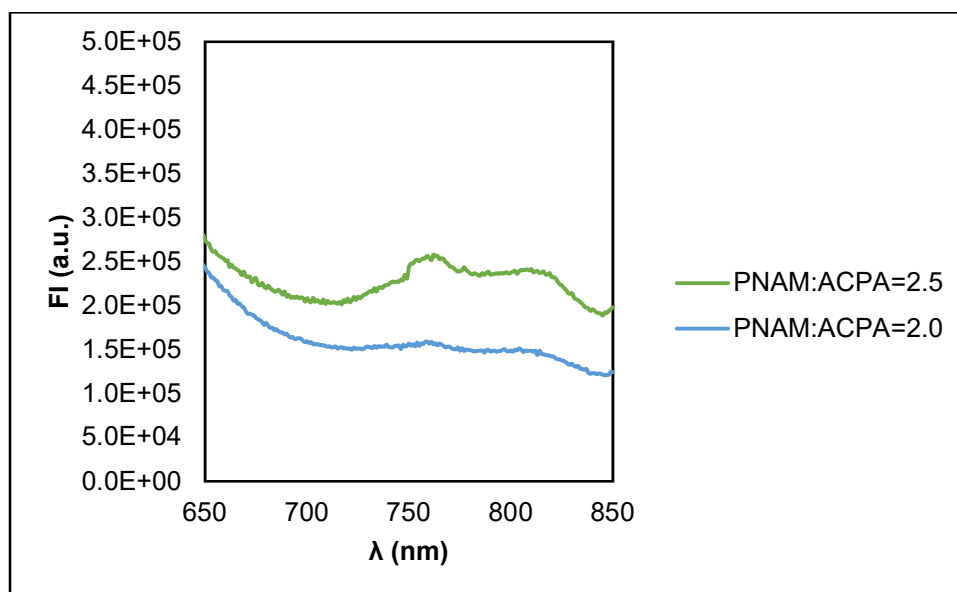

*Figure 84.. Fluorescent emission spectra of PISA-RAFT with AuNCs solutions after 2h at 80°C, varying the PNAM: ACPA ratio (**PISA 15** and **PISA 20**), with λ_{exc}=450 nm.*

In conclusion the ratio PNAM:ACPA=2 does not bring any advantages compared to PNAM:ACPA=2.5.

ii.   nBA: PNAM molar ratio

Another studied parameter is the ratio nBA:PNAM by changing the volume of nBA. By reducing the initial volume of nBA in 50%, the ratio ACPA:nBA increases, which means that there is more radicals per unit of nBA. It should increase the rate of polymerization.

Visual aspect of reaction medium

The decrease of the nBA:PNAM ratio does not affect the aspect (Figure 85). Both solution have a brown colour right after the polymerization is stopped. After about 15min, 2 phases were visible. The top phase is dark brown, being constituted by nBA, acetonitrile e AuNCs. The bottom phase, the aqueous phase, is now salmon with a tone of brown.
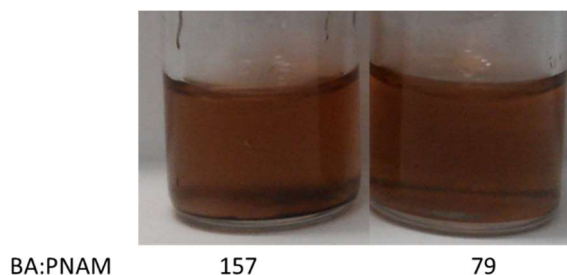

BA:PNAM   157   79

*Figure 85.Visual aspect of PISA-RAFT with AuNCs solutions after 2h at 80°C, varying the nBA: PNAM ratio (**PISA 15** and **PISA 21**).*

Kinetics

Kinetic curves show similar evolution (Figure 86). The decrease in the amount of nBA does not influence the initial concentration of nBA in the aqueous phase. In both cases, the nBA is in excess. So, in terms of nBA concentration, the influence would be at higher conversions, after the micelles formation, since the concentration of nBA inside the micelles would be lower.
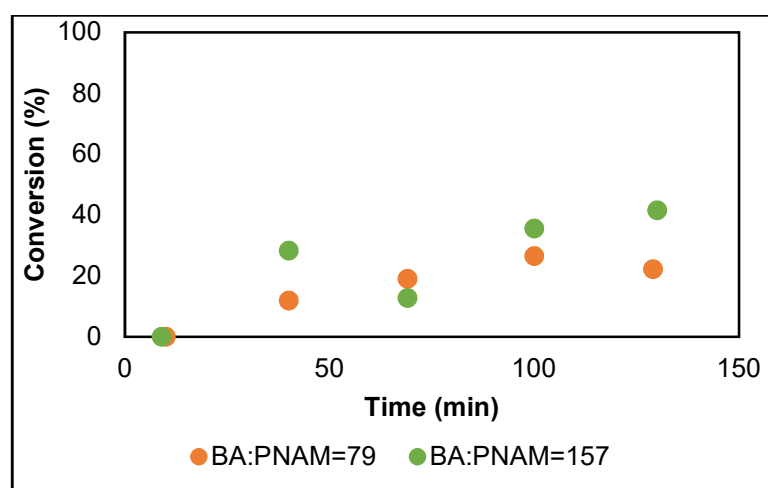

*Figure 86. Kinetics of PISA-RAFT with AuNCs solutions after 2h at 80°C, varying the nBA: PNAM ratio (**PISA 15** and **PISA 21**).*

Even though the amount of nBA was half from one experiment to the other, the final conversion is similar. So, only the equivalent to ¼ of the nBA in nBA:PNAM=157 actually reacted in nBA:PNAM=79.

PNPs size

The PNPs size is slightly smaller for nBA:PNAM=79, which can be due to the lower conversion (Figure 87). The smaller size of PNPs may be due to the lower concentration of nBA, keeping the polymerization rate inside. On the other hand, the lower concentration of nBA may have led to micelles with lower concentration of nBA, which decreases the rate of polymerization.
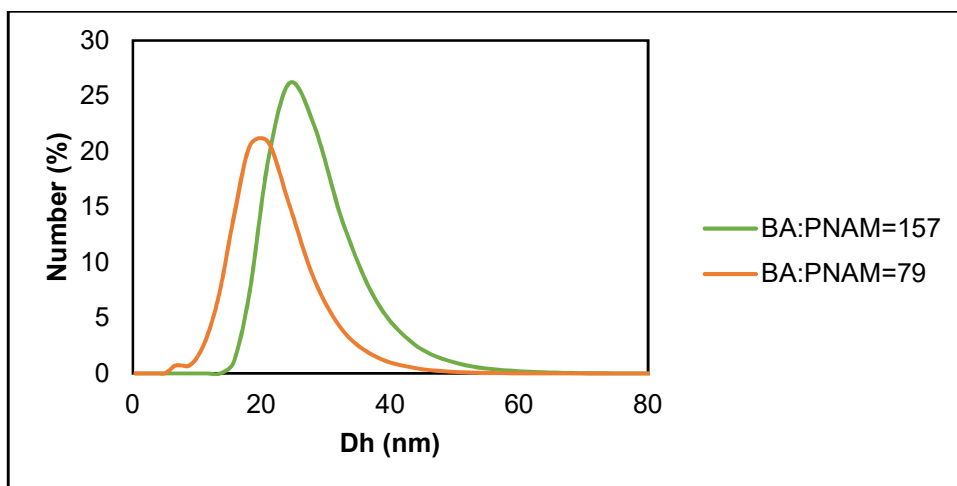
*Figure 87. Size distribution of PISA-RAFT with AuNCs solutions after 2h at 80°C, varying the nBA: PNAM ratio (**PISA 15** and **PISA 21**).*

VI.   [AuNCs] in nBA

To confirm the effect of [AuNCs] with the optimized parameters, PISA-RAFT for two different concentrations was done at 80°C for 2h.

Visual aspect of reaction medium

The tone of brown changes according to the concentration of AuNCs (Figure 88). Higher concentrations originate darker solution, like in [AuNCs]=0.140mM, while lower concentration originate a color between salmon and brown ([AuNCs]=0.070mM).
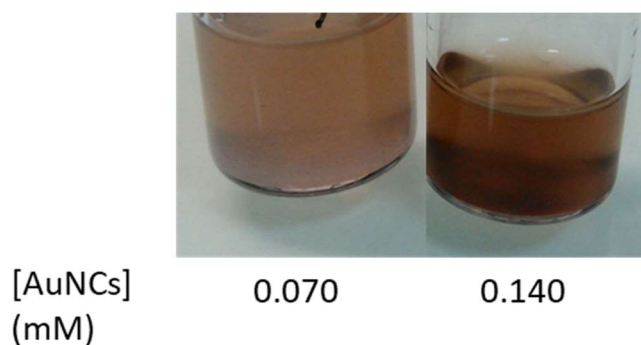

Figure 88. Visual aspect of PISA with AuNCs solutions after 2h at 80°C, varying the [AuNCs] (PISA 22 and PISA 24).

In both cases, after a few minutes with stirring, the samples show the presence of 2 phase: aqueous phase and organic phase. As expected by the solutions color right after the polymerization, in the solution with higher concentration, the top phase (organic phase) is darker.

Kinetics

In terms of polymerization the rate, there is no influence from the concentration of AuNCs, as shown previously in section 3.3.4.3 (Figure 89). The presence of AuNCs seems not to influence the rate of polymerization, even thought that in the end it originates smaller PNPs.
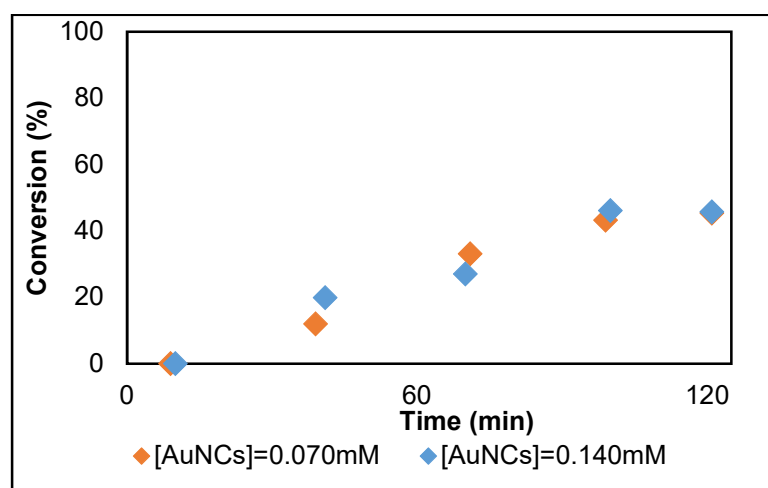

Figure 89. Kinetics of PISA with AuNCs solutions after 2h at 80°C, varying the [AuNCs] (PISA 22 and PISA 24).

PNPs size

The size, at this conversion (46% for [AuNCs]=0.140mM and 45% for [AuNCs]=0.070Mm), shows an influence of [AuNCs] in the PNPs size, leading to bigger particles for lower [AuNCs] (Figure 90). For [AuNCs]=0.070Mm, the size is 33.5±0.7 nm, while for [AuNCs]=0.140Mm, the size is 28.0±1.7 nm. As showed

in section 3.3.4.3, for lower concentrations of [AuNCs], the PNPs tend to have a slightly higher size. This due to the concentration of CTAB, which increases proportionally to the [AuNCs] in the organic phase.
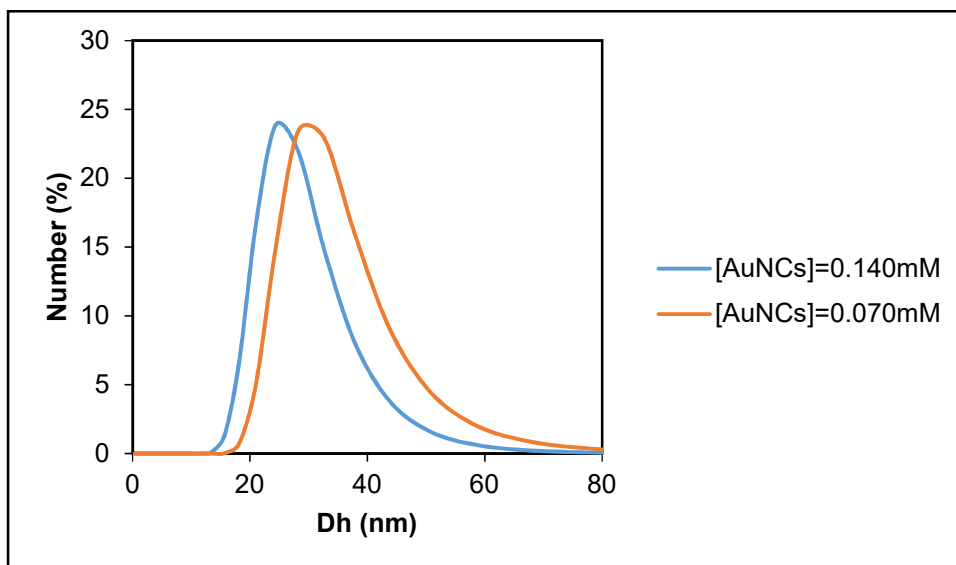

Figure 90. Size distribution (DLS) of PISA with AuNCs solutions after 2h at 80°C, varying the [AuNCs] (PISA 22 and PISA 24).

In this case, the difference of sizes is only a slight difference since the conversion is quite low. It was shown, in section 3.3.4.3, the difference of size starts to be more noticeable from 60% conversion.

Optical properties

With the decrease in concentration, the detection of AuNCs was not possible. Which can be due to the low concentration or some time evolution from the AuNCs.